UNIVERSITÀ DEGLI STUDI DI UDINE

DOTTORATO DI RICERCA IN

TECNOLOGIE CHIMICHE ED ENERGETICHE

CICLO XXVII

SYNTHESIS AND CHARACTERIZATION OF NEW ORGANIC MATERIALS WITH POTENTIAL APPLICATION IN WATER TREATMENT

Thandu Merlyn Mathilda

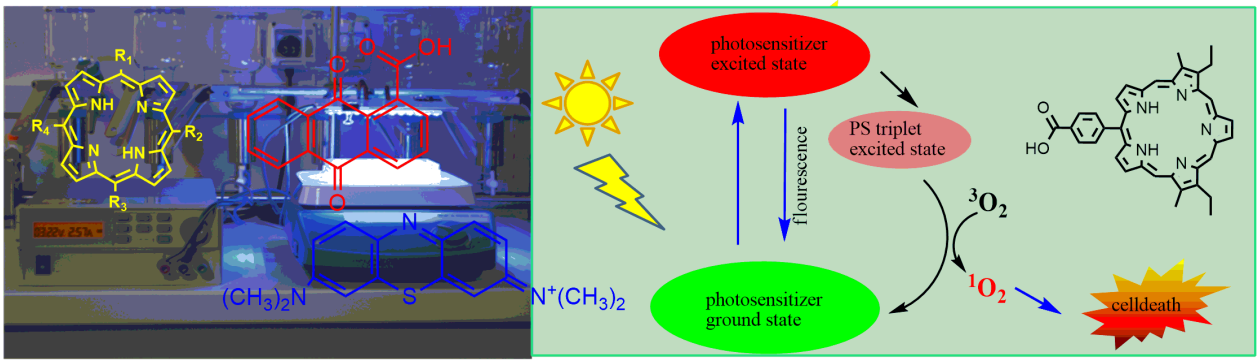

COMMISSION

Prof. Marina Zacchigna	REVIEWER
Dr. Silvia Cavalli	REVIEWER
Prof. Carla de Leitenburg	REFEREE
Prof. Pietro Mastrorilli	REFEREE
Prof. Barbara Milani	REFEREE
Prof. Daniele Goi	SUPERVISOR
Dr. Clara Comuzzi	CO-SUPERVISOR
Prof. Alfredo Soldati	DIRECTOR OF PH.D. PROGRAM

Academic year 2015-2016

To science for always giving more room to be explored for betterment of humanity
To my whole family especially Sunil and Satyen for always believing in me and loving me

Introduction

The fast and rapid growth of unwanted microbes distributed far and wide in the environment pose a threat to human health and other animals. These unwanted and harmful microbes grow and multiply in air, soil and water causing both environmental and health hazard. Water borne diseases alone account for millions of deaths annually worldwide [1]. Water borne transmission of parasitic protozoa has caused the eruption of almost two hundred human diseases in a span of just 7 years (2004-2010) [2]. The fast growing global population and contamination of water resources by human activities and/or industries poses a challenge in achieving clean, microbe-free water for drinking and other domestic purposes. Scientists worldwide believe that waterborne diseases are affecting both the developed and the developing nations [1-4]. Acquiring pure water free of contaminants and pathogens is a matter of concern which calls for new, effective and low cost water disinfection techniques.

Conventional disinfection mainly involves chlorination or ozonization. Another cheap alternative for disinfection is using direct sunlight (SODIS) (solar disinfection) [4]. But these methods face limitations like production of harmful by products, involving high cost, limited water volume and time consuming. In order to overcome these inadequacies, remarkable efforts have been carried out to develop more effective water disinfection methods than the conventional systems that will be environment friendly, cost effective and highly efficient [1-6]. Photocatalytic disinfection of water is gaining much interest as it involves three components that are individually harmless to the biological environment namely the photosensitizer, light and molecular oxygen [7].

Some organic and inorganic catalyst on light irradiation in presence of oxygen produce reactive oxygen species (ROS) like singlet oxygen, hydroxyl radical (superoxide anion) that are cytotoxic species and are capable of killing bacteria, fungi and viruses [1, 5, 6, 8, 9]. Not only disinfection, but these ROS can also cause the oxidation of unwanted contaminants present in water, thereby carrying out dual function of disinfection and decontamination [1, 10, 11, 12]. Organic dyes like methylene blue, rose bengal, porphyrins and phthalocyanines are used as photosensitizers [5, 8, 12] for water disinfection while common

inorganic catalysts are TiO_2, ZnO, ZnS, CdS, Fe_2O_3 and WO_3 [1, 8, 13, 14]. Among the inorganic semiconductors, TiO_2 is the most widely used in photocatalysis.

In consideration with the above theoretical evaluation, the PhD project is aimed at developing new organic materials that upon light irradiation are able to produce reactive oxygen species (ROS) especially singlet oxygen, which is responsible for destroying pathogens in contaminated water. The project is mainly carried out in the following steps:

- Immobilization of TPP (5-*p*-carboxyphenyl-10,15,20-triphenyl porphyrin) on solid supports :
    - Magnetic porphyrin nanoconjugate (SPION-TPP)
    - Polymeric porphyrin composite (PVC-TPP)
- Phototreatment of contaminated water using immobilized and free photosensitizers.
- Synthesis of expanded porphyrins and their characterization.

Photodynamic therapy undoubtedly is a potential technique for destruction of unwanted microbes. But analysing recovery and reusability of photosensitizers can be an important breakthrough in the field of photodisinfection.

Magnetic nanoparticles are not gaining the required attention in water photodisinfection although they are used to a greater extent for biomedical applications. Magnetic nanoparticles can prove to be potential carriers for photosensitizers as they allow to be recovered at the end of treatment and thereby reuse the photosenstizer. Here we report a successful immobilization of TPP on SPION and the evaluation of photodisifection efficiency of the nanoconjugate.

Another support studied was a common polymer polyvinyl chloride (PVC). To our knowledge, PVC has not been used in the past as a support for photosensitizer. The study has proved that PVC can be a promising support for photosensitizers with high yield of singlet oxygen/ROS generation and significant toxicity against *S. aureus* in presence of light

Trial syntheses of new photosensitizers were performed to study the behaviour of expanded porphyrins. The desired characteristics can be tailored by choosing the right precursors with different functional groups in expanded porphyrins . The study performed has given an insight for future modelling of novel photosensitizers.

1 Literature Survey

1.1 PHOTOSENSITIZATION/PHOTOCATALYSIS

Photosensitization process or photodynamic therapy (PDT) principally involves three components namely, the photosensitizer, light and oxygen. On illumination at appropriate wavelength, the photosensitizer transfers its energy to molecular oxygen giving rise to reactive oxygen species (ROS) [6, 8, 15-17]. ROS are cytotoxic in nature which enables to employ this phenomenon in destroying unwanted microorganisms like bacteria, fungi and viruses (Figure 1). These ROS are also capable of oxidizing organic pollutants into CO_2 and water [18].

Depending on the nature of photosensitizer/photocatalyst, the photodynamic action proceed through type I or type II mechanism or both. Type I mechanism involves electron transfer from excited sensitizer to substrate molecule or oxygen yielding free radicals and superoxide ion whereas in type II mechanism, energy transfer between photosensitizer and oxygen produces singlet oxygen [8].

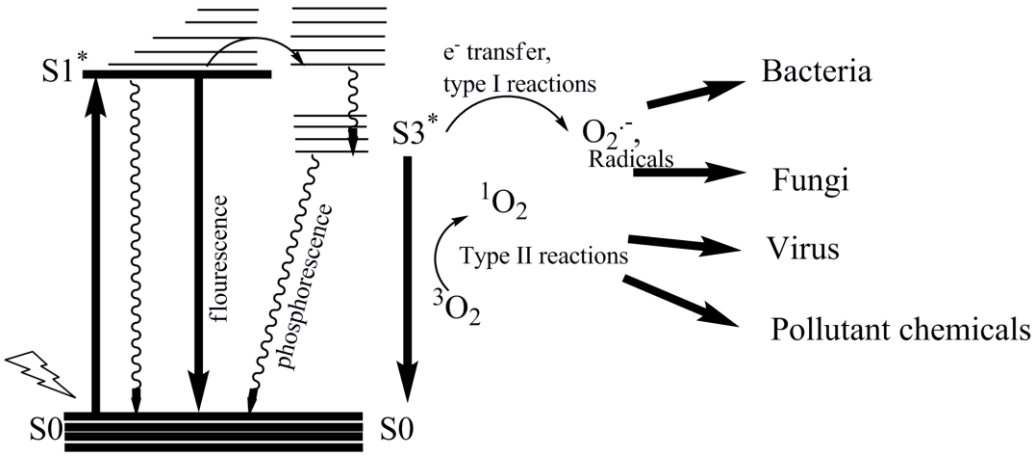

Figure 1.1 The Jablanski diagram

1.1.1 VISIBLE LIGHT PHOTODISINFECTION

Organic dyes and photosensitizers are generally absorbed in the visible range (400-800 nm) and excitation is achieved by one photon transition ($h\nu$) from the ground state (S0) to singlet excited state ($S1^*$) eq.1.1. $S1^*$ can undergo intersystem crossing (ISC) to give the triplet excited state ($S3^*$) (eq.1.2). The relaxation of $S1^*$ and $S3^*$ to ground state results in fluorescence and phosphorescence, respectively [8, 21] (eqs. 1.3 and 1.4). Alternatively, since $S3^*$ has a longer lifetime than $S1^*$, it can also undergo radiationless transition by transferring its energy to another molecule [17]. In the presence of oxygen, the photosensitizer easily transfers energy to triplet ground state oxygen via type II mechanism producing $^1O_2$ (eq.1.5).

$S0 + h\nu \rightarrow S1^*$ (1.1)

Intersystem crossing (ISC) $S1^* \rightarrow S3^*$ (1.2)

Relaxation $S1^* \rightarrow S0 + h\nu$ (fluorescence) (1.3)

$S3^* \rightarrow S0 + h\nu$ (Phosphorescence) (1.4)

Or energy transfer $S3^* + {}^3O_2 \rightarrow S0 + {}^1O_2$ (1.5)

Electron transfer $S3^* + O_2 \rightarrow S^{\bullet+} + O_2^{\bullet-}$ (1.6)

It is considered that photodamage to cell is predominantly caused by singlet oxygen via type II reactions [19, 20], but it is also proved that photosensitized action is caused by both type I and type II pathways [21, 22]. Ergaieg et al. [21] have reported that type I reactions had a significant role in inactivation of Gram-negative bacteria whereas the photoinactivation rate of Gram-positive bacteria was unchanged even in the absence of superoxide anion. Silva et al. [23] also have considered the production of $O_2^{\bullet-}$ (eq.1.6) and propose that it may be involved in PDT apoptosis.

1.1.2 UV-BASED PHOTOCATALYSIS

Semiconductors such as TiO_2, Fe_2O_3, WO_3, ZnO and CdSe require light energy in the UV-A ($\lambda < 400$nm) range to carry out photochemical activity. Such molecules have a band gap between the valence band and conduction band which can be activated by light. The light energy to excite the valence electron

must be higher or equal to the band gap. The band gaps of some semiconductors are listed in Table 1.1. The different band gaps also suggest the efficiency of the materials. Larger the band gap more is the photocatalytic activity of the semiconductor [24].

Table 1.1 Band-gap of some inorganic semiconductors

Semiconductors	**TiO_2 (anatase)**	**TiO_2 (rutile)**	**ZnO**	**SnO_2**	**WO_3**	**ZnS**
Eg (eV)	3.2	3.0	3.2	3.9	2.8	3.7

The energy required for excitation of such electrons lies in the UV region (λ<400nm) [1, 18]. On illumination with sufficient energy, one of the electrons from the valence band excites to the conduction band forming electron-hole pair. The photoreactions follow type I mechanism resulting in formation of radicals (Eqs. 1.7- 1.11). The electron-hole pair can oxidize water yielding $HO^{\bullet}$ radicals which are powerful oxidizing agents that cause oxidation of pollutants into CO_2 and H_2O (Eqs. 1.12-1.14). The electron in the conduction band can combine with oxygen to form superoxide radical anion $O_2^{\bullet -}$ that can react with H^+ to produce hydroperoxyl radical $HOO^{\bullet}$ further protonation of which gives H_2O_2. These ROS are responsible for the oxidative degradation of contaminants and disinfection. The generation of singlet oxygen by TiO_2 has also been proved recently [25, 26]. Konaka et al. [26] have shown that $^1O_2$ is formed by direct photosensitization or by ion-annihilation of $O_2^{\bullet -}$ (Eqs. 1.15 and 1.16)

$TiO_2 + h\nu \rightarrow h_{VB}^+ + e_{CB}^-$ (1.7)

$h_{VB}^+ + H_2O \rightarrow HO^{\bullet} + H^+$ (1.8)

$e_{CB}^- + O_2 \rightarrow O_2^{\bullet -}$ (1.9)

$O_2^{\bullet -} + H^+ \rightarrow HOO^{\bullet}$ (1.10)

$HOO^{\bullet} + HOO^{\bullet} \rightarrow H_2O_2 + O_2$ (1.11)

$HO^{\bullet}$ + pollutant $\rightarrow CO_2 + H_2O$ (1.12)

$O_2^{\bullet -}$ + pollutant $\rightarrow CO_2 + H_2O$ (1.13)

$HOO^{\bullet}$ + pollutant $\rightarrow CO_2 + H_2O$ (1.14)

Direct photosensitization $TiO_2 + O_2 \rightarrow {}^1O_2$ (1.15)

Ion annihilation $TiO_2^+ + O_2^{\bullet -} \rightarrow {}^1O_2$ (1.16)

1.2 PHOTODISINFECTION MECHANISM

It has been known for almost a century that light and photosensitizer can cause destruction of microorganisms [5], and during these years many have discussed and some have put forward their results to explain the mechanism of cell killing [9, 27, 28-31, 22, 32-36]. The photoprocess successfully causes reduction in survival of bacteria (Gram-positive and Gram-negative), yeast, fungi and viruses [30]. The accumulation of the photosensitizer in the bacteria was thought to be the prerequisite for its destruction [9]. Basically, two main approaches of photokilling were elucidated, (i) Breaking of the cell membrane and its constituents (ii) DNA damage. Many results have been put forward to prove that phototreatment induces alterations in the membrane as well as cell constituents. Depending upon the type of microorganism, the mechanism of photoinactivation and the cellular targets could vary as discussed in the following sections.

1.2.1 BACTERIA

The photodynamic effect of TMPyP (Figure 1.2 displays the structure of different organic photosensitizers and the abbreviations are indicated in brackets) on four different *E. coli* strains (O_4, WP2 TM9, Bs-1 and TG1) was studied by Valduga et.al [37]. All the cell suspensions on photosensitization underwent about 5 log decrease in cell survival after 30 min irradiation. They observed alterations in the electrophoretic mobility of outer membrane proteins as well as cytoplasmic proteins. Lactate and NADH dehydrogenases were readily inactivated by irradiation in presence of TMPyP. Similarly, the activities ATPase and succinate hydrogenase were impaired. A decrease of plasmid DNA extracted from irradiated *E. coli* TG1 cells was also observed. Further, Bertoloni et al. [30] have studied the mechanism of photosensitizing activity of Hp on *S. aureus*. Electrophoretic analysis of visible light irradiated Hp sensitized *S. aureus* show that the photoprocess induces a modification consequent to protein-protein crosslinking formation at the level of cytoplasmic membrane proteins but not at the level of cytoplasmic proteins. But, changes in both plasmidial and

chromosomal DNA strands were observed both *in vivo* and *in vitro* photoprocesses at long irradiation time.

1.2.2 FUNGI

Likewise, membrane and intracellular damage is caused by photosensitization of fungi as well. Lambredhts et al. [38] observed that in dark conditions, the cationic porphyrin TriP4 binds to the cell envelope of *Candida albicans* and does not enter into the cell. Upon illumination, the cell membrane is damaged and becomes permeable for TriP4 and a lethal damage of the cell occurs. Cationic porphyrins interact strongly with DNA and cause photocleavage in solution [33]. Quiroga et al. [34] used $TFAP^{3+}$, $TMAP^{4+}$ and TMPyP to study the photoinactivation of *C. albicans*. All the cationic porphyrin exhibitied a photosensitizing activity causing about 3.5 log decrease in cell survival. The interaction of the porphyins with DNA was confirmed by the alterations in the spectral properties (mainly Soret band) of the porphyrins. However, their studies did not find any significant cleavage of isolated genomic DNA in *C. albicans*.

1.2.3 PROTOZOA

Ferro et al. [39] studied the inactivation of *Acanthamoeba palestinensis* (pathogenic protozoa) with photodynamic treatment with a tetra cationic Zn (II)-phthalocyanine (RLP068) and found that the survival of the cysts dropped down considerably. Further, the study on the mechanism of photosensitized inactivation of *A. palestinensis* [29] proved that the activities of mitochondrial enzymes (NADH, SDH and CS) showed no significant decrease, while that of cytoplasmic enzyme LDH were inhibited upto 35 ± 4 %. Transmission electron microscope images of the trophozoites incubated with 2 μmol l^{-1} for 10 min and irradiated for 10 min at 500 Wm^{-2} (600-700 nm) showed several subcellular sites to be severely damaged. The cytoplasm was highly vacuolized and various vesicles surrounded by a membrane were visible while plasma and nuclear

membrane were unchanged in comparison with control cells. Photoinactivation, thus induces both functional and morphological damage to the microorganism resulting in its complete destruction.

There are numerous evidences for the interaction of photosensitizers with cell components and thereby their destruction in presence of light but cell death is not due to the alteration of intracellular components but the primary cause being the cell membrane and the cell wall. This is evident because, *D. radiodurans* having very efficient DNA repair mechanism easily undergoes photosensitization [40, 41]. TMPyP-mediated photosensitization of *D. radiodurans* [42] revealed the leakage of potassium and magnesium from cells and a significant loss of phosphate which could be followed as a function of light dose. Thus, the cell wall is the primary target in photoinactivation and the destruction of intracellular components is the possible consequence of membrane damage [40, 43 and 44].

1.2.4 VIRUSES

The primary target in antiviral PDI depends on the type of virus [36]. Envelope lipids and proteins, caspid and core proteins, DNA and RNA all are the different components that can be targets of photoproccess [32, 35]. Smetana et al. [45] studied the photoinactivation of herpes simplex virus type 1 (HSV-1) with two cationic phthalocyanines and an anionic dye. They observed major changes in viral proteins in particular glycoprotein D (gD), a structural protein of the HSV envelope. The inactivation of envelope protein impairs their ability to enter into host cell thereby reducing viral infection. Non-enveloped T7 phage effectively undergoes photoinactivation in presence of cationic porphyrins TriP4 and TMPyP [35]. The porphyrins efficiently bind to DNA even in the dark but total virus inactivation occurs after illumination. At appropriate doses of porphyrins, the structural integrity of DNA and viral proteins are affected leading to reduction in the viability of T7 bacteriophage. The effect of MB on reverse transcriptase (RT), HIV-1 associated protein p24 and viral RNA in HIV-1 was studied by Bachmann et al. [32]. RT was completely inhibited after the whole virus inactivation by MB/light treatment. Also, western blotting and polymerase chain reaction (PCR) inhibition assay showed alteration in HIV-1

p24 and the destruction of its RNA. All the results discussed above lead to the conclusion that phototreatment of viruses in presence of photosensitizers are effective in their destruction and this could be promising alternative in treating viral infections.

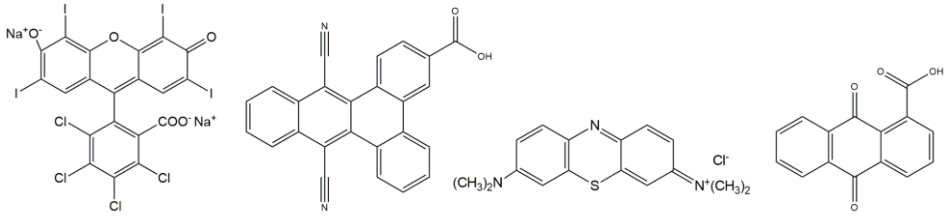

Figure 1.2 (a) Structures of some aromatic dyes used as photosensitizers

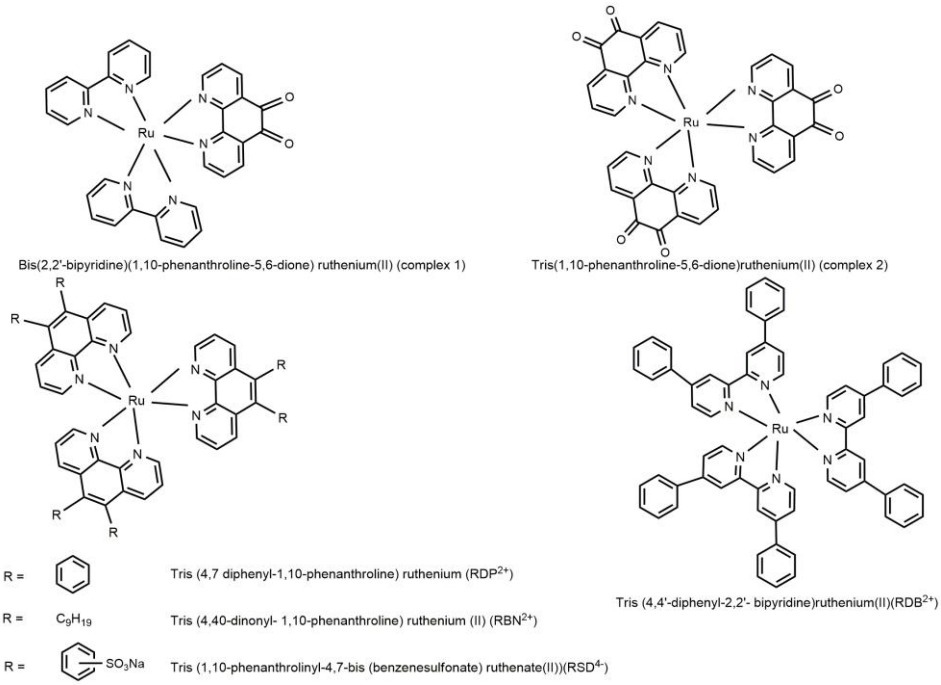

Figure 1.2 (b) Ruthenium complexes as photosensitzers

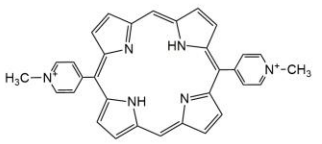

5,15-Di(N-methyl-4-pyridinium) porphyrin (DMPyP)

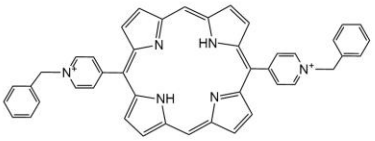

5,15-Di(N-benzyl-4-pyridinium)porphyrin (DBPyP)

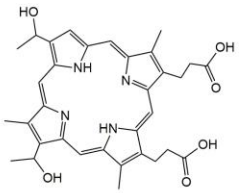

Hematoporphyrin (Hp)

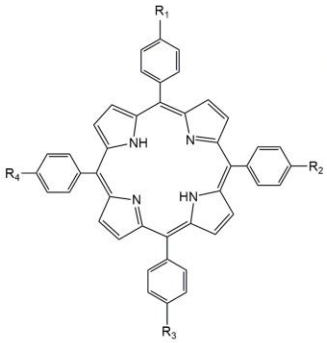

R_1= R_2=R_3=R_4 = A= 4-(3-*N*,*N*,*N*-trimethylammoniumpropoxy)-O$(CH_2)_3N^+(CH_3)_3I^-$(A_4^{4+})

R_1= R_3= A R_2=R_4= B = 4-(trifluoromethyl) phenyl- CF_3 ($ABAB^{2+}$)

R_1= A R_2=R_3=R_4=B (A_3B^+)

R_1= R_2=R_3=R_4=H 5,10,15,20-tetraphenyl porphyrin (TPP)

R_1= R_2=R_3=R_4= $SO_3^-Na^+$ 5,10,15,20-tetrakis(4-sulfonatophenyl) porphyrin($TPPS_4^{4-}$)

R_1= R_2=R_3=R_4=  5,10,15,20-tetrakis(4-*N*,*N*-diphenylaminophenyl) porphyrin (TDAP)

R_1= R_2= R_3 = R_4= COOH 5,10,15,20-tetrakis (4-carboxyphenyl) porphyrin (H_2TPPC)

R_1= R_2 = R_3 = R_4= NO_2 5,10,15,20-tetrakis (4-nitrophenyl) porphyrin (TNO_2PP)

R_1= R_2=R_3=R_4= OH 5,10,15,20-tetrakis(*p*-hydroxyphenyl)porphyrin (p-THPP)

R_1= R_2=R_3=R_4= NH_2 5,10,15,20-tetrakis(*p*-aminophenyl)porphyrin (p-TAPP)

R_1= R_2=R_3=R_4=  5,10,15,20-tetrakis(4-*N*,*N*,*N*-trimethylanilinium) porphyrin ($TMAP^{4+}$)

R_1= CF_3 R_2=R_3=R_4  5-(4-trifluorophenyl)-10,15,20-tris(4-*N*,*N*,*N*-trimethylammoniumphenyl) porphyrin ($TFAP^{3+}$)

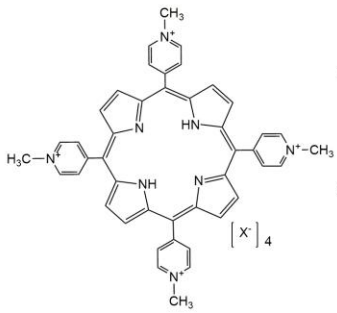

X^- = 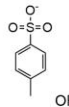 5,10,15,20-tetrakis (*N*-methylpyridinium-4-yl) porphyrin tetratosylate (TMPyP)

OR

X^- = I^- 5,10,15,20-tetrakis(1-methylpyridinium-4-yl) porphyrin tetra-iodide (Tetra-Py^+-Me)

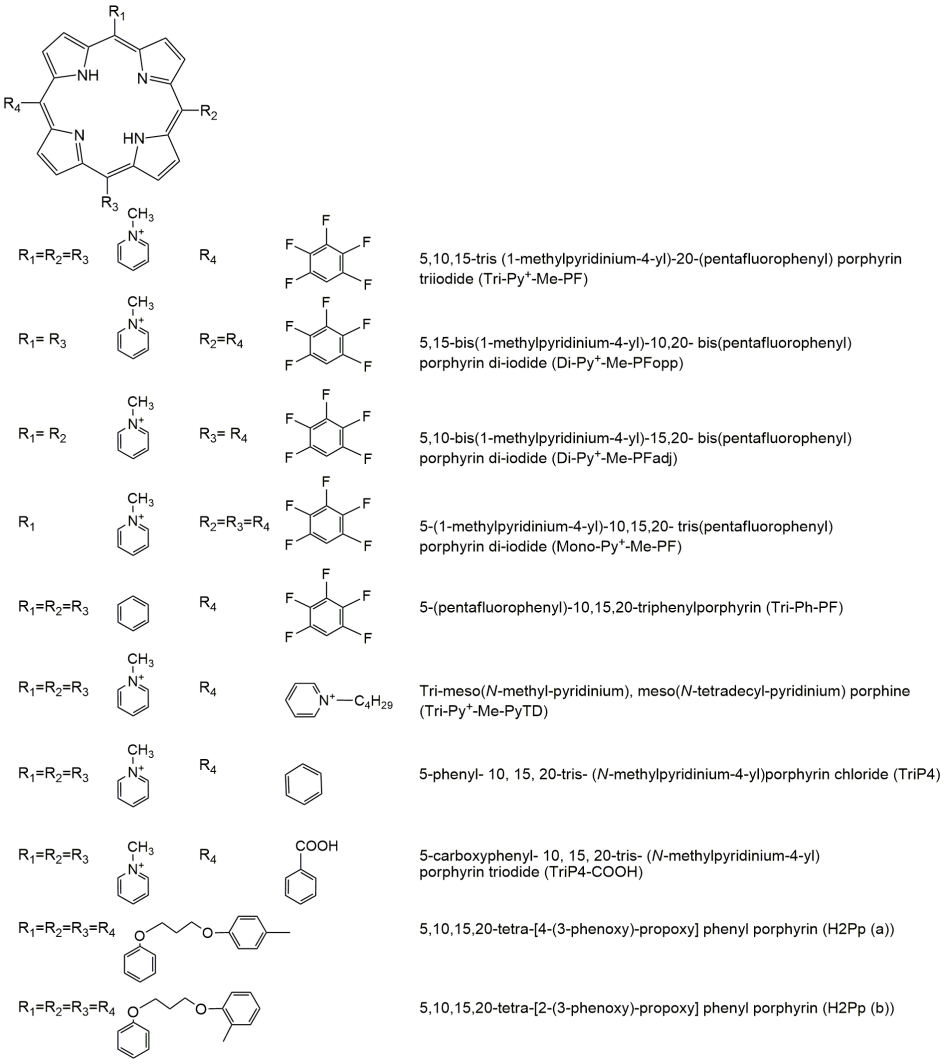

Figure 1.2 (c) Stuctures of wide range of porphyrins available or synthesized

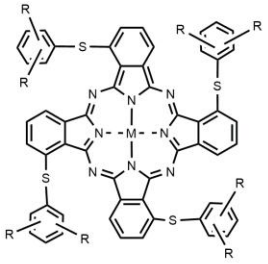

M= Zn, R = CH_2Cl 3-tetra [di(chloromethyl)phenylthio] phthalocyaninato zinc ($ZnPc(Sph)4Clm_8$) on silica ($D/ZnClm_7$)

M= Zn, R= CH_2-$N^+(CH_3)_2$-CH_2CH_2OH- 3-tetra [di(chloromethyl)phenylthio] phthalocyaninato zinc hydroxide ($D/ZnChol_7$)

M= Al, R = CH_2Cl 3-tetra [di(chloromethyl)phenylthio] phthalocyaninato Aluminium ($AlPc(Sph)4Clm_8$) on silica ($D/AlClm_7$)

M= Al R= CH_2-$N^+(CH_3)_2$-CH_2CH_2OH- 3-tetra [di(chloromethyl)-phenylthio] phthalocyaninato aluminium hydroxide ($D/AlChol_7$)

M= Al, R= CH_2-NH-$CH_2CH_2SO_3$-Na^+-tetra [di(taurylmethyl)phenylthio] phthalocyaninato) ($D/AlTaur_7$)

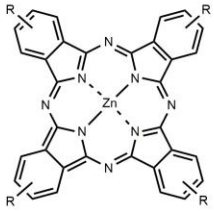

R= zinc(II) 2,9,16,23- tetrakis [4-(*N*-methylpyridyloxy)] phthalocyanine ($ZnPPc^{4+}$)

R= NO_2 zinc(II) tetranitrophthalocyanine (ZnTNPc)

R=  zinc(II) tetra(phenyloxy)phthalocyanine (ZnTPhOPc)

R= 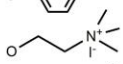 zinc(II) tetra(*N*,*N*,*N*-trimethylaminoethyloxy) phthalocyaninate tetraiodide (ZnTTMAEOPcI)

R= 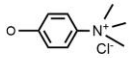 1(4),8(11),15(18),22(25)-tetrakis-3-(*N*,*N*,*N*-trimethylammonium) phenoxy-phthalocyanato zinc (II) chloride (RLP068)

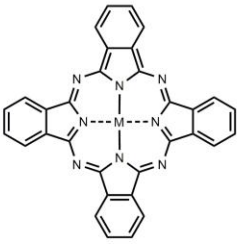

Phthalocyanine = PCH

M = Ti (TiPCH)

M = Zn (ZnPCH)

M = Si (SiPCH)

M = Al (AlPCH)

M = Co (CoPCH)

M = Ni (NiPCH)

M = Cu (CuPCH)

Metalfree PCH (MeFPCH)

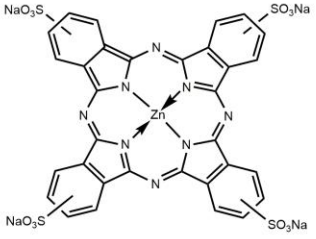

Zinc(II) phthalocyanine tetrasulfonic acid tetrasodium salt (ZnPcS)

Figure 1.2 (d) Phthalocyanines

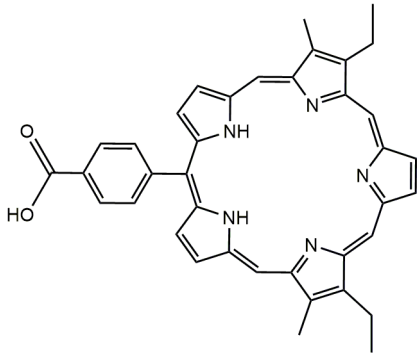

20-(4-carboxyphenyl)-2,13-dimethyl-
3, 12-diethyl-(22p) pentaphyrin (PCCox)

Figure 1.2 (e) Pentaphyrin

1.3 INFLUENTIAL PARAMETERS IN WATER PHOTOTREATMENT

1.3.1 PHOTOSENSITIZERS

Several photosensitizers are available that can be employed in photodisinfection. In order to display superior photodynamic action, the photosensitizer must fulfil certain criteria. Some properties which must be possessed by an ideal photosensitizer are listed as follows:

- High absorption coefficient in the spectral region of the excitation light especially blue light as it is the most penetrating in waters.
- Long lived triplet excited state and high quantum yield for the generation of ROS (in particular singlet oxygen).
- Photo stability.
- Broad spectrum of action in order to efficiently act on infections involving a heterogeneous flora of pathogens.
- The photoinactivation mechanism with minimal risk of inducing selection of resistant strains or promoting the onset of mutagenic processes.
- Low or no toxicity in the dark.

Organic photosensitizers such as **MB**, **RB**, porphyrin related molecules as well as transition metal complexes (in particular bipyridine and phenanthroline complexes of Ru (II)) have been the focus of research and development in the last few years [8, 19, 21,46-48]. In order to have an antimicrobial activity in the broad spectrum, the photosensitizers must effectively kill bacteria (both Gram positive and Gram negative), fungi and viruses. Gram negative bacteria are more resistant than the Gram positive bacteria owing to the presence of complex lipopolysaccharide layer in addition to the thick peptidoglycan cell membrane which limits the permeability of the photosensitizer into the cell. Hence disinfection of Gram negative bacteria with organic sensitizers either require the presence of membrane disrupting agents (cationic polypeptide polymixin B or EDTA) or that the photosensitizer bears a positive charge so that

it binds to the negatively charged surface and displace cations thereby changing the arrangement of lipopolysaccharide resulting in alteration of the barrier properties of cell wall [49]. Many authors have successfully reported the inactivation of Gram negative bacteria like *E. coli* using positively charged photosensitizers. Merchat et al. [50] while using 4 different meso substituted porphyrins (2 cationic and 2 anionic) found that the all porphyrins were effective against Gram positive whereas Gram negative bacteria were almost insensitive to anionic porphyrins. However, Jemli et al. [51] have reported the better activity of RB (di anionic) than MB (mono cationic) against fecal coliforms referring the enhanced activity of the former to better photophysical properties (high quantum yield of singlet oxygen and better absorption). Nonetheless, more recent studies proving that cationic dyes are more effective in destroying Gram negative bacteria are published [48, 52 and 53]. Caminos et al. [54] have studied the effect of an anionic and four cationic porphyrins with different pattern of meso-substitution by 4-(3-*N*, *N*, *N*-trimethylammoniumpropoxy) phenyl (A) and 4-(trifluoromethyl) phenyl (B) groups. They have found that cationic porphyrins are rapidly bound to *E. coli* cells with the highest binding for A_3B^{3+} porphyrin (tricationic) and the photosensitized inactivation followed the order $A_3B^{3+} > A_4^{4+} >> ABAB^{2+} > AB_3^{+}$. Under the same conditions, anionic sensitizer ($TPPS_4^{4-}$) had negligible effect on *E. coli*. Similar results were obtained by Hernández et al. [55] supporting the condition of presence of positive charge on photosensitizer to inactivate Gram negative bacteria. Providing more evidence in this area, Lopes et al. [44] show that the number of charge on photosensitizer and their distribution had clear effect on lipid oxidation and photoinactivation efficiency in *E. coli*. The order of total inactivation efficiency after 270 min of irradiation was Tetra-Py^+-Me and Di-Py^+-Me-PF_{adj} with higher efficiencies followed by Tri-Py^+-Me-PF and Di-Py^+-Me-PF_{opp}. Formation of lipid hydroperoxides and saturated fatty acids (photo-oxidation products) follow a different order of efficiency. Overall, they conclude Tetra-Py^+-Me, Di-Py^+-Me-PF_{adj} and Tri-Py^+-Me-PF were more efficient photosensitizers than Mono-Py^+-Me-PF and Di-Py^+-Me-PF_{opp}.

1.3.2 CONCENTRATION OF PHOTOSENSITIZER

The photocatalytic inactivation rate depends on the concentration of the photosensitizers used. It is expected that the inactivation rate increases with increase in photosensitizer concentration. This behavior is actually observed by many [56, 57, 53, 58, 59,]. Acher and et al. [56, 57] have studied the photoactivity of MB and RB in water treatment. They reported that microorganisms were more sensitive to singlet oxygen inactivation than organic pollutants as they succeeded in destroying sewage coliforms (1.3×10^9 coliforms in 100 ml) with mild photo-oxidation conditions (3.5 m g L^{-1} MB at 68 µ E m^{-2} s^{-1} of sunlight). Complete bacterial inactivation was obtained with 0.5 mg L^{-1} with 28 min of sunlight irradiation. The same group achieved complete destruction of algae at as less concentration as 0.25 mg L^{-1} of MB and 0.60 mg L^{-1} of RB. Gerba et al. [60] have shown that polio virus could be readily photoinactivated by MB (about 4 mg L^{-1} = 5 µM) and visible light in 5 minutes of illumination. They have observed that above 8-9 mg L^{-1} of MB concentration had little effect on the efficiency and that considerable inactivation occurs in dark above 20 mgL^{-1} of MB. Similar other studies have shown that small concentrations in the range of 5 to 20 µM are sufficient to achieve efficient disinfection [46, 61 and 62]. Manjón et al. [63] have studied the photoefficiency of RDP^{2+} and RDB^{2+} on porous silicone at a loading of 2 g m^{-2} to inactivate *E. coli* and *E. faecalis*. The films produced 2-3 log reduction in the microbial population with initial concentration 10^2 and 10^4 CFU ml^{-1}. This efficiency was unchanged regardless the type of bacteria and their initial concentration.

1.3.3 pH EFFECT

Acher et al. (1990) [64] have found that increasing the pH of the effluent of waste water treatment plant from 7.1 - 7.6 to 8.6 - 8.9 improved the photodisinfection efficiency with MB as a sensitizer. Schäfer et al. [40] also have observed in photosensitization with RB, a significant decrease in *E.coli* survival at higher pH than 7.0. They report that at pH indices below and above pH= 7.0, the survival of bacteria reduces by several logs. But, at pH=9.6 without the

sensitizer showed remarkable increase in photoinactivation (the alkaline pH is rendering toxicity) whereas no photo killing is observed at pH = 7.0 and 4.5 in the absence of sensitizer. On the other hand, Cooper and Goswami [65], on changing the pH from 7.0 to 10.0, did not observe any significant change in the photodisinfection rates by methylene blue. Another factor which influences the effect of pH is the pretreatment of Gram-negative bacteria with polycationic agents. Polycations like peptides bind tightly to the negatively charged cell membrane thereby exchanging divalent cations and changing the physical arrangement of lipopolysacchharide [66]. While using such polycations, the sensitizer is bound to the polycation which facilitates the latter's penetration into the cell membrane. Nitzan et al. [49] report that decreasing the pH from 8.5 to 6.5 increased the binding constant of deuteroporphyrin (DP) to polycationic agent polymyxin nonapeptide (PMNP) consequently increases the penetration of sensitizer into *E. coli* and *P. aeruginosa* cell membrane.

1.3.4 INCIDENT LIGHT-WAVELENGTH AND INTENSITY

Organic dyes, aromatic hyrdrocarbons, porphyrin and related compounds, phthalocyanine and transition metal complexes have strong absorbance in the UV-visible region with high quantum yield of singlet oxygen [8]. Dyes like MB, RB and eosin absorb in the visible region ($\lambda > 400$ nm). It is important to irradiate the system under study with light of appropriate wavelength so that the photosensitizer can transform itself to the longer lived triplet state and transfer its energy to molecular oxygen to generate ROS. Porphyrins and related compounds however absorb at several wavelengths in the UV-visible region with the Soret band in the blue region (360-400 nm) enabling to use the most penetrating blue light in water [8, 67 ,68] and the Q-bands in the red region (600-800 nm). This makes it possible to use visible light for photodisinfection as these materials can produce ROS in presence of light of wavelength ranging from 360- 800 nm. Schäfer et al. [40] have indicated the wavelength dependence of disinfection. They found a very small effect of the wavelengths below 435 nm (UVA) and above in the absence of sensitizer than in the presence of RB. It means that the photocatalytic activity is a combined action of light and the photosensitizer in the presence of oxygen and the

contribution of only UV component is negligible. Many researchers have used sunlight or solar simulated light sources for photodisinfection [47, 57, 51, 63, 64, 69 and 85]. Also, while using organic sensitizers, the intensity of the light is not a limiting factor for photocatalytic disinfection [57]. Acher et al. [64, 71] carried out disinfection experiments in all the four seasons of the year, the sunlight intensity varying from 700 to 2100 µE m^{-2}. In spite of the different sunlight intensities, they obtained good microbiological results in all the seasons. The same group [72] carried out photodisinfection under concentrated sunlight using heliostats to reflect sunlight. Concentrated sunlight (17×10^4 W m^{-2}) caused 5 logs decrease in the microrganisms survival in 3 seconds as compared with normal sunlight (850 W m^{-2}). Alouini and Jemli [19] have reported increase in percentage destruction of Ascaris eggs and Taenia with increasing light intensities from 800 to 5000 W m^{-2} in presence of TMPyP. Cooper and Goswami [65] have obtained complete destruction of *E.coli* in less than 10 min with 10 mg L^{-1} (31 µM) MB with average sunlight intensity of 715 - 775 W m^{-2}. Magaraggia et al. [70] employed Quartz halogen lamp with UV and IR filters with fluence rate of 1000 W m^{-2} in combination with cationic porphyrins. The photosensitizers caused reduction in survival of *S. aureus*, *E. coli* and fungal pathogen *Saprolegnia spp*. after just 20 min irradiation. Jemli et al. [51] carried out photodisinfection of fecal coliforms using TMP_yP, RB and MB under sunlight (400-700 nm) with fluence rate of 9.5×10^{-2} W m^{-2}. The best result was achieved by TMPyP at a concentration of 5 µM with 180 min of irradiation. Carvalho et al. [73] have used white light with intensity of 90 W m^{-2} and successfully photoinactivated fecal coliforms in 240 min respectively even at low concentration of 1 µM of cationic porphyrins (Tetra-Py^+-Me, TriP4-COOH). On the other hand, Orlandi et al. [74] irradiated cultures with 500 W halogen tungsten lamp (fluence rate 480 W m^{-2}) and found that cationic porphyrins caused considerable log reduction in both laboratory model microorganisms as well as waste water microflora in 75 min irradiation. Two fold increasing the irradiation time (i.e. doubling the light dose) resulted in further decrease of only 1 log unit of the monitored microflora. Rossi et al. [46] have used two different light sources with very low intensities; incandescent light bulb (white light with UV radiation cut off, 40 W m^{-2}) and multi-LED lamp at different fluence rates (24 W m^{-2} and 40 W m^{-2}). They observe that irradiation with incandescent light bulb in presence of pentaphyrin PCCox at a fluence of 40 W m^{-2}, caused almost

5 logs reduction in the *S. aureus* survival within 15 min of treatment and 6 logs after 60 min while with multi-LED lamp caused only 2 logs in 15 min and almost 5 logs in 60 min. This indicates that using a wider spectrum of the light energy (incandescent lamp) is more efficient than a small part of the spectrum (multi-LED lamp). Also, it is seen that almost halving the fluence rate (from 40 to 24 W m^{-2}) does not have a significant effect on the photodisinfection. These results imply that sunlight can be effectively used for water purification which emits in the visible range of electromagnetic spectrum.

1.3.5 WATER QUALITY

The presence of contaminants (organic or inorganic), turbidity and the pH of water all affects the rate of photocatalytic disinfection. The fact that the photodisinfection efficiency is greatly influenced due to suspended solids, dissolved oxygen (DO) and pH has been reported by many [75, 19, 56, 64, 51, 72]. In their pilot plant studies, Acher et al. [64] found that the photodisinfection efficiency fell sharply when the turbidity exceeded 25 NTU. Back in 1977, Acher and Rosenthal [56] had observed reduction in photodisinfection efficiency as the colloids in the effluent tend to adsorb the photosensitizer, protect the microorganism and reduce the light penetration into the waters. However, they succeeded in reducing the turbidity by flocculating the effluent with bentonite clay while aiming for the dye removal by the clay. Acher et al. [72] suggest that the turbidity of the entering effluent should be < 20 NTU for efficient photodisinfection process. Photodisinfection process proceeds in presence of the dissolved oxygen in the water to be treated. The minimum DO required for an efficient disinfection process is approx 2.0 mg O_2 L^{-1} as per the studies of Acher et al. [86]. They have also carried out photodisinfection with MB [72] with varied amount of DO (8 and 35 mg O_2 L^{-1}) and found that increasing the DO from 8 to 35 mg O_2 L^{-1} did not affect the results.

1.3.6 FREE AND FIXED PHOTOSENSITIZERS

While using photodynamic systems for water treatment, it is worthwhile to use photosensitizers on a solid support (heterogeneous phase). Employing the photosensitizer as a suspension or a homogenous solution poses a problem of removing the photosensitizers from the water. In their preliminary experiments in 1977, Acher and Rosenthal [56] made an effort to adsorb the dyes on solid ion exchange resin and natural clays but were unsuccessful in efficient photodisinfection as the dye-binded resins reacted with ions in the sewage and released colored compounds. They however chose to carry out photodisinfection using dissolved MB in water followed by removal of dye using bentonite. Similarly, Parakh et al. [62] are of the opinion that the removal of photosensitizers post illumination proves to be efficient in dye separation as well as adsorb other suspended pollutants. They have employed two water soluble Ru (II) pyridyl complexes (complex 1 and complex 2) as promising candidate for light inactivation of bacteria and used activated carbon and silica as adsorbents to remove the photsensitizers from water. These efforts are worth mentioning, although scientists are looking forward to adopt heterogeneous systems. Organic photosensitizers, owing to their wide range of functional groups available on them and their solubility in water or solvents are much feasible for immobilization on solid supports. The anchoring of photosensitizers onto solid supports can be carried out by adsorption [76], polymerization [77], electrostatic interaction [55] conjugation [78] and click reaction [79]. Many researchers have carried out the immobilization of photosensitizers on supports such as magnetic nanoparticles [52, 80], glass [77], resins [81], polymer [82] and silicones [83]. Savino and Angeli [81] immobilized MB, RB and Eosin covalently on polystyrene beads and also coated MB on granular activated carbon, silica gel and XAD-2 polystyrene resin. The adsorption of MB was carried out by suspending the supports in hot agitated water to which a solution of MB in water was added till it reached saturation. They found that MB covalently bonded to polystyrene beads was the best photosensitizers with 97.55% inactivation of *E. coli* in 30 min of exposure to electrofluorescent cold white light. Activated carbon was found to be the best support for the adsorption of the dye. Jimenez-Hernandez et al. [55] synthesized two cationic Ru (II)

phenanthroline complexes $RDP^{2+}$and RBN^{2+}, and one anionic RSD^{4-}. RDP^{2+} and RBN^{2+} were immobilized on porous silicone cylinders via adsorption in boiling solutions. RSD^{4-} was immobilized via electrostatic interaction on cationic nylon, cellulose and polyvinilydine difluoride. The sensitizer loading was in the order of 1-30 mg g^{-1} of the polymer in all the cases. The excited state lifetimes of RBN^{2+} was measured to be 0.3 μs and that for RSD^{4-} and RDP^{2+} were in the range of 2.4 to 4.2 μs. RDP^{2+}on silicone had highest O_2 quenching efficiency and singlet oxygen lifetime yielding 5 logs decrease in *E. coli* and *E. faecalis* count in one hour under a solar simulator lamp. RSD^{4-}/ cationic polymer systems produced no disinfection at all. Moreover, photosensitizer leaching was observed in Nylon and cellulose polymers. Yet in another attempt to achieve higher sensitizer loading and increase efficiency of RSD^{4-}, they incorporated it into cationic silicone [47]. Though the surface charge neutralization provides a promising strategy to enhance its photodisinfection properties, the efficient loading on to the polymer still remains a drawback for RSD^{4-}/ p-Sil. On the other hand, RDP^{2+} has a high loading on the anionic polymer, longer singlet oxygen lifetimes and better bacterial inactivation rates. The same research group in Spain have evaluated the disinfection efficiency using sunlight, 0.8 m^2 compound parabolic collectors and RDP^{2+} on siloxane films (2 mg m^{-2}) [75]. They employed two CPC prototypes with different configuration of photosensitizers, namely co-axial and fin type. With both the photoreactor designs and regardless the bacteria used, the average bacterial inactivation rate was calculated to be 2 x 10^4 and 2 x 10^6 CFU L^{-1} h^{-1}. They have also studied the effect of various factors influencing the performance of solar reactors using immobilized sensitizers on silicone [63] and the effect of dye reloading to water disinfection with solar reactors [83]. The reloading of the dye on the polymer is readily achieved and performs better than the original ones. They have successfully demonstrated that immobilized dyes can be a potential tool for drinking water disinfection using solar reactors. Loading of the dye on different polymers have been studied by other researchers as well [61, 82, 84, 85]. Bonnett et al. [82] have used chitosan membrane to support 2 different porphyrins (p-THPP and p-TAPP) and a Zn (II) phthalocyanine (ZnPcS), by adsorption, dissolution and casting and by covalent attachment. Photomicrobicidal studies on *E. coli* were conducted using static photoreactor and circulating water photoreactor systems. ZnPcS/chitosan membrane with a loading of 9 μg cm^{-2}

gave the best performance with complete disinfection in 90 min of illumination. These membranes were still 50% effective even after 9 months of storage in the dark. The drawback of brittle chitosan membrane was also overcome with reinforced membranes which were prepared by casting the polymer on nylon net support. Nakonechny et al. [84] studied the disinfection efficiencies of RB and MB immobilized on polystryrene membranes. 99% enclosure of the photosensitizer in the polymer was ensured and the films exhibited high antimicrobial properties against *S. aureus* and *E. coli*. An interesting alternative to prepare immobilized photosensitizers on optically transparent indium tin oxide (ITO) is reported by Funes et al. [77]. The films were formed by electrochemical polymerization of a metal free porphyrin TDAP and Pd-porphyrin (Pd-TDAP) complex on ITO, the two electrochemical active centers being the porphyrin core and the triphenylamine (TPA) moieties. Also, the TPA groups undergo radical cation dimerization to produce tetra phenyl benzidine (TPB). Experiments with these films in solution showed photoxidation of dimethyl anthracene and L-Tryptophan was observed indicating the presence of photodynamic action of the polymeric films. In vitro experiments with *E. coli* and *Candida albicans* caused a decrease of ≈ 3 logs and ≈ 2.5 logs respectively. Phthalocyanines of zinc and aluminum were covalently immobilized to nano amino propyl silica gel by Kuznetsova et al. [61]. In this paper, they have reported that the photodisinfection efficiencies of photosenstizers immobilized on nanoparticles are comparable to those in homogenous solutions due the enormous surface of nanocarriers. However, in such systems the separation of photosensitizers and increase in turbidity due to silica gel remain the drawbacks. Such limitations can be overcome by using magnetic nano particles as supports for the photosensitizers. Photosensitizers on nanomagnets are successfully prepared and their use and reuse in photodisinfection are described [52, 86, 87]. Carvalho et al. [52] have synthesized cationic nanomagnet-porphyrin hybrids and studied their photodisinfection capabilities against *E. coli*, *E. faecalis* and T4-like phage. They have reported good stability of these hybrids in water and effective antimicrobial activity. The hybrid materials possess good photostability as well, hence can be efficiently recovered and reused for photodisinfection. Recycling and reuse capability of such nanomagnet-porhyrin hybrids were also studied by Alves et al. [80]. Two nanomagnet-porphyrin hybrids differing in core particle (Fe_3O_4 and $CoFe_2O_4$)

were subjected to recycling and reuse along with reuse assays of a non-supported cationic porphyrin Tri-Py^{+}-Me-PF. Results showed that the hybrids maintained high bactericidal efficiencies as comparable to the non-supported porphyrin even after several photoinactivation cycles. The photostability and the efficiencies retained by these nanomagnet-prophyrin hybrids broaden new horizons of photoinactivation, in particular for water treatment.

1.4 ENVIRONMENTAL APPLICATIONS OF PHOTOSENSITIZATION

1.4.1 DISINFECTION OF WATER

Photosensitization efficiently produces ROS which causes toxic effects in bacteria leading to their irreversible death by oxidation of cell wall proteins and membrane disruption [88]. It is nearly a century since the discovery of singlet oxygen and its use for disinfection has been studied widely. However, its application for water disinfection gained attention only in the 1970's (26, 28-31-). Acher et al. have performed in their various experiments and plant studies, the disinfection of coliforms, enterococci [71], algae [69] and polio virus [64] from sewage water, secondary effluent from wastewater treatment plants and industrial wastewater. More recently, numerous studies have shown that photodynamic inactivation of water is a successful tool for obtaining microbe-free water. Table 1.2 lists the different microorganisms that can be photoinactivated by organic sensitizers. The concentration giving the best efficiency is indicated in the table although various different concentrations may have been studied in the corresponding cited references. The photodisinfection efficiencies of these materials and the type of irradiation used are also displayed.

Table 1.2

Type of Microorganism	Photosensitizer	Light dose/irradiance	Efficiency

Coliforms	MB (4 mg L^{-1}), RB (10 mg L^{-1}) [56]	Hanovia UV lamp 450 W and Sunlight at 1980 µE m^{-2}	Complete destruction
	Tetra-Py^{+}-Me (5µM), TriP-COOH (5µM), Tri-Py^{+}-Me-PF (5µM) [73]	White lamps of 18 W, 90 Wm^{-2}	83.5 % , 99%, 99.8 % reduction respectively
Gram negative bacteria			
E.coli	MB (5 mg L^{-1}) [57]	Sunlight , 2,030 µE m^{-2}	9 log reduction
	MB, RB, Eosin on PS beads [81]	Electrofluorescent cold white TLE 22 W	97.55 %, 92.2% and 81.6% respectively
	MB (10 mg L^{-1}), RB (10 mg L^{-1}) [65]	Sunlight, 650-900 Wm^{-2}	> 99% reduction
	Tetra-Py^{+}-Me,$TMAP^{4+}$, $TPPS_4^{4-}$, Hp (10µg ml^{-1}) [41]	Tungsten lamps 250 W, 60 Wm^{-2}	4 log, 5 log, no reduction and no reduction respectively.
	TMPyP, Tri- Py-Me-PyTD, [70]	Quartz halogen lamp with UV and IR filters, 1000 W m^{-2}	6-7 log reduction.
	p-THPP, p-TAPP, ZnPCS on chitosan (9µg cm^{-2}) [82]	Halogen lamp 500 W	> 2 log reduction
	RDP^{2+}, RDB^{2+} immobilized on porous poly(dimethyl siloxane) (2gm^{-2})[63]	Solar simulated reactor in lab and sunlight for solar reactor 0.6–0.8 MJ m^{-2} L^{-1}	Approx.3 log decrease with both film
	TDAP and its Pd complex (PdP-film) on optically transparent indium tin oxide (ITO) electrodes[77].	150 W lamp, 900 W m^{-2}	3 log reduction
	TMPyP, MB (0.73 and 3.65 µmol L^{-1})[48]	High-pressure arc xenon lamp 300 W, 28 W m^{-2}	TMPyP and MB caused reduction by several logs
	Tri-Py^{+}-Me-PF (5µM) [89]	13 white light lamps, each of 18 W and	6 log reduction

		fluence rate of 40 W m^{-2}	
	Tri-Py-Me-PF, Tri-Py^{+}-Me-PF, Tri-Ph-PF) on magnetic nanoparticles.[52]	White light of 18 W, 40 W m^{-2}	Cationic hybrids showed 4-5 log reduction
	DBTP-COOH, ANT on silica (2.5g L^{-1})[15]	125 W lamp	7 log reduction.
	$ZnPc(Sph)_4Clm_8$ on silicagel D/10µM-ZnChol7), $Al(OH)Pc(Sph)_4Clm_8$ on silica gel (D/5µM-$AlClm_7$, D/5µM-$AlChol_7$, D/5µM-$AlTaur_7$) [61]	Halogen lamp, 75 W m^{-2}	PDI of positively charged D/5µM-$AlChol_7$ (95%) was markedly higher than negatively charged D/5µM-$AlTaur_7$(50%).
	Complex 1 and complex 2 (10µM) [62]	LED array, 950 W m^{-2}	7 log decrease.
	DBPyP (5 µM)[126]	Artificial white light, 480 W m^{-2}	6 log reduction.
	PbTepyPc [127]	Quartz lamp 1.0 x 10^{19} photons cm^{-2} s^{-1}	10 log reduction.
V. anguillarum	Tetra-Py^{+}-Me,$TMAP^{4+}$, $TPPS_4^{4-}$, Hp (10µg ml^{-1}) [50]	Tungsten lamps 250 W, 60 Wm^{-2}	5, 3, 0.5 and 0 log reduction respectively.
	Tri-Py^{+}-Me-PF (5µM) [43]	13 white light lamps, each of 18 W and fluence rate of 40 W m^{-2}	5-8 log reduction
V. fischeri	Tri-Py^{+}-Me-PF (5µM) [89]	13 white light lamps, each of 18 W and fluence rate of 40 W m^{-2}	5.5 log reduction.
	Tri-Py^{+}-Me-PF on magnetic nanoparticles Fe_2O_3 and $CoFe_2O_4$ at (5µM of nonsupported and 20µM of nanohybrids)[80]	White light, 40 W m^{-2}.	
Vibrio	Tri-Py^{+}-Me-PF (5µM) [89]	13 white light lamps,	6-8 log reductions in

parahaemolyticus, Aeromonas salmonicida, Photobacterium damselae subsp. damselae, Photobacterium damselae subsp. piscicida, Pseudomonas sp		each of 18 W and fluence rate of 40 W m^{-2}	all bacteria.
Gram positive bacteria			
S. aureus	TMPyP, Tri- Py-Me-PyTD [70]	Quartz halogen lamp with UV and IR filters, 1000 W m^{-2}	5 log and 7 log reduction respectively.
	Tri-Py^{+}-Me-PF (5µM) [43]	13 white light lamps, each of 18 W and fluence rate of 40 W m^{-2}	7-8 log reduction.
	PCCox (0.05, 0.5 and 5 µM) [46]	Multi-LED monochromatic lamp 40 W m^{-2}	99.997 % reduction.
E. faecalis	RDP^{2+}, RDB^{2+} immobilized on porous poly(dimethyl siloxane) (2gm^{-2})[63]	Solar simulated reactor in lab and sunlight for solar reactor 0.6–0.8 MJ m^{-2} L^{-1}	2-3 log reduction.
	Tri-Py-Me-PF, Tri-Py^{+}-Me-PF, Tri-Ph-PF) on magnetic nanoparticles.[52]	White light of 18 W, 40 W m^{-2}	5 log reduction with all the nanohybrids.
	RDB^{2+}/pSil, RDP^{2+}/pSil, RDP^{2+}/pSil-a (aged for 250 h) and RDP^{2+}/pSil-r (reloaded with PS after ageing) [83]	Xe lamp, 150 W, 5 MJ m^{-2}	2-3 log reduction with all materials.
	DMPyP (10µM), DBPyP (5 µM) [74]	Artificial white light, 480 W m^{-2}	6 log reduction

E. seriolicida	Tetra-Py^{+}-Me,$TMAP^{4+}$, $TPPS_4^{4-}$, Hp (10µg ml^{-1}) [50]	Tungsten lamps 250 W, 60 Wm^{-2}	5, 7, 4, 6 log respectively.
D. radiodurans	RB (1-5 ppm) [40]	Xenon lamp, 1000 W, 100 J cm^{-2}	5 log reduction.
E. hirae	TMPyP, MB (0.73 and 3.65 µmol L^{-1}) [48]	High-pressure arc xenon lamp 300 W, 28 W m^{-2}	8-9 log reduction.
Fungi			
Saprolegnia spp.	TMPyP, Tri- Py-Me-PyTD (10 µM) [70]	Quartz halogen lamp with UV and IR filters, 1000 W m^{-2}	2 log and 6 log reduction respectively
C. albicans	TDAP and its Pd complex (PdP-film) on optically transparent indium tin oxide (ITO) electrodes [77].	150 W lamp, 900 W m^{-2}	2.5 log reduction.
	$ZnPPc^{4+}$(10 µM) [90]	150 W lamp, 300 W m^{-2}	5 log reduction.
Viruses			
Poliovirus	MB (13 µM)[60]	Artificial light, 20 W m^{-2}	2.5 log reduction.
T-4 like phage	Tri-Py-Me-PF, Tri-Py^{+}-Me-PF, Tri-Ph-PF) on magnetic nanoparticles.[52]	White light of 18 W, 40 W m^{-2}	Cationic hybrids cause 6.9 log reduction.
	Tetra- Py^{+}-Me, Tri-Py^{+}-Me-PF (5.0 µM) [91]	White PAR light (40 W m^{-2}), sunlight (600 W m^{-2})	Both photosensitizers were able inactivate T4-like phage to the limit of detection (> 99.9999%).
Enterovirus 71 (EV71)	MB (0.1 mM) [92]	LED light source 200 J cm^{-2} (2000 W cm^{-2})	>6.5 log reduction

1.4.2 DECONTAMINATION OF WATER

The solar detoxification of a stable pesticide, bromacil with MB was studied by Acher et al. [72]. Bromacil was readily decomposed when the ratio of bromacil: O_2 was > 1. Gryglik et al. [92] applied photosensitized oxidation to the degradation of 2-chlorophenol (causes considerable damage to aquatic bodies and human health). The oxidation was carried out using RB in solution and immobilized on silica gel and satisfactory results were obtained so as to use this method for further investigations in purification of water. Phenol and its chlorinated derivatives were degraded using different phthalocyanines (AlPHC, ZnPHC, SiPHC and Metalfree PHC) [11, 93] in presence of light. Among the photosensitizers used, AlPHC was the most active and metal free PHC was virtually inactive. Also, sulphonation of the benzene rings of these phthalocyanines render the photosensitizers water soluble [93]. Three zinc phthalocyanines immobilized on mesoporous aluminosilicate have been successfully employed in the degradation of pesticides fenamiphos and pentachlorophenol by Silva et al. [94]. They report 98% conversion of fenamiphos after 300 min of irradiation into fenamiphos-sulfoxide and fenamiphos-sulfone. The main photodegradation product of pentachlorophenol after 300 min of irradiation was 2, 3, 5, 6-tetrachloro-hydroquinone. Recently, TiO_2 catalysts photosensitized with porphyrins are investigated for phototreatment of water [95-97]. Wang et al. [95] report the photodegradation of 4-nitrophenol using functionalized porphyrin-TiO_2 catalyst. They synthesized two kinds of meso substituted porphyrins, $H_2Pp(a)$ and $H_2Pp(b)$ and their corresponding copper(II) complexes Cu $H_2Pp(a)$, Cu $H_2Pp(b)$. TiO_2 based photocatalysts were prepared by dissolving these photosensitizers at different concentrations in $CHCl_3$ and adding to these 1 g of ground TiO_2, stirred for 8 h and solvent was removed under vacuum. The most efficient photodegradation was obtained for an optimal amount of porphyrin equal to 18 μmol per 1 g of TiO_2. The photo efficiencies of the porphyrins impregnated with an optimal amount of 18 μmol per 1 g of TiO_2 decreased in the order TiO_2-CuH_2Pp (b) > TiO_2-$CuH_2Pp(a)$ > TiO_2-H2Pp(b) > TiO_2-$H_2Pp(a)$. Li et al. [84] have investigated the photodegradation of acid chrome blue K (ACBK) using TiO_2 sensitized porphyrins H_2TPPC or TNO_2PP. Their results indicated that

there was remarkable effect of H_2TPPC-TiO_2 on degradation of ACBK. Upto 94% of decolorization was observed in 15 min under incandescent lamp with initial ACBK concentration of 10 mg L^{-1}. Murphy et al. [97] have also prepared a composite photocatalyst to photodegrade the pharmaceutical Famotidine. They absorbed H_2TPPC on TiO_2 by two methods. In method A, H_2TPPC was absorbed onto TiO_2 in methanol at room temperature and in method B, H_2TPPC was absorbed on TiO_2 in dimethylformamide (DMF) at reflux. Photodegradation experiments were carried out both under visible light and solar light irradiation. Famotidine was found to degrade into series of intermediate products with S-oxide of Famotidine as the major product but complete mineralization of the drug was not achieved. Also, they have observed that under halogen lamp, TCPP-TiO_2 A was more efficient than TCPP-TiO_2 B. TCPP alone showed minimal photodegradation and also TiO_2 alone displayed poor degradtion. Hence, the result was due to the combined action of composite photocatalyst and not the individual components.

1.4.3 OTHER ENVIRONMENTAL APPICATIONS

The use of photodynamic process along with decontamination and inactivation in water was also employed to treat infections in fisheries due to invasion by *Saprolegnia spp*. by in vivo studies [70]. Treatment of rainbow trout (Oncorhynchusmykiss) with submicromolar doses of porphyrin causes 10-13% of decrease in the infection on fishes and complete remission of infection was induced within 1 week. In a similar study aimed at destruction of fish pathogens, cationic porphyrin was utilized to test against nine pathogenic bacteria found in aquaculture systems [43]. 7-8 logs reduction in the bacterial isolates was observed after 60-70 minutes of irradiation. In another interesting scope of application RB, MB, safrannin and toluidine blue were employed to treat corrosion producing biofilms and planktonic bacteria on oil and gas pipelines [98]. Desulfovibrio vulgaris and Desulfovibrio desulfuricans are well known for aggravating corrosion on steel and other alloys. The studies show that photoinactivation using photosensitizers gave better performance than the commonly used biocide, benzalkonium chloride.

Enterovirus (EV71) spread on solid surface was inactivated by MB-mediated photodynamic action by Wong et al. [91]. No detectable virus was noted when surface-bound EV71 was treated with MB at a light dose of 50 J cm^{-2} after 3 days. MB-PDI also prevented EV71 transmission to mice. 1 day-old mice that had been in contact with high concentration of EV71 ($3x10^7$ pfu) for 4 h exhibited serum conversion, weight loss and death whereas no infection was observed in mice exposed to same dose of virus after MB-PDT (0.05 mM, 25 J cm^{-2}). Ismail et al. [99] employed MB-light-activated antimicrobial coatings for disinfecting hospital surfaces. MB with or without gold nanoparticles was coated on silicone polymers. The coated polymers were inoculated with bacterial suspensions of *S. aureus* (MRSA) and irradiated with light intensity of 2,305 lux. After 24 hours illumination, both the MB coatings with and without gold nanoparticles achieved 99.99 and 99.33 % reduction of bacterial population.

Luksiene et al. [100] studied the possibility to control microbial contamination of strawberries by Na-Chl. *Listeria monocytogenes* contamination was reduced by 98% after 30 min of illumination with visible light at 120 W m^{-2}. Naturally occuring yeasts/microfungi ans mesophiles were also inhibited by 86 and 97 % thereby increasing its shelf life by 2 days with no negative impact on antioxidant activity, and phenols anthocyanins or colour formation.

1.5 LIMITATIONS

1.5.1 RECOVERY AND REUSE

One of the drawbacks of photosensitized water treatment that is often discussed is the recovery of the photosensitizer and its reuse for subsequent treatments. As discussed earlier, sedimentation, coagulation and filtration processes are time consuming and expensive. It is important to develop methods for easy recovery of photosensitizer. The immobilization of photosensitizers on solid supports like polymers, ITO and nanocarriers seems promising alternative. However, there are reports on ways to overcome these problems and some have also treated water on immobilized systems on CPC solar reactors [75].

Immobilized systems with maximum photosensitizers loading, improved utilization of available photons and enhanced activity comparable to free photosensitzers are desirable. Nanocarriers are also advantageous in this regard as the problem of limited light penetration is reduced to some extent due to the availability of large surfaces on the nano particles [52]. Another factor limiting the reuse of photosensitizers is their degradation due to prolonged exposure to light. MB, RB and some porphyrins have been reported to undergo bleaching thereby reducing their photoinactivation efficiencies [52, 53]. Photosensitizers with excellent light stability and capable of absorbin visible light should be employed.

1.5.2 REISITANCE OF GRAM NEGATIVE BACTERIA

While TiO_2 proves to be efficient in destroying practically both Gram-positive and Gram-negative bacteria, organic photosensitizers without positive charge have failed to destroy Gram-negative bacteria [50, 55]. It is essential to contain a positive moiety on the photosensitizer or the support carrying the sensitizer in order to destabilize the Gram negative bacteria wall (as discussed in 1.3.1)

1.5.3 EFFECT OF PHOTOTREATMENT ON NON-PATHOGENIC ORGANISMS

At photochemically active doses, the photosensitizers are generally non-toxic to the large majority of biological system. However, it is necessary to evaluate the process for toxic effects on non-pathogenic agents. Fabris et al. [101] have studied the effect of porphyrin doses in the rane of 0.1-10 μM to protozoan Ciliophora (*Colpoda inflate and Tetrahymena thermophili*) and the Crustacea Branchiopoda (*Artemia franciscana and Daphnia magna*). *A. franciscana* was very resistant to phototreatment whereas *T. thermophilia* was resistant to doses upto 3 μM. On the other hand, *C. inflata* and *D. magna* were sensitive to the action of porphyrin. This poses as a potential drawback as *D. magna* were senstitive to the action of porphyrin. This poses as a potential drawback as *D. magna* is often selected as a reference standard for assessing the environmental safety.

Highlighting similar concerns, Arrojado et al. [43] have also suggested a careful evaluation of environmental impacts of PDT in particular to aquaculture waters. Renovation of the water at each tidal cycle helps to return the non-pathogenic bacteria. Since PDT is not selective for pathogenic bacteria, the non-pathogenic bacteria responsible for turnover of organic matter are also affected. Moreover, dissolved and particulate matter in water also competes for ROS and reduces the efficiency of phototreatment. Therefore, while constructing molecules for photoinactivation purposes, one should also evaluate the toxicity effects to non-pathogenic microorganisms and other larger living bodies in water.

1.6 EXPANDED PORPHYRINS

Porphyrins and related compounds are the most chosen and most widely used photosensitizer for PDT. However, in recent years expanded porphyrins are gaining attention due to their different photophysical, electronic, co-ordination properties and reactivities which are evidently superior to porphyrin [102-104]. Expanded porphyrins are compounds containing at least one pyrrolic ring more than porphyrins [105]. Among the various expanded porphyrins; pentaphyrins, sapphyrin and smaragdyrin containing 5 pyrrolic units have been studied extensively during the last few years [106]. These molecules are interesting due to their potential application in PDT [103, 108], sensing agents [106,107], as MRI agents, coordination of large metal ions [104] and disinfection [46]. Expanded porphyrins have an increased degree of conjugation, which shifts their absorption spectra in the red region (Bathochromic shift) making them feasible to use light of higher wavelength which is more penetrating in biological systems [103, 113]. Also, it has been shown that these molecules have short half-life in biological systems which make them easy to get rid of after a specific PDT [7].

The 22π electron macrocycles having 5 meso carbons are of the interest in this project. Few reports of synthesis of such molecules are reported [103, 104, 108 and 110] and fewer are investigated for their photosensitizing ability [103, 108 and 114]. The first such pentaphyrin was synthesized by Rexhausen and

Gossauer [110], who have performed the condensation of a tripyrrane dialdehyde with dypyrromethane in presence of hyrdrobromic acid in acetic acid followed by oxidation with chloranil to give a fully β-substituted pentaphyrin. Similarly, Král et al. [108] syntheisized a non-ionic water soluble pentaphyrin by introducing 4 hyrdroxyl groups at the periphery of the molecule. They found that the synthesized pentaphyrin caused toxicity in human T lymphoma cells at a concentration in the range of μM which is in comparison with other water soluble, pophyrin-type systems. Comuzzi et al. [103] successfully synthesized 2 macroccyclic species, one a non-aromatic isopentaphyrin with 24π electrons and an aromatic pentaphyrin with 22π electrons. The condensation of tripyrrane dicarboxylic acid with 1,9-diformyl-5-phenyldipyrromethane in presence of trifluoroacetic acid resulted in the 24π electron isopentaphyrin, which on oxidation with DDQ resulted in the 22π electron aromatic macrocycle pentaphyrin. The biological activities of the two pentaphyrins were evaluated on four different human cell lines and they observed that the aromatic pentaphyrin had a better uptake by the cells and also displayed better photodynamic effect. In another study, an isopentaphyrin namely 20-[[4'-(Trimethylsilyl) ethoxycarbonyl]phenyl-2,13-dimethyl-3,12-diethyl-[24]iso-pentaphyrin (PCRed) was synthesized and consequently metallated by Lu(III) [114]. On assessment of the bioactivity of the metallated pentaphyrin, it was found that metallated pentaphyrin displayed significantly higher cellular uptake and phototoxicity as compared to the non-metallated macrocycle. Most of the planar, aromatic and non-fused pentaphyrins are *β*-alkylated and non-meso substituted [103, 104, 108 and 110] derived from *β*-substituted dipyrromethanes and tripyrranes[111,112 and 115]. *meso*-aryl-substituted pentaphyrins are forced to take a *N*-fused conformation with one or more inverted pyrroles due to severe steric congestion [109,116]. By reducing one meso substitution on the pentaphyrinic macrocycle, Yoneda et al. [109] have successfully synthesized a stable tetrakis (pentafluorophenyl) pentaphyrin by the condensation of a dipyrromethane dialdehyde and a tripyrrane in presence of *p*-toluene sulfonic acid and subsequent DDQ oxidation. In this project we have tried to synthesize a pentaphyrinic macrocycle with 5 meso carbons. The aim was to synthesize pentaphyrinic macrocycle with pyridine substitution at *meso positions*. The pyridine functionality undergoes quaternization which can give rise to positively charged photosensitizers. The

positive charge is a prerequisite for photosensitizers to effectively disinfect both Gram-positive and Gram-negative bacteria.

2 MATERIALS AND METHODS

2.1 CHEMICALS AND REAGENTS

All the chemicals and the reagents were purchased from commercial sources and used as received.

5-(4-carboxy-phenyl)-10,15,20- triphenyl-21H, 23H-porphyrin (CAS 95051-10-8) was purchased from Frontier Scientific Inc., Logan, UT, USA.

Nanomag®-D–spio (SPION-NH_2) were obtained from Micromod Partikeltechnologie GmbH. The SPION nanoparticles were in the form of aqueous suspension with NH_2 surface, 20 nm in size. The solid content was 5 mg/L with $8x10^{14}$ particles per ml and $1.6x10^{14}$ particles per mg. Poly vinyl chloride (PVC) (high molecular weight) was purchased from Sigma-Aldrich.

12-azido-4,7,10-trioxadodecanoic acid NHS ester (≥98%)was purchased from Cyanagen.

Di n-octyl adipate was purchased from Chem Service inc. **di n-butyl adipate, bis-(2-ethyl hexyl) adipate** and **di capryl adipate** was purchased from Sigma-Aldrich.

All the other reagents and solvents used were purchased from Sigma-Aldrich and were of the highest purity commercially available.

2.2 CHROMATOGRAPHIC TECHNIQUES

2.2.1 THIN LAYER CHROMATOGRAPHY (TLC)

TLC was used for monitoring all the reaction pathways. Both silica gel and aluminium oxide TLC sheets were used depending upon the basicity required. **Silica gel** on Al foils/PET sheets and **Aluminium oxide** on Al foils were purchased from Sigma-Aldrich. The sample spots were detected by one of the following:

- UV-absorption

- Staining with a solution of potassium permanganate.
- Staining with a solution of ammonium molybdate or ninhydrin followed by charring at 150°C.
- Only charring at 150°C.

2.2.2 COLUMN CHROMATOGRAPHY

Silica gel for column chromatography was purchased from Merck. The type used was Silica gel 60 (particle size 0.015-0.040 mm).
Aluminium oxide (0.05-0.15 mm, pH = 10±0.5) was purchased from Sigma-Aldrich.

2.3 SPECTROSCOPIC TECHNIQUES

2.3.1 UV-VISIBLE MEASUREMENTS

UV-visible measurements were carried out on Varian Cary 50 spectrophotometer. Spectra were measured from 200 to 1000 nm. The absorbances of samples were either measured by placing them in quartz cell (path length 1 cm, 3.5 ml capacity) or using a Fibre optic dip probe into the sample solution. Concentration calculations are carried out following the Beer-Lambert's law using the formula in eq.2.1.

$$A = \varepsilon . c . l \qquad (2.1)$$

A= Absorbance
ε = molar absorption co-efficient (L mol^{-1} cm^{-1})
c = concentration (mol L^{-1})
l = path length of the sample/cuvette (cm)

Absorbances of bacterial cultures were measured with Jasco SSE-343 spectrophotometer at 600 nm.

2.3.2 NMR SPECTROSCOPY

^{1}H NMR spectra were acquired with a Bruker 200 NMR spectrometer (200 MHz). Chemical shifts are reported in ppm with tetramethylsilane (TMS) as an internal reference. The abbreviations used are: s=singlet, d=doublet, dd=doublet of doublets, m=multiplet, and br=broad. 1H-HRMAS-NMR experiments were performed on a Bruker DMX 500 (11.7 T) equipped with an HRMAS ^{1}H–^{13}C indirect detection probe with gradients on the magic angle. MAS experiments were performed at spinning rates up to 8 kHz (15 kHz maximum MAS rotation available) using a 50 mL zirconia rotor. In general, lyophilised nanoconjugate powder (1–2 mg) was dispersed in deuterated DMSO (60 mL). Proton spectra were obtained by using 1024 scans for each experiment. The sample temperature was kept constant at RT.

2.3.3 MASS SPECTROSCOPY

ESI-mass spectra were carried out on a Bruker Esquire 4000 ion-trap mass spectrometer equipped with a pneumatically assisted electrospray ionization source, operating in positive mode and negative mode at ± 110.7 volt of capillary exit.

2.4 PHOTOINACTIVATION

2.4.1 SET UP

The set up used for illumination experiments is as shown in Figure 2.1 and schematically representated in Figure 2.2 consists of the following:

- Magnetic stirrer C-MAG MS7 (Ika);
- Stirring bar (5 x 22 mm);
- Light source (see section 2.4.2);
- Stand with clamp for supporting the light source

- Multi-well plate (containing the sample to be illuminated)with 48 wells of diameter 1 cm and 1.5 ml capacity;
- Power supply U8002A (Agilent).
- Radiometer (DeltaOhm HD 2302.0 connected to an LP 471 RAD probe)

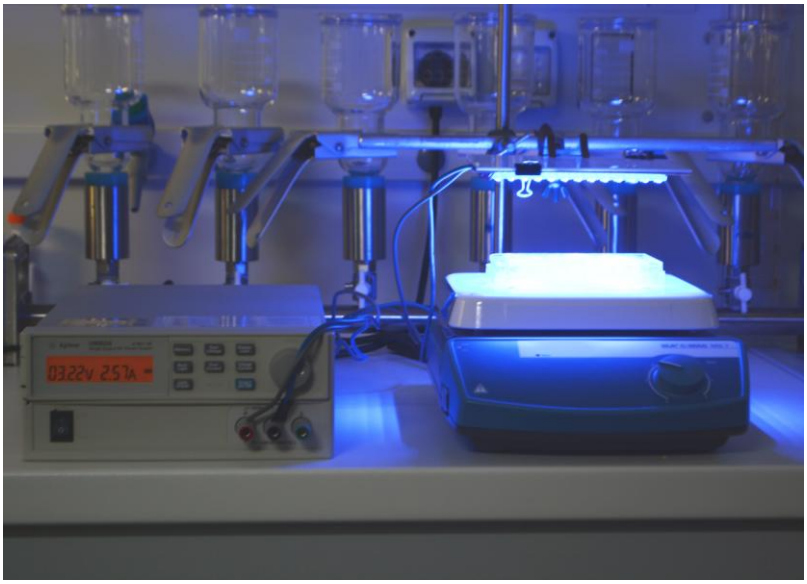

Figure 2.1 Setup of the photoxidation experiments

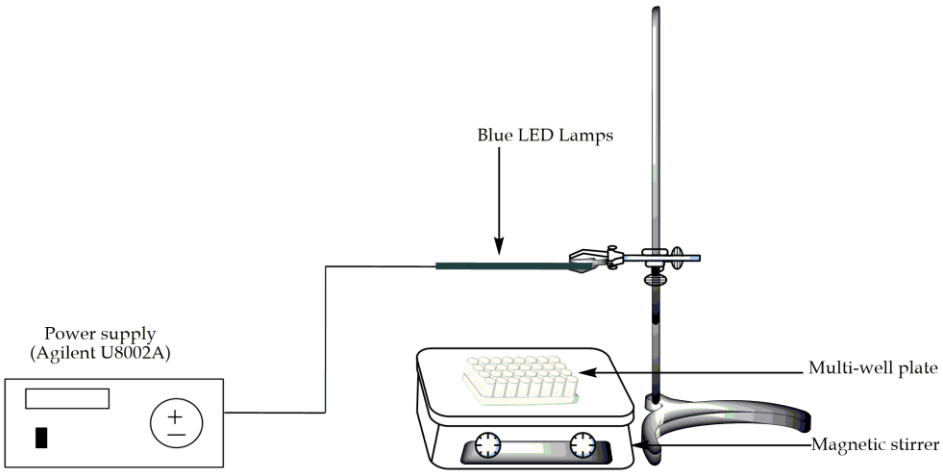

Figure 2.2 Schematic representation of Photodisinfection experiment

2.4.2 LIGHT SOURCE

In literature one can find different type of light sources used for photodisinfection experiments (ref chapter 1.3.4 and Table 1.2). In this project only one type of light source was used for all the illumination experiments in order to have identical conditions for all the experiments. The lamp used is a homemade multi-LED (130 blue LEDs TLWB7600 Vishay) with emission maximum at 470 nm, which is connected to a power supply which regulates the fluence rate of 24 to 50 W/m^2 (measured by Delta OHM HD 2302.0 Light meter).

2.4.3 ILLUMINATION CONDITIONS

As the setup already shown in Figure 2.1 depicts, all the illumination experiments were carried out at similar illumination conditions which contained the following:

- Bacterial culture with the photosensitizer;
- Bacterial without the photosensitizer;
- Dark controls;
- Constant distance between light source and the multi-well plate.

The samples were exposed to light for a fixed time period ranging from 15 minutes to 180 minutes depending upon the photoefficiency of sensitizer. At regular intervals aliquots were drawn from each well for analysis (read in detail in sec **2.5**)

2.5 BACTERIOLOGY

2.5.1 THE MICROORGANISMS

All the different water bodies are contained with several kinds of bacteria derived from either human or animal metabolism. In this project however, the target microorganism was grown in-vitro using monocultures. The monocultures used for the evalution of photodisinfection efficiency contained the following bacterial strains:

- *Staphylococcus aureus* ATCC 6538 (Leibniz Institut DSMZ –Deutsche Sammlung von Mikroorganismen und Zellkulturen GmbH)
- *Escherechia coli* DSM 11250 (Leibniz Institut DSMZ –Deutsche Sammlung von Mikroorganismen und Zellkulturen GmbH)
- *Streptococcus mutans* Clarke 1924 DSM 20523 (Leibniz Institut DSMZ – Deutsche Sammlung von Mikroorganismen und Zellkulturen GmbH)

Nutrient Broth N° 2 (Sigma-Aldrich) was used to grow *S. aureus* and *E. coli*. *S.mutans* was grown in Tryptic Soy Broth (Sigma-Aldrich).
The bacterial strains are cultured in 10 ml of Broth and allowed to grow to the logarithmic phase at 37°C. The culture is then centrifuged at approximately 3,200 rpm to obtain a pellet of the bacteria culture. The excess medium is removed using a sterile Pasteur pipette connected to a vacuum pump. The pellet is resuspended in 0.01 M sterile phosphate-buffered saline (Sigma-Aldrich) to arrive at a bacterial concentration of 10^8 CFU/ml. This concentration was achieved by reaching an optical density of 0.1 at 600 nm for *S. aureus* and *E. coli* and 0.4 for *S. mutans*.

2.5.2 CULTURE MEDIA

The agar media used for microbiological analyses are available as powders containing a mixture of ingredients which have to be resuspended in a specific amount of water and subsequently boil and sterilize.
The following media were used in this project for microbiological analyses:

- *E. coli* direct MUG agar (Fluka) suitable for coliforms and selective for *E. coli,* which are recognized by colonies those are UV-fluorescent.
- Mitis Salivarius Agar (Fluka) suitable for streptococci which is made selective for *S. mutans* by adding 100 units/L of bacitracin (Sigma Aldrich) to the medium.
- Mannitol Salt Phenol Red Agar (Fluka), containing mannitol, sodium chloride 75% w/v and the pH indicator phenol red selective for *S. aureus*.

The desired amount of medium is weighed and dissolved in distilled water. The mixture is allowed to boil along with continuous stirring and autoclaved for 20 minutes at 120°C. When the temperature of the mixture reaches 60-80°C, 7 ml of medium are poured into Petri dishes and once they are solidified stored in sterile packets at 4°C.

When the sample is subjected to microbial analysis, the culture is plated on the selective agar medium and incubated in a thermostat for sufficient period of time depending on the type of microorganism. After the incubation period, the bacterial colonies formed are counted and back calculated to a concentration of bacteria present in the sample expressed as the ratio between CFU (*Colony Forming Units*) and volume of the sample used.
The bacteria are identified through precise morphological characteristics, which microorganisms assume after contact with the medium in which they are grown:

- Coliforms form round white colored colonies on the agar ECD MUG. This medium helps identify *E. coli* via fluorescence stimulated by UV at the wavelength which can hydrolyze the MUG (4-methylumbelliferyl-β-D-glucuronide) present in the medium to the glucuronide and 4-methylumbelliferone.
- *S. aureus* form yellow coloured colonies with a halo around of the same colour, because the micro-organism is able to acidify the medium and then turning the pink color of the medium to yellow.
- *S. mutans* form white to pale yellow colonies with granular surface.

2.5.3 DETERMINATION OF BACTERIAL COUNT

During the photo-illumination experiments, aliquots of the microbiological sample were taken out and the concentration of bacteria at regular time intervals was determined according to the agar-germi method 9215 B proposed by the Standard methods for the Examination of Water and Wastewater [130]. The analyses were conducted on the monocultures of the bacterial species mentioned above.

The disinfection and cleaning of the environment and the apparatus used proved to be very important for the success of the measurement. The procedure followed was conducted under a microbiological hood, and hence in a sterile environment. All the equipment and reagents used were previously sterilized at 120 deg for 20 min.

- Sterile nitrocellulose membranes with porosity 0.45 μm and diameter 4.7 cm (Millipore);
- Petri dishes (diameter 5 cm);
- Selective medium;
- Wood's lamp;
- Kovac's reagent;
- Lighted Magnifying lamp
- Sterile Pyrex flask of 1 l;
- Graduated cylinder;
- Distilled water;
- Thermostat;
- Micropipette with adjustable volume;
- Pipette controller;
- Sterile pipette tips.

The steps in the procedure are as follows:

1. The sample under analysis was serially diluted (10^{-1}, 10^{-2}, 10^{-3}, 10^{-4}, 10^{-5}, 10^{-6}) with 0.01 M sterile phosphate buffer saline (PBS). This enables to count an optimal number of colonies on the agar plate typically between 10 to 100 as the concentration of bacteria in monocultures is very high (10^{-5} to 10^{-8}).

2. 100 µl of the diluted sample were aliquoted in small doses on the respective agar medium in Petri: the Petri dish is then agitated horizontally to distribute the sample over the entire surface available. The plated Petri was then placed in the thermostat for a time period suitable for a particular type of bacteria.
3. After the completion of incubation time, the Petri was removed to count the colonies grown on the agar medium.
4. The bacterial concentration in the original sample was calculated using the equation 2.2.

$$\frac{CFU}{ml} = \frac{N\ x\ D}{V} \qquad (2.2)$$

Where
CFU = colony forming units
N = number of colonies counted
D = dilution factor
V = volume of the aliquot (in ml)
The bacterial count is generally reported in CFU (*Colony Formation Unit*) per ml of the sample.

3 SYNTHESIS OF MAGNETIC PORPHYRIN-NANO CONJUGATE AND ITS PHOTOEFFICIENCY

3.1 INTRODUCTION

Porphyrin based photosensitizers are well known for their photodisinfection properties. TPP was attached to SPION nanoparticles via Cu-catalysed click reaction. The aim of immobilization of TPP is to enable the photosensitizer to be recovered and reused after photoillumination.

3.2 EXPERIMENTAL

3.2.1 SYNTHESIS OF PORPHYRIN-PEG ALKYNE

3.2.1.1 Synthesis of compound 2

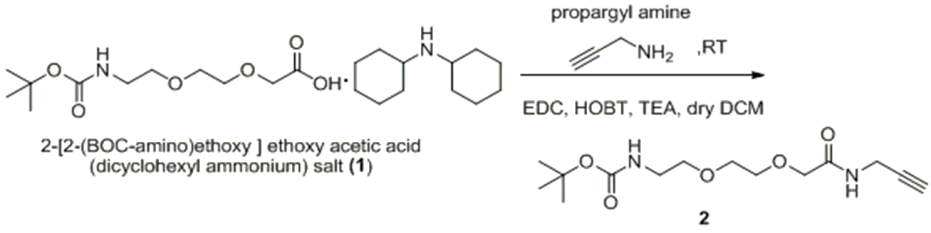

Scheme 3.1 synthesis of BOC-protected PEG alkyne (**2**)

Table 3.1 Reactants and reagents used for synthesis of **2**

Material	Molecular weight	Weight taken (mg)	Moles (μmol)
1	444.61	100	224.29
EDC	191.70	52	270
HOBT·H_2O	153	41.3	270

TEA	101.19 (d=0.727)	45.45 (62.5µl)	450
Propargyl amine	55.08 (d=0.86)	14.87 (17µl)	270

Compound **1** was taken in a round bottom flask to which 10-15 ml of dry DCM was added. EDC, HOBT and TEA were added to the solution and stirred for 2-3 minutes. Propargyl amine was added to the mixture and stirred (**Scheme 3.1**). In order to render the mixture homogenous, the total volume of DCM required was ~ 40 ml. The reaction mixture was stirred overnight at room temperature. The reaction was monitored using TLC (5% MeOH in DCM). After the completion of the reaction, the reaction mixture was evaporated to remove solvent to obtain colorless, viscous liquid. The evaporated contents were purified directly by column chromatography (3% methanol in DCM) without any prior separation. 57.0 mg (yield 89.23%) of the pure product. ^{1}H NMR spectrum of the product was recorded. NMR (200 MHz, $CDCl_3$, 25°C): δ= 1.37 (s, 9 H), 2.21 (t, 2 H), 3.29 (t, 2 H), 3.48-3.67 (m, 7 H), 3.99 (s, 2H), 4.0-4.07 (m, 2 H), 5.00 (br s, 1 H), 7.20 (br s, 1 H)

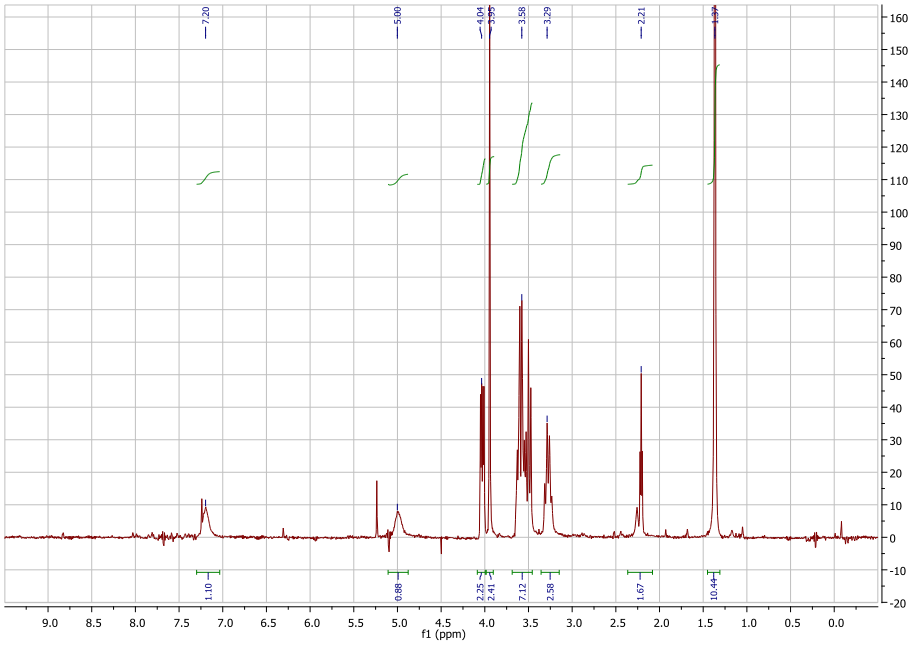

Figure 3.1 ^{1}H NMR spectrum of compound **2**

3.2.1.2 Synthesis of compound 3

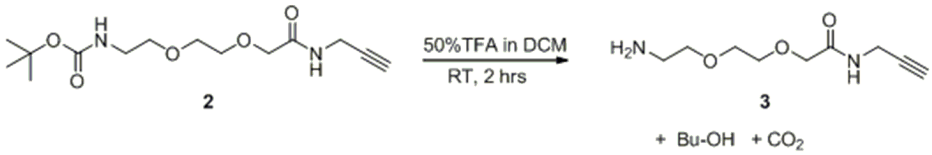

Scheme 3.2 Deprotection of **2**

8.6 mg (2 equivalents) of **2** was taken in a round bottom flask. To this, 50% of TFA in DCM were added and the solution was allowed to stand for 2 hours at room temperature to evaporate CO_2. The solution is evaporated followed by co-evaporation with toluene 3 times.This was followed by co-evaporation with TEA 3 times. The contents were dissolved in DCM, evaporated and dried on the pump to ensure the removal of volatile components. The deprotection was monitored by TLC (5 % MeOH in DCM). The product **3** was used as such for the next step without any further purification. ^{1}H NMR (200 MHz, 25°C), δ= 2.24 (t, 1H), 2.69 (br s, 2 H), 3.34 (t, 2H), 3.63 (m, 8 H), 4.00 (dd, 2 H), 4.97 (br s, 1 H)

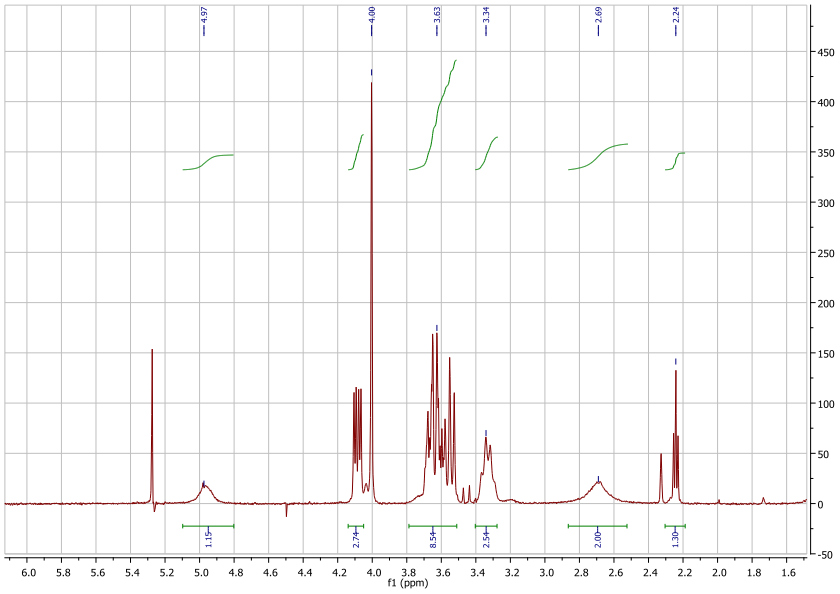

Figure 3.2 ^{1}H NMR spectrum of compound **3**

3.2.1.3 Synthesis of compound 5

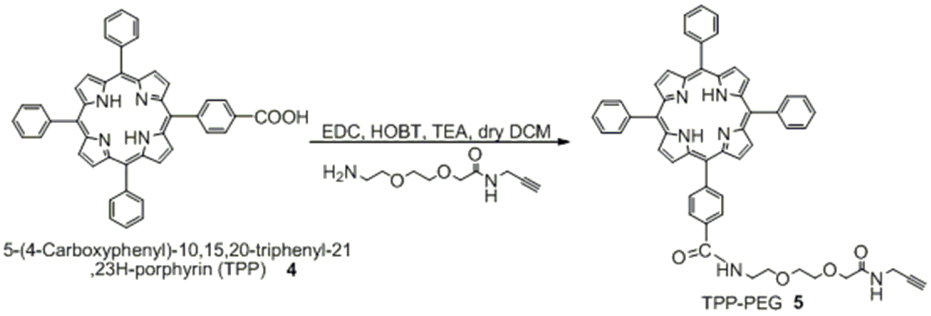

Scheme 3.3 Synthesis of TPP-PEG

Table 3.2 Reactants and reagents for synthesis of TPP-PEG

Material	Molecular weight	Weight taken (mg)	Moles (µmol)
TPP	658.7	10	15.18
EDC	191.7	4.4	22.77
HOBT.H_2O	153	3.5	22.77
TEA	101.19	3.07	30.36
Compd **3**	200	6	30.36

TPP (**4**), EDC and HOBT were dissolved in dry DCM. TEA was added to this solution and let stand for few minutes. Compound **3** dissolved in dry DCM was added to the mixture and the reaction mixture was stirred overnight at room temperature. The reaction was monitored by TLC (5% MeOH/DCM). The resulting product was evaporated and purified using column chromatography (3% MeOH/DCM) to obtain 8.8 mg of TPP-PEG. TPP-PEG was analysed by UV-visible, ^{1}H NMR and mass spectroscopy. ^{1}H NMR (200 MHz, $CDCl_3$, 20) δ= -2.79 (s, 2H), 2.26 (t, 1 H), 3.60 (dd, 2H), 3.67-3.7 (m, 6H), 4.10 (s, 2H), 4.12-4.16 (dd, 2H), 7 (br s, 1H), 7.7-7.8 (m, 9 H), 8.15-8.31 (m, 6 H), 8.19 (d, 2H), 8.20 (d, 2H), 8.78 (d, 2 H), 8.34 (s, 4 H), 8.86 (d, 2 H). Molecular weight of **5**=841.34, m/z=841.5 $[M+1]^{+1}$

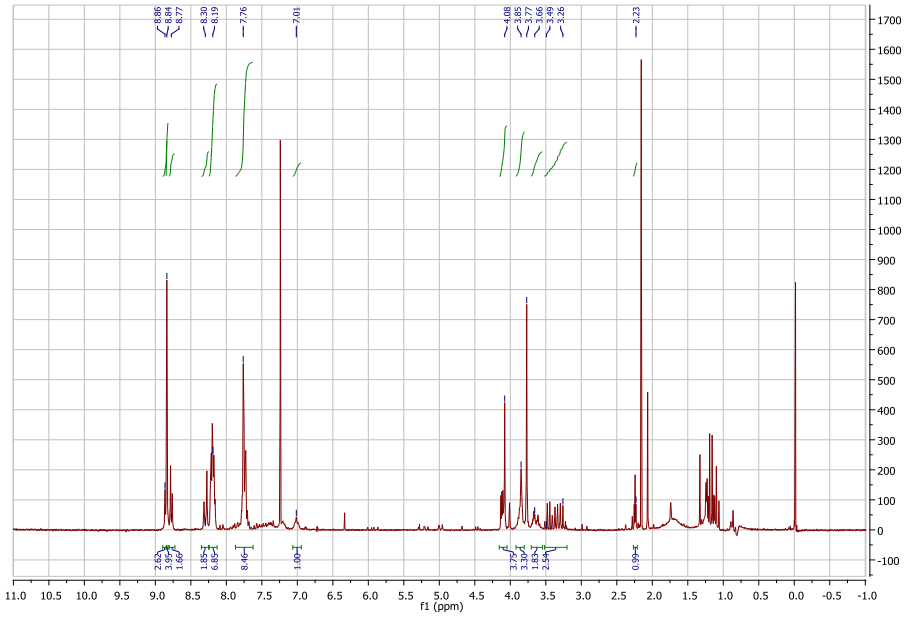

Figure 3.4 ^{1}H NMR spectrum of compound **5** (TPP-PEG)

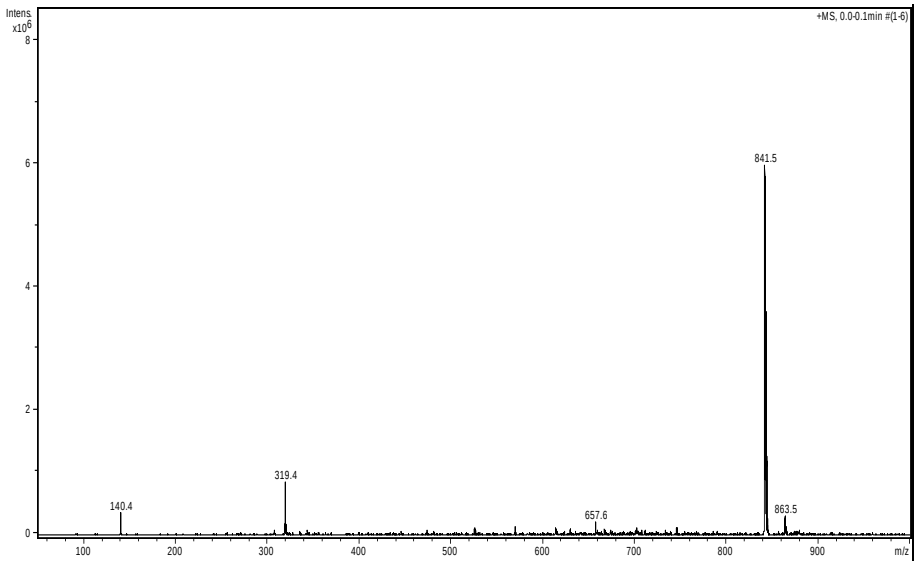

Figure 3.5 Mass spectrum of compound **5** (TPP-PEG)

3.2.2 CLICK REACTION BETWEEN PORPHYRIN-PEG AND SPION

3.2.2.1 *Synthesis of SPION-N_3*

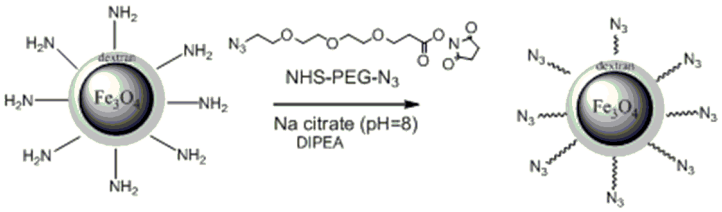

Scheme 3.4 Synthesis of SPION-N_3

SPION-N_3 (SPION azide) nanoparticles were prepared by the reaction of SPION-NH_2 with NHS ester of 12-azido-4, 7, 10-trioxadodecanoic acid in presence of DIPEA (10 µl) and 2 ml of 0.1 M citrate buffer (pH 7.4). The reactants were placed in a falcon and rotated overnight and then dialysed (SpectraPor regenerated cellulose, 3.5 KDa molecular weight cut-off) with pure deionised water for three to five days with occasionally changing the water. The resulting SPION-N_3 solution was diluted to a volume of 10 ml with deionised water and this solution was used as SPION-N_3 stock solution.

3.2.2.2 *Click reaction*

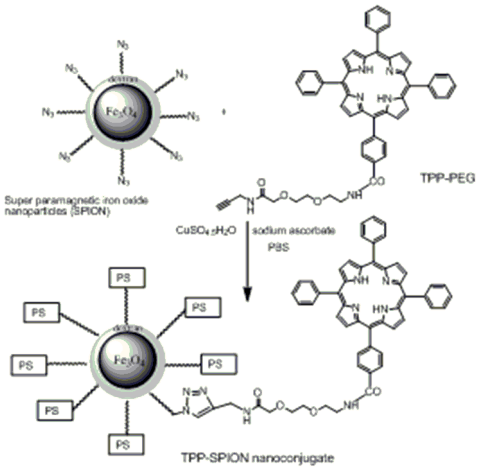

Scheme 3.5 Cu(I)-catalysed click reaction between SPION-N_3 and TPP-PEG

Table 3.3 Reactive components for SPION-TPP

Material	Molecular weight	Weight taken (mg)	Moles (μmol)
Compd 5 (TPP-PEG)	840.34	2.00	2.4
$CuSO_4.5H_2O$	249.69	0.30	1.2
Sodium ascorbate	198.11	0.87	4.8
SPION-azide		500 μl	
PBS		500 μl	

SPION-TPP nanoconjugate was synthesized via Cu (I) catalysed Huisgen 1, 3 dipolar cycloaddition or the "click reaction". TPP-PEG (1 equivalent) was weighed into an eppendorf and 1-2 μl of DMSO was added to it. To this, 0.5 equivalent of $CuSO_4.5H_2O$ and 2 equivalents of sodium ascorbate were added followed by addition of 500 μl of PBS and 500 μl of SPION-azide. The eppendorf with the contents was placed on a vibrator and allowed to react overnight. The contents of the eppendorf were transferred into a molecular exchange membrane and dialyzed with 500 ml of EDTA (3 times at intervals of 00 hrs, 3 hrs, 1 hr) followed by dialysis in 5 L water (4 times at intervals of 00 hrs, 15 hrs, 7 hrs and 15 hrs). After this, the membrane along with the contents was transferred to a falcon containing PBS in which it was dialyzed in order to change the medium of the contents into PBS. This was done 2-3 times in order to ensure the medium is fully in PBS. The contents of the membrane were then removed and UV measurements were carried out to find the concentration of the nanoconjugate. SPION-TPP in PBS was then stored in the fridge at 5°C.

3.3 RESULTS AND DISCUSSION

The Cu (I) catalysed click reaction was chosen to construct the conjugate molecule (SPION-TPP) because of its wide range of biomedical applications [131-133]. Moreover, the hydrolytic and thermal stability of the cycloadduct is of great interest in the field of bioconjugation. The click reaction has also been used in the field of porphyrin synthesis and also for their immobilization on different materials [119, 134]. SPION possessing strong magnetic property and the triazole with its stability and biocompatibility are efficient carriers for TPP

and hence were synthesized and studied for their photodynamic effect of bacterial strains.

3.3.1 CHARACTERIZATION AND CONCENTRATION DETERMINATION OF SPION-TPP

UV/Vis spectra were measured on a Varian Cary 50 spectrophotometer. Spectra were measured from 200 to 1000 nm, and PBS was used as the baseline The TPP conjugation on SPIONs was checked through UV/Vis spectroscopy. The Q-band changes were the most significant.

In order to calculate the right concentration of nanoconjugate, ε for TPP in PBS was calculated by preparing a series of TPP solution with known concentration. The UV-visible spectrum for each concentration was recorded and ε was calculated knowing the absorbance of the solution using beer-lambert's law and using the equation 2.1. The average of all the calculated ε was 1.43 x 10^5 and this value was used for further computation and expressed as M^{-1} cm^{-1}.

Two methods were used to estimate the concentration of TPP loaded on the nanoparticles. One method was based on the correction of the TPP-SPION absorbance ($A_{TPP\text{-}SPION}$) by the SPION absorbance (A_{SPION}). In this approach, the Beer–Lambert law was applied to (eq. 3.1)

$$\Delta A = A_{TPP-SPION} - A_{SPION} \quad (3.1)$$

at λ_{max} 422 nm (ε=1.43 x 10^5 M^{-1} cm^{-1}). The second method was based on a designed [135] deconvolution spread sheet. This procedure allows the complex absorbance spectrum of TPP-SPIONs to be resolved into individual absorption bands (Figure 3.6). The peak ascribable to the TPP loaded on SPIONs was calculated directly, and its absorbance value was used to calculate the concentration. The concentration values obtained with the two approaches were in good agreement.

Figure 3.6 (A)The absorption spectrum (black line) of a 6 μM solution of TPP in PBS is depicted, together with the deconvolution individual bands (red lines) and the calculated convolution spectrum (light violet line). The TPP Soret band at 423 nm is composed of two peaks, the highest of which is centered at 425 nm (log ε= 5.20). B) The absorption spectrum (black line) of a solution of SPION in

PBS (diluted from commercially available SPION-NH_2 as in SPION-TPP samples) is shown, together with the deconvolution individual bands (orange lines) and the calculated convolution spectrum (light violet line). The optimized data of FWHM and λ_{max} for each deconvolution individual band of TPP and SPION spectra were used to solve the SPION-TPP spectra. C) Figure reports the absorption spectrum (dark blue line) of 50 µl of SPION-TPP nanoconjugates in 450 µl PBS, together with the deconvolution individual bands (red lines) and the calculated convolution spectrum (light violet line).

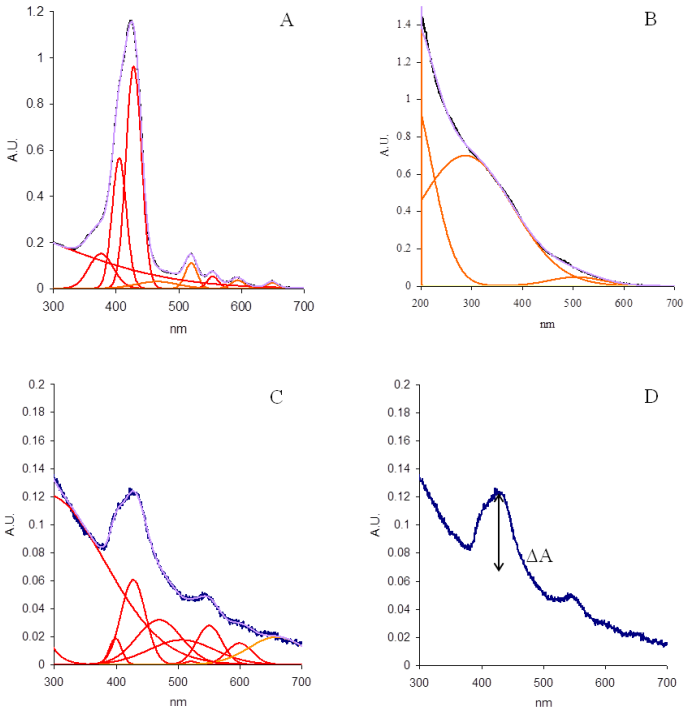

Figure 3.6 UV-visible absorption of TPP-SPION and the resolution of individual peaks

The deconvolution band at 425 nm was used to evaluate the concentration of TPP clicked to the nanoparticle (log ε= 5.20). D) Figure reports the absorption spectrum of 50 µl of SPION-TPP nanoconjugate in 450 µl PBS, together with the graphical evaluation of ΔA ($\Delta A = A_{TPP-SPION} - A_{SPION}$) used to calculate the concentration of conjugated TPP (log ε= 5.20).

The concentration obtained using the deconvolution method was 3.87 x 10^7 M in the diluted solution (50 µl of SPION-TPP nanoconjugate in 450 µl PBS). Hence, the concentration of the stock solution in terms of TPP = 3.87 µ M.

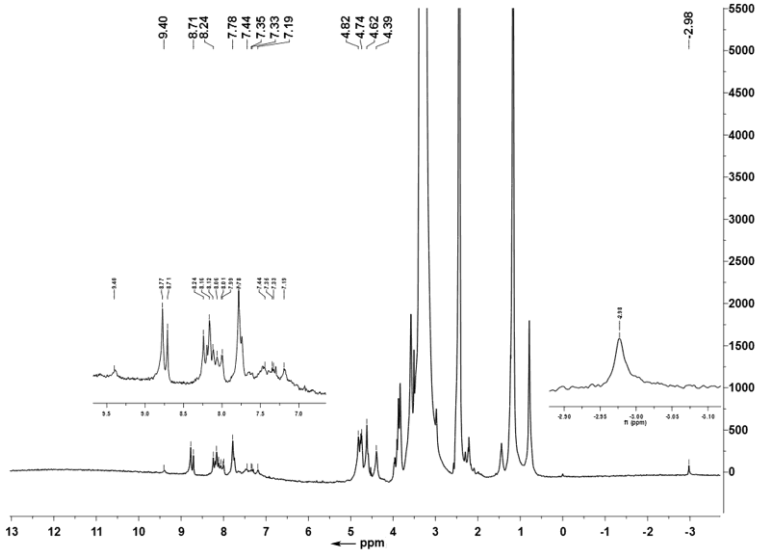

Figure 3.7 ^{1}H HRMAS-NMR of SPION-TPP. 2 mg of lyophilised nanoconjugate powder was dispersed in 60 µL of deuterated DMSO (1024 scans at RT)

The incidence of the reaction and the formation of the triazole ring upon conjugation was also verified through 1H highresolution magic angle spinning (HRMAS) NMR spectroscopy. As shown in the NMR spectrum in Figure 3.7, the CH of the triazole was identified as the singlet peak at 9.40 ppm. Furthermore, as expected, the peaks of the pyrrole and phenyl groups related to the porphyrin molecule were observed in the aromatic region (from 7.19 to 8.71 ppm) and at negative ppm (-2.98 ppm). Finally, the peaks related to the CH2O group of the short ethylene glycol linker were found between 4.39 and 4.82 ppm. The remaining peaks (0.5–4 ppm) were ascribed to the dextran-coated SPION and to the deuterated DMSO used as solvent for the NMR experiments (in addition, the usual broad peak of water related to the solvent was found at around 3.4 ppm).

3.3.2 CALCULATION OF NUMBER OF TPP MOLECULES PER SPION

An estimate of TPP per particle in SPION-TPP was calculated as follows:
According to the TDS of commercial SPION-NH_2, the number of nanoparticles per mL is $8.0x10^{14}$.
According to UV measurements, TPP concentration in the SPION-TPP stock solution (considering all dilution step applied during the synthesis) was found equal to 3.87 µM.
Thus the number of TPP particles/mL was $3.87x10^{-9}$ moles.
As 1 mole is equal to $6.23x10^{23}$ particles (Avagadro number), $3.87x10^{-9}$ moles = $6.23x10^{23}$ x $3.87x10^{-9}$ = $2.41x10^{15}$ particles/mL of TPP.
This means that 1 mL of SPION-TPP (stock solution) contained $8x10^{13}$ nanoparticles and $2.41x10^{15}$ particles of TPP.
Thus the number of TPP per nanoparticle in the SPION-TPP stock solution was $2.41x10^{15}/8x10^{13}$ = 30.12 TPP molecules per nanoparticle.

3.3.3 EVALUATION OF PHOTODISINFECTION EFFICIENCY OF MAGNETIC SPION-TPP

SPION-TPP was previously synthesized and tested not only as theranostic agents but also was found to cause photodynamic effect on murine amelanotic melanoma B78-H1 cells [125]. SPION-TPP possessed IC_{50} values in the range of 800 nm, which was similar to free TPP. These results proved that SPION-TPP can be promising agents for theranostic and PDT applications. Since the singlet oxygen generating capability of SPION-TPP was similar to free TPP [125], the application of the same to water disinfection appeared as a potential initiative.
With regard to the above, the photodsinfection efficiciency of SPION-TPP was tested on bacterial monocultures prepared in the laboratory. The bacterial strains used for this test were two Gram-positve (*S.aureus*, *S.mutans)* and one Gram-negative (*E.coli)*. The cultures used were in the logarithmic phase of their growth, which was prepared as mentioned in sec 2.5.3. A specific volume of SPION-TPP suspension was calculated to reach a 2 ml (total volume) of 0.3 µM

SPION-TPP solution in the bacterial suspension, which was previously prepared in sterile 0.01M PBS. 1 ml of this solution was placed in multi-well plate and placed above a magnetic stirrer and under the light source (blue LED light TLWB7600 Vishay) having fluence of 48 W m^{-2}. The solutions were stirred with magnetic stirrer throughout the treatment. Control experiments were conducted with or without SPION-TPP under illumination as well as in the dark. The treatment of photo-oxidation was 60, 120 and 180 minutes.

3.3.3.1 Disinfection of S.aureus with SPION-TPP

The effect of photodisinfection on *S.aureus* with SPION-TPP is shown in Figure 3.8 along with TPP-COOH in solution and the control samples SPION-N_3 and SPION-NH_2. As can be seen SPION-TPP at a very low concentration of 0.3 µM causes more than 2 log decrease (99.43 % abatement) in the cell survival in 180 minutes. This efficiency of SPION-TPP is close to the percent abatement caused by free TPP-COOH in solution (99.9999%) (Table 3.4). The non-conjugated nanoparticles SPION-NH_2 and SPON-N_3 cause at the maximum 56.23 % reduction in *S.aureus* survival, which is less than one order of magnitude and has no significant contribution in the total antibacterial efficiency of SPION-TPP. This proves that magnetic nanoparticles can be reliable carriers for photosensitizers to provide recovery and reusability of the photosensitizers after the treatment. Also, as shown in Figure 3.9, the nanoconjugate is not toxic in dark which is evident that the photodisinfection is due to the formation of ROS and not due to toxicity of the molecule or the nanoparticles itself.

Table 3.4 Percent abatement of *S. aureus* (10^7 CFU/ml as the initial concentration) with the nanoconjugate

Time (min)	SPION-TPP (0.3µM)	Free TPP-COOH (0.5 µM)	SPION-NH_2	SPION-N_3
60	-3.03		15.15	48.48
120	70.65	99.99375	29.65	9.85
180	99.43	99.9999	54.66	56.23

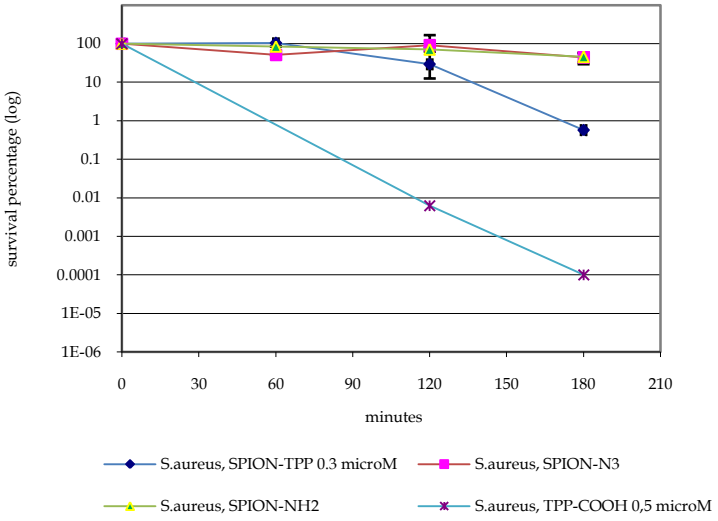

Figure 3.8 Effect of photosensitized treatment on *S.aureus* with SPION-TPP in comparison with TPP-COOH, SPION-N_3 and SPION-NH_2

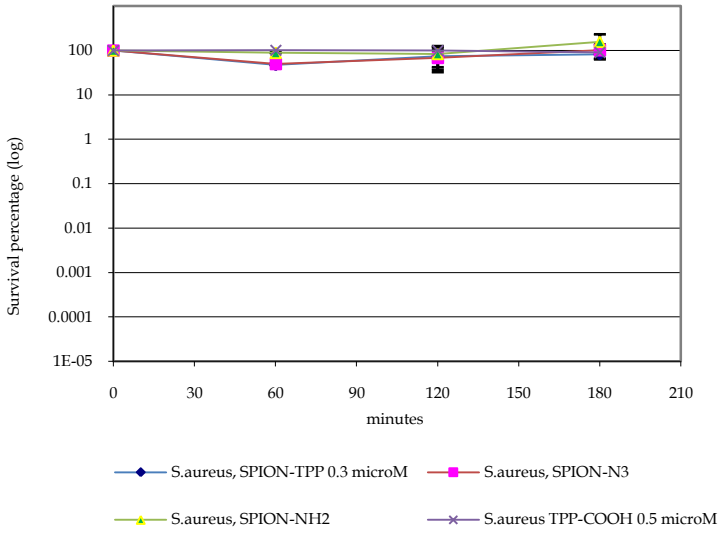

Figure 3.9 Toxicity of the materials on *S. aureus*

3.3.3.2 Photodisinfection of S.mutans with SPION-TPP

The effect of photodisinfection on *S. mutans* was carried out in the same conditions as *S. aureus* and for the same illumination period (180 minutes). SPION-TPP caused 95.10488% abatement in *S.mutans* at the end of the treatment (Table 3.5). As seen in Fig 3.10, only 1.5 log reduction was seen in the *S. mutans* survival after illumination with SPION-TPP. Unlike *S. aureus*, *S. mutans* cultures were found to be less susceptible to photoxidation by immobilized TPP-COOH over an illumination period of 180 min. On the other hand, TPP-COOH in solution caused several orders of reduction in the survival of *S. mutans* in 60 minutes itself. This can be explained by the fact that *S. mutans* posses the ability of forming biofilms i.e. they synthesize extracellular polysaccharides [136] and this reduces the possibility of interaction between the photosensitizer and the cell membrane. During photodisinfection process, it is well identified that the primary target in the pathogenic bacteria is it outer cell membrane and its constituent proteins [37and 60]. Hence, TPP-COOH in solution which has much lower particle size than SPION-TPP can easily penetrate or has larger surface to be in contact with the cell wall at the same concentration and break the cell membrane releasing its constituents and ultimately resulting in cell death.

Table 3.5 Percent abatement of *S. mutans* with SPION-TPP and TPP-COOH

Time (min)	SPION-TPP (0.5 µM)	TPP-COOH(0.5 µM)
60	57.21393	99.9994
120	56.33499	100
180	95.10488	100

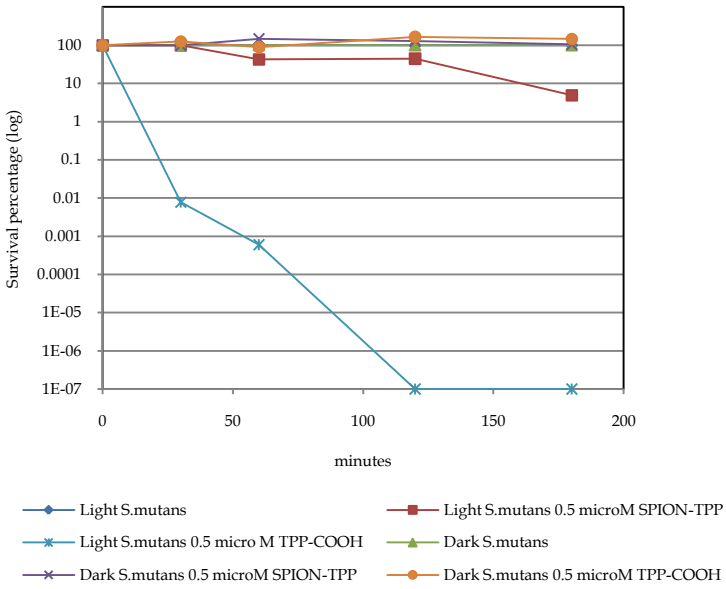

Figure 3.10 Effect of the phototreatment on *S. mutans* with SPION-TPP and evaluation of its toxicity

3.3.3.3 Photoillumination of E. coli with SPION-TPP

E. coli, Gram negative bacteria was also tested for photodisinfection by SPION-TPP. SPION in its original form bears amine functionality. Gram-negative bacteria are more resistant than Gram-positive bacteria due to the complex lipopolysaccharide membrane surrounding the cell membrane. In order to break this kind of barrier, it is either required to have a positive charge on the photosensitizer or its carrier. However, SPION-TPP does not bear any positive charge and appropriately as can be seen in Fig 3.11, *E. coli* is not affected by photoillumination in presence of SPION-TPP even in 180 minutes. TPP in its free form was previously tested on *E. coli* [137] and was found that the *E. coli* survival does not reduced with free TPP under light.

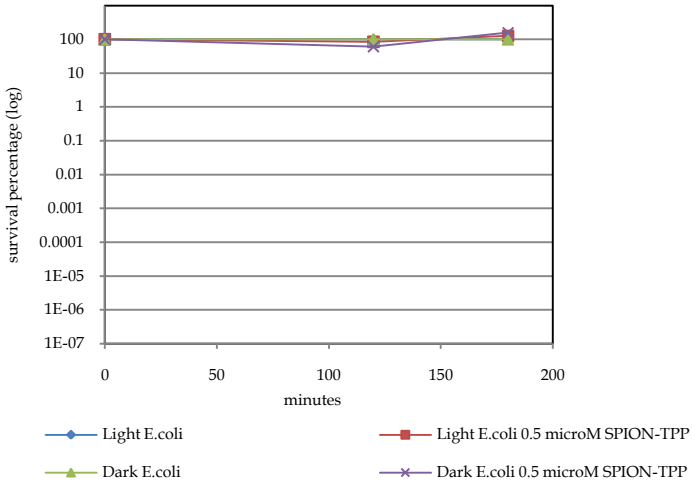

Figure 3.11 Effect of phototreatment of *E. coli* with SPION-TPP

These experiments show that SPION-TPP can be used for disinfection of water with the possibility to recover and reuse them after phototreatment (Fig. 3.12). These trials have not been conducted yet but such nanomagnetic particles are being studied for their use in photodisinfection of water [54, 96]. Their reuse properties have also been evaluated and it was found that the nanomagnet-porphyrin hybrids retained their photodynamic efficiencies even after 6 cycles of photodisinfection.

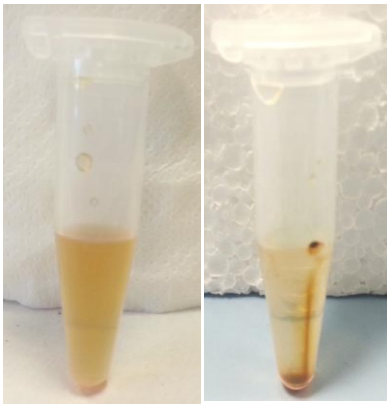

(a) (b)

Figure 3.12 Photographic pictures of SPION-solutions (a) before (b) after contact with neodinium magnet.

4 POLYVINYLCHLORIDE (PVC) SUPPORTED TPP

4.1 INTRODUCTION

As already discussed in Sec 1, the immobilization of photosensitizers proves to be more advantageous over free photosensitizers in solution. Solid support like polymers, nanoparticles and clothes can be used to produce self-disinfecting materials for medical application, protective clothing, environment (water and exposed surfaces) etc. Polymeric layers of PS on ITO [77], nanolayer coating of PS on NiTi alloy [20] and simple mixing of PS with different kinds of porous polymers [47,110] are the few reports available on supported reactive oxygen systems. Polymers or plastics find innumerable applications in day to day life and can prove to be efficient supports for developing singlet oxygen generating systems. Among the polymers used for support, the most common ones are polystyrene [81, 84, 117], porous silicones [63, 55, 47, 83] and cellulose [118, 119]. Selecting the right polymer with desired compatibility, porosity and PS uptaking capacity is an important task. Here we report a simple, easy and non-tedious technique for incorporating PS onto poly vinyl chloride (PVC). Polyvinyl chloride (PVC) is one such polymer that has vast application in the form of sheets, pipes, linings, cling films etc. It is used in the field of electrical, medicine, packaging, sports material, clothing etc. It is a light but strong, low cost polymer, has good biological and chemical resistance and available in flexible and rigid forms [120]. In this project, PVC films were prepared with a well known and commercially available porphyrin 5-(4-carboxy-phenyl)-10,15,20- triphenyl-21H, 23H-porphyrin (TPP). Different types of adipates were used as additives in the polymeric film and interestingly was found that the adipates play an important role in the morphology of the films and thereby the photodisinfection ability. The films prepared were tested for their anti-microbial activity in presence of light and their efficiencies are reported as abatement percentage.

4.2 EXPERIMENTAL

4.2.1 IMMOBILIZATION OF PHOTOSENSITIZER (TPP) ON THE PVC POLYMER WITH DIFFERENT ADIPATES

The PVC films were prepared by simple solution cast technique with tetrahydrofuran (THF) as the solvent. PVC films with 5% of TPP were prepared using different kinds of plasticizers/adipates. Also, PVC films without TPP were prepared as control films to verify the toxicity of the PVC films. The following different formulations were used to prepare the PVC composites:

Table 4.1 PVC film formulations

Name	Ingredients (mg)			
	PVC	TPP	Adipate	Film Thickness (µm)
TP5-OA	100	5	19.60 (20 µl)	70
TP5-BA	100	5	19.24 (20 µl)	50
TP5-EHA	100	5	18.60 (20 µl)	65
TP5-NA	100	5	00	50
TP5-CA	100	5	20 µl	75
PVC-OA	100	00	19.60 (20 µl)	70
PVC-BA	100	00	19.24 (20 µl)	55
PVC-EHA	100	00	18.60 (20 µl)	45
PVC-NA	100	00	00	50

Where

TP5-OA	5% TPP-PVC film with di-n-octyl adipate (OA)
TP5-BA	5% TPP-PVC film with di n-butyl adipate (BA)
TP5-EHA	5% TPP-PVC film with bis (2-ethylhexyl adipate) (DEHA)
TP5-NA	5% TPP-PVC film without any adipate
TP5-CA	5% TPP-PVC film with di capryl adipate (CA)
PVC-OA	PVC films with OA and without PS
PVC-BA	PVC film with BA and without PS
PVC-EHA	PVC film with DEHA and without PS
PVC-NA	PVC film without adipate and PS

Procedure

100 mg of PVC (high molecular weight) was taken in a 10 ml beaker and dissolved in 1.5 ml of tetrahydrofuran (THF). To this, 20 µl of di n-octyl adipate was added and the mixture was stirred till a homogeneous viscous mixture was obtained. 5 mg of TPP was weighed accurately and added to the polymer solution. The whole mixture was again stirred for 15 minutes to disperse the photosensitizer into the mixture very well getting rid of any lumps of TPP. The polymer mixture was then poured onto glass slides and spread with the help of a glass rod. The formulation was left to dry in a dark environment to evaporate the solvent completely. The film thus obtained had dimensions of 3 cm x 2 cm and thickness of film ranged between 50 to 100 microns. Similarly, all the films were prepared only changing the type of adipate required. PVC (blank) films were also prepared following the same procedure excluding the addition of TPP.

4.2.2 PVC-PHOTSENSITIZER COMPOSITE WITH VARYING CONCENTRATIONS OF TPP

Photosensitized PVC films with two different concentration of TPP (1% and 5%) were prepared. Di n-octyl adipate (OA) was the plastizer used in both the films. A control film without the photosensitizer was also prepared to test the toxicity of the polymer in light as well as in dark. The formulations of the films prepared is given in Table 4.2

Table 4.2 Formulation of photosensitized PVC films with different TPP concentrations

Name	Ingredients (mg)			
	PVC	TPP	Adipate	Film Thickness (µm)
TP1-OA	100	1	19.24 (20 µl)	40
TP5-OA	100	5	19.60 (20 µl)	70
PVC-OA	100	00	19.60 (20 µl)	70

TP1-OA 1%TPP-PVC film with di n-octyl adipate

TP5-OA 5% TPP-PVC film with di n-octyl adipate

PVC-OA 0% TPP-PVC film with di n-octyl adipate

4.2.3 5%TPP-PVC FILMS WITH VARYING CONCENTRATION OF DI N-OCTYL ADIPATE

In order to evaluate the effect of adipate on the photodisinfection efficiency of the composite films, TPP-PVC films with 3 different concentrations of di n-octyl adipate were prepared. The different concentrations of the adipate used were 20 and 40 µl in the total formulation. The formulations are given in Table 4.3

Table 4.3 Formulation for films with varying amount of adipate

Name	Ingredients (mg)			
	PVC	TPP	Adipate	Film Thickness (µm)
TP-520	100	5	19.60 (20 µl)	90
TP-540	100	5	39.20 (40 µl)	70
PVC-20	100	00	19.60 (20 µl)	70

Pictures of some composite films prepared are shown in Fig 4.1

Figure 4.1 Photographic images **(a)** PVC with 20 µl OA **(b)** 5% TPP-PVC with 20 µl OA **(c)** 5% TPP-PVC with 40 µl OA **(d)** 1% TPP-PVC with 20 µl OA

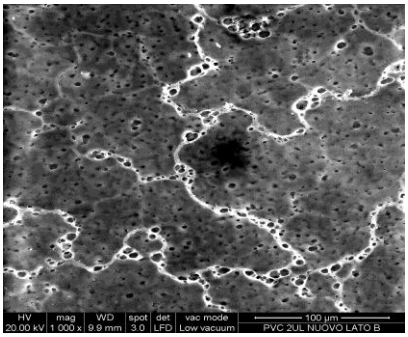

(a) PVC-20 µl OA

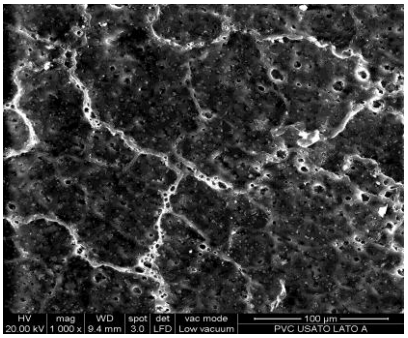

(b) LPVC-20 µl OA

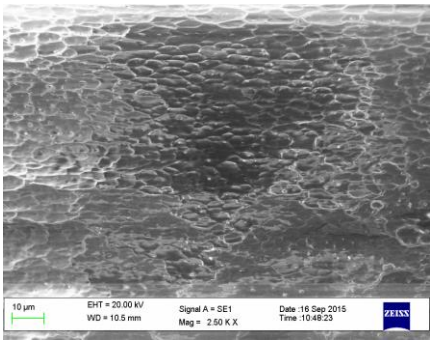

(c) TP-520

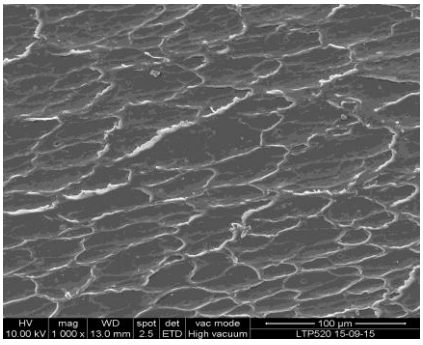

(d) LTP-520

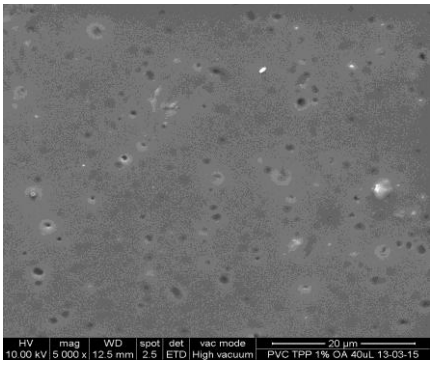

(e) TP-120

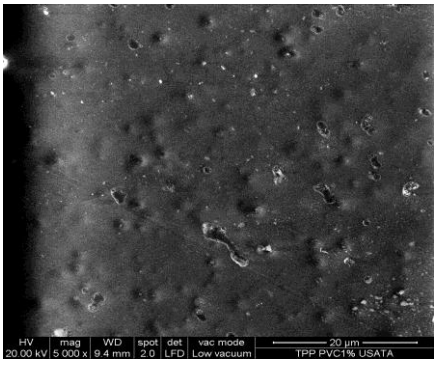

(f) LTP-120

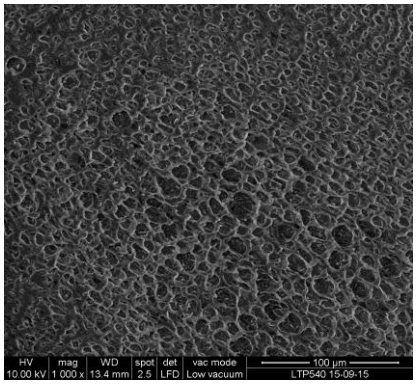

(g) LTP-540

Figure 4.2 SEM images of **(a)** PVC film with 20 µl OA x 1000 magnification **(b)** PVC film after illumination x 1000 magnification **(c)** 5% TPP-PVC film with 20 µl OA **(d)** 5% TPP-PVC film after illumination **(e)** 1% TPP-PVC film with 20 µl OA x 5000 magnification **(f)** 1% TPP-PVC film with 20 µl OA after illumination x 5000 magnification **(g)** 5% TPP-PVC with 40 µl OA after illumination.

4.2.4 PHOTODISINFECTION EXPERIMENTS WITH PVC COMPOSITE FILMS

For the photodisinfection experiments, the same setup as shown in Fig 2.1 was used. All the films prepared as above were tested for antimicrobial activity under light as well as their toxicities were tested in the dark. Each film was cut into a circular shape so as to fit into the multi-well (48 well) plate with diameter of 1 cm and capacity of 1.5 ml. The film so obtained weighed 7 mg. Hence, 7 mg of each film was used consistently in order to obtain constant concentration of the photosensitizer in all the experiment. The polymer films prior to illumination were washed with sterile PBS to remove any traces of free TPP on the surface of PVC film. UV-visible spectra of the washings were recorded and was seen that the concentration of TPP in the washings was negligible (<0.1 µM). This also proves that the TPP is successfully incorporated in the PVC matrix with very less or no free PS on the surface. However, the use of TPP eliminates the possibility of any free PS activity in solution as TPP is insoluble in water.

Volumes of 1 ml of bacterial solution (*S. aureus*) in sterile PBS at concentration of 10^8 CFU ml^{-1} were placed in multi-well plate. The films to be tested were introduced in the bacterial suspensions and the plates were positioned above a magnetic stirrer and under the light source (blue LED light TLWB7600 Vishay) having fluence of 48 W m^{-2}. The solutions were stirred with magnetic stirrer throughout the treatment. Control experiments were conducted with or without PVC films under illumination and on plates with PS-PVC films in the dark. The treatment of photo-oxidation may have different duration (15, 30, 60, 90, 120 and 180 minutes of illumination) depending upon the concentration of the photosensitizer.

At regular intervals of treatment time, the survival of microorganisms is analyzed and expressed as CFU ml^{-1}. 50 µl of the bacterial solution under treatment was aliquoted and diluted in 0.01 M PBS using a dilution factor optimal for the cultivation of bacteria. From each dilution, 100 µl of bacterial suspension are collected, seeded in selective media on Petri dishes and incubated in the dark at 37°C for 18-24 hours.

The same procedure is followed for the control samples to test the activity of PS-PVC film in the dark, the toxicity of PVC films both in light and dark; and the vitality of bacterial suspension without photosensitizer, subjected to light or incubated in the dark. Each test is performed at least in triplicate, the survival data in terms of CFU ml^{-1} are expressed through mean and standard deviation. The survival rate is calculated in relation to the concentration of bacteria measured on the control sample subjected to light, to subtract any interfering toxic effect from the photosensitizer effect.

To exclude the possibility of any photodynamic activity due to some TPP release into solution during illumination, the TPP-PVC films were suspended in sterile water and illuminated for similar time duration (90 minutes). Control tests were conducted by illuminating only sterile water samples and PVC films in water. The same set of water samples were placed also in the dark. ESI-TIC chromatograms of all the water samples were recorded [Fig 4.7]

4.3 RESULTS AND DISCUSSION

4.3.1 EFFECT OF PHOTOXIDATIVE TREATMENT ON S.AUREUS BY 5% TPP-PVC FILMS WITH DIFFERENT ADIPATES

For easy understanding, the films TP-NA, TP-BA, TP-EHA and TP-OA after illumination will be abbreviated as LTP-NA, LTP-BA, LTP-EHA and LTP-OA, respectively. Figure 4.1 shows the photographs of the PVC films with and without TPP. The abatement percentages of the TPP-PVC films with different adipates are listed in Table 4.4. As can be seen in the table and graphical presentation of data (Fig 4.3), the presence of adipate and the type of adipate plays an important role in the photodisinfection ability of the composite films. TPP-PVC films with no adipate caused 94.1176% abatement in the bacterial survival at the end of 90 minutes of illumination. LTP5-BA and LTP5-EHA have similar efficiencies 90.9973% and 92.9885% abatement, respectively in 90 minutes. These three films showed within 1 order of ability to destroy *S. aureus* strain. Interestingly, LTP5-OA displays the same order of activity in 30 minutes of irradiation itself and remarkably causes several orders of reduction (100% abatement) in the microorganism within 60 minutes of illumination. None of the films showed any toxicity in the dark (Fig 4.4 and 4.5). Elucidation of the toxicity of the PVC films without TPP but in presence of adipates helped to rule out the possibility that the high antibacterial activity of LTP5-OA is due to di n-octyl adipate itself (Fig 4.5). Such a significant difference in the photodynamic activity of the different films led to following uncertainties:

- The anti-bacterial activity was due to presence of some contaminant in di n-octyl adipate. This was solved by recording an ESI-mass spectrum of the adipate (Fig 4.7) molecular weight of d n-octyl adipate = 370.57 m/z= 393.6 $[M+1]^{+1}$. ESI-mass spectrum showed that the compound was in the pure form without any contamination
- The anti-bacterial activity was due to release of some toxic component in presence of OA in the film during the irradiation procedure. For this, the ESI-TIC chromatogram (Fig 4.8) solved the dilemma that there was no release into the water system during the illumination. The

chromatogram show that there is no difference between the component peaks of the blank water samples and the water samples with suspended PVC films with or without TPP. Also, the figure compares the chromatograms of samples in the dark.

In addition to the above evidences, it would be interesting to know how the morphology of polymeric films affects the release of singlet oxygen into the water system. The following mechanisms can be proposed for the activity of the TPP-PVC films

- Close proximity of the microorganisms to the surface TPP molecules of the films disseminating singlet oxygen into the cell structure within its decay time.
- Slow release of photosensitizer into the bacterial suspension during illumination.
- Porous voids in the polymer matrix to contain bacterial colonies thereby providing more contact and time for the singlet oxygen to diffuse and cause cell death.

The second mechanism of disinfection is not acceptable in water disinfection systems and also it was proved that there was no release of the PS during the illumination. If the first proposed mechanism is true, then the films without adipate and also TP5-BA and TP5-EHA are expected to show similar activity as TP5-OA at the same concentration of TPP. However, this was not true in this case as it was observed that TP5-OA and TP5-CA films have significantly different photodynamic efficiencies with respect to others. Hence, the third mechanism appears more relevant in this case. A polymer in its glassy state has its molecules closely packed with strong polymer-polymer interactions making the polymer rigid and hard. According to *Free volume* theory of plasticization, when a plasticizer is added to a PVC it lowers its glass transition temperature *Tg* by separating the PVC molecules, adding free volume and making it more flexible and rubbery [121]. Di n-octyl adipate and di capryl adipate are well known for their co-solvent properties and imparting flexibility and porosity to the polymer structure. Both the adipates have a molecular structure with a long straight chain of carbon skeleton as compared to BA and EHA. Here it is evident that the molecular structure of the adipate plays an important role in imparting porous properties to the polymeric films (Fig. 4.6). Hence, it is capable of providing more free volume into the PVC matrix. The porosity of the

PS carrier plays a crucial role in the photodisinfection mechanism. F. Manjón and co-workers have carried out photodisinfection on a large scale using heterogeneous systems by using porous silicones as PS supports [75, 55, 63]. According to them, porous silicone is optically translucent, mechanically robust, significantly photostable and chemically inert with excellent interaction with microorganisms. They have also proved that the lifetime of singlet oxygen produced by PS in these polymers is higher than in water by 10 times. Also, polystyrene a porous polymer was used to support RB and MB with a concentration of 0.1 to 1% of the dye onto to the polymer [84]. At such a low concentration and considerably lower fluence of irradiated light of 21 W m^{-2}, they found 2-3 log decrease in bacterial count. Also, the bactericidal activity was higher with a lower initial concentration of bacteria (10^3 CFU ml^{-1}). In this study, we have used 1% and higher concentration of the dye and fluence of incident light at 48 W m^{-2}.

Table 4.4 Percentage of abatement of the bacteria *S. aureus*

	LTP5-NA	LTP5-BA	LTP5-EHA	LTP5-OA	LTP5-CA
30	36.7647	44.51613	46.5517	95.64733 ± 3.203	99.4476 ± 1.1481
60	58.7254	69.54839	76.2835	100	99.9873
90	94.1176	90.99735	92.9885	100	100

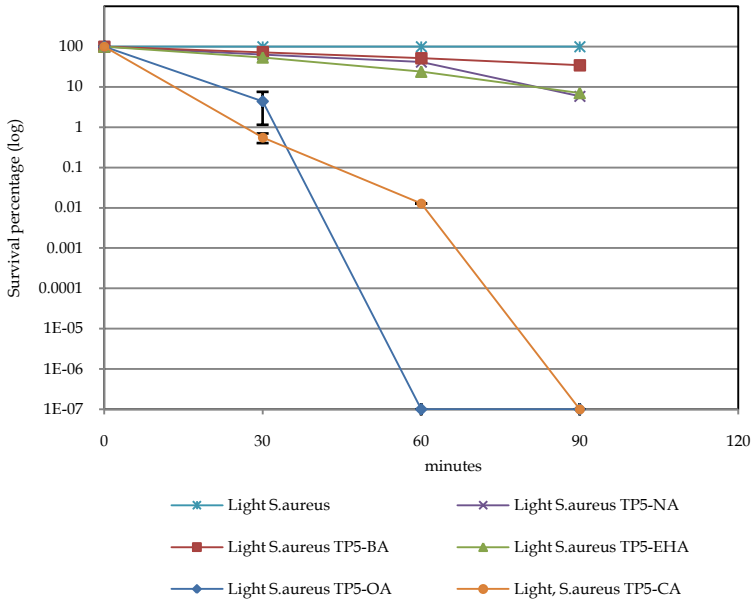

Figure 4.3 Photodisinfection efficiency of 5% TPP-PVC films containing different adipates on *S.aureus*

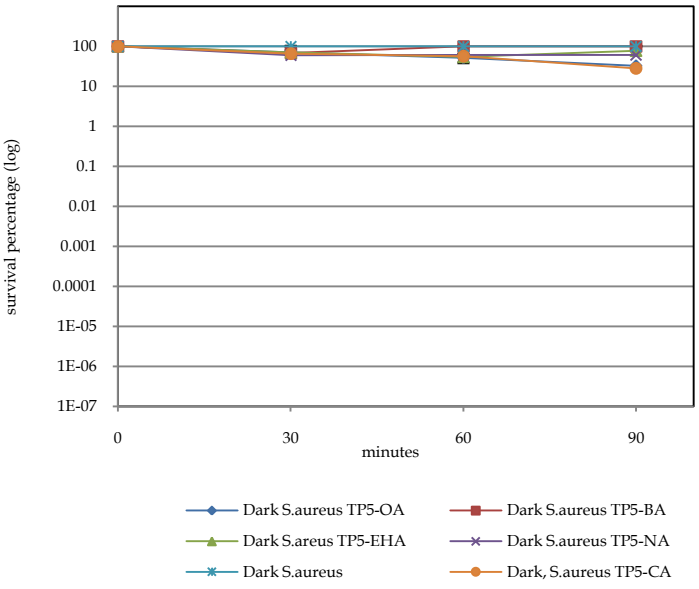

Figure 4.4 Toxicity of the PVC film on *S.aureus* in the dark

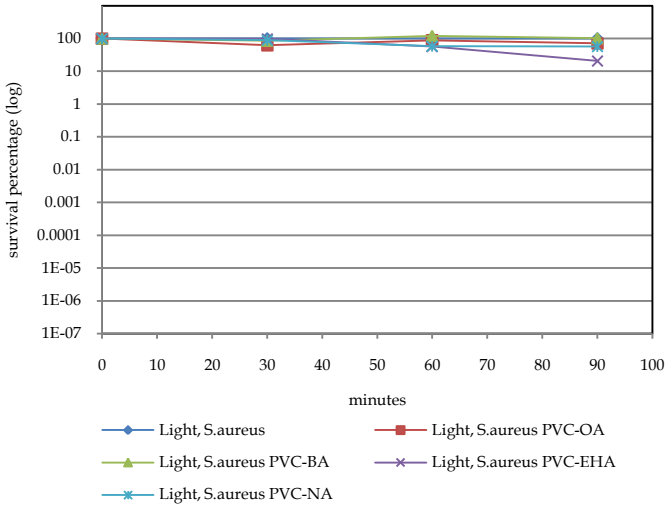

Figure 4.5 Effect of irradiated PVC control films on *S. aureus*

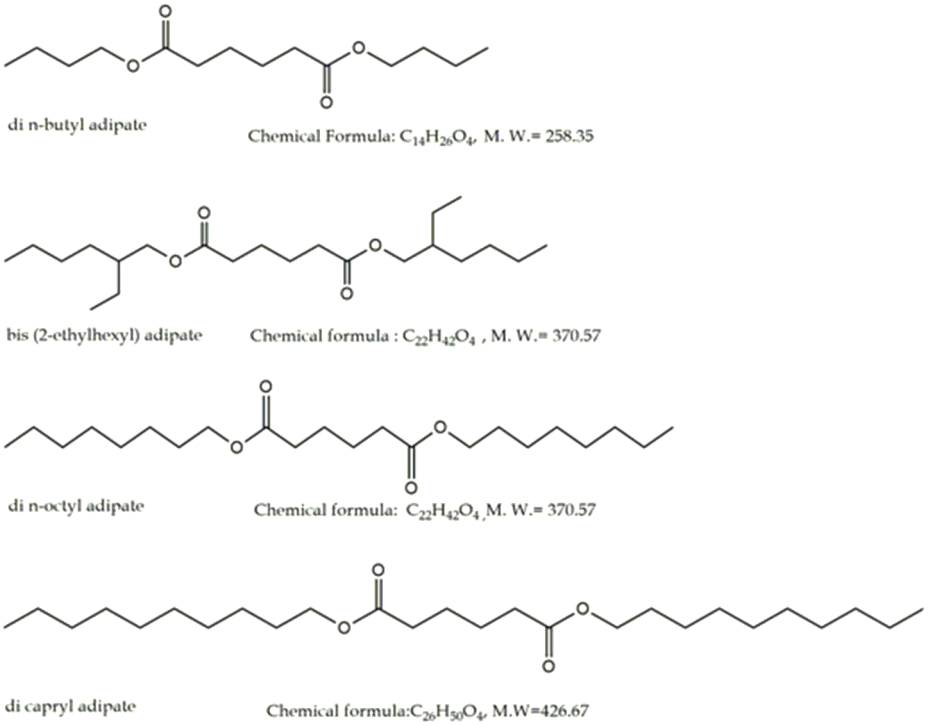

Figure 4.6 Molecular structures of different adipates used

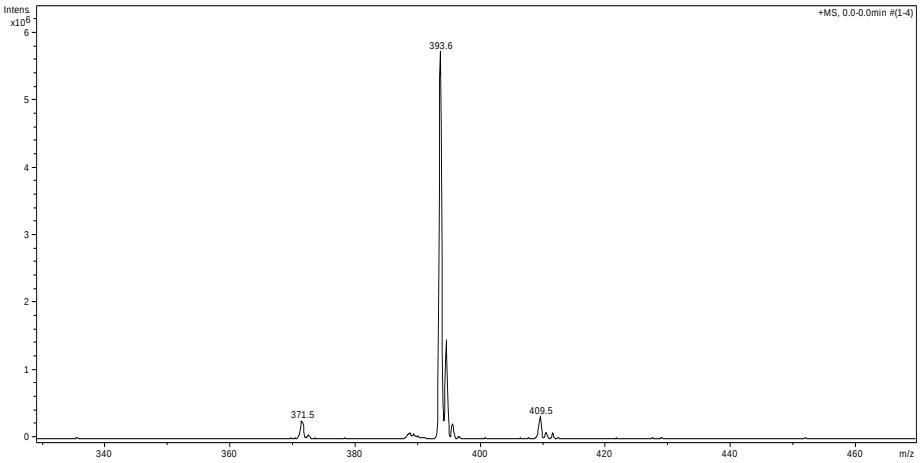

Figure 4.7 ESI-mass spectrum of di n-octyl adipate

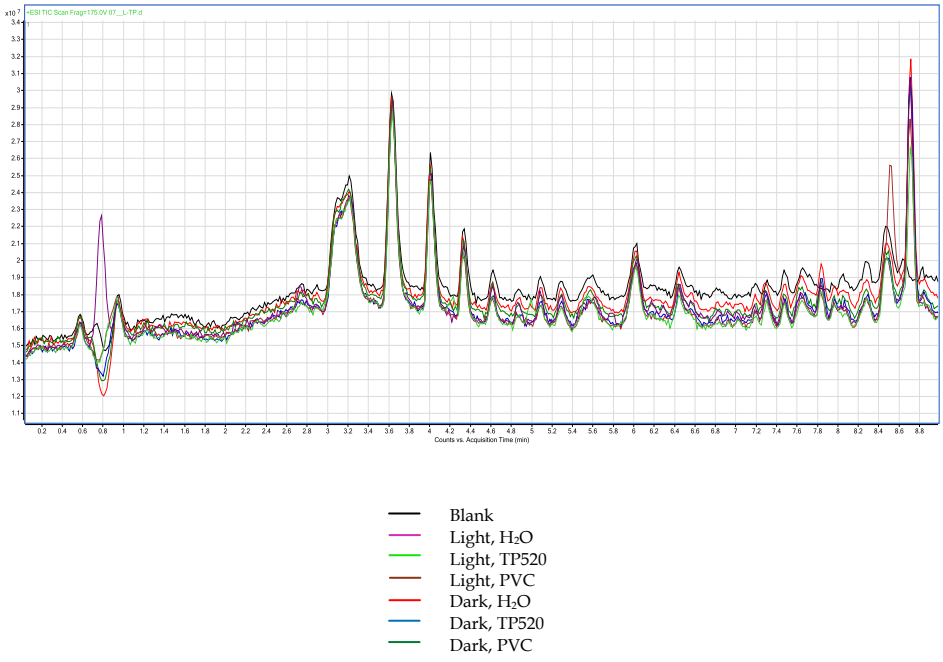

Figure 4.8 ESI-TIC chromatograms of the illuminated water samples

In Figure 4.2 are shown SEM micrographs of PVC films with and without TPP. Only PVC film with OA (Fig 4.2a) shows a pattern of porous network and it retains this structure even after illumination (Fig 4.2b). On the other hand,

addition of TPP causes a smooth effect in the polymeric surface and there can be seen a more uniform pattern. This change in the morphology can be explained by the structure of TPP. TPP contains 4-phenyl substituents at the meso positions and the molecule has a planar structure. The planar structure with a huge delocalization of electrons is capable of stacking in a parallel array of molecules and thereby forming a uniform network and this is seen in the SEM micrographs. This property of TPP possibly contributes to a more uniform and even network of free volume (Fig 4.2c).

4.3.2 COMPARISON OF PHOTOEFFICIENCY OF 1%TPP-PVC AND 5% TPP-PVC

The effect of different TPP concentration on the photodisinfection efficiency of PVC films is shown in Figure 4.2. As can be seen, both 1% and 5% TPP-PVC films show remarkable efficiency in reducing the bacterial survival. Also, as expected, increasing the concentration of TPP from 1% to 5% causes an increase in the abatement of bacterial survival by more than 4 orders at 60 minutes of irradiation itself. At 90 minutes, the survival of *S. aureus* dropped by 4 log in presence of 1% TPP-PVC and by several orders (100 % abatement) in presence of 5% TPP-PVC.

Another factor to be considered here is the thickness of the films (Table 4.2). TP1-OA (40 μm) has roughly half of the thickness of TP5-OA (70 μm) and as seen in Figure 4.1, the photograph of LP1-OA reveals that it is almost transparent and TPP is well incorporated into the PVC matrix. The SEM micrographs of TP1-OA (Fig. 4.2 (e) and (f)) show a rather smooth structure. TPP at 1% concentration (w/w) seem to level the irregularity in the PVC. Large and porous voids are lesser in this film as compared to PVC-OA (Fig. 4.2 (a) and (b)). This shows that the PS-polymer displayed significant photoefficiency irrespective of the size of the porous free volume. Even at low thickness and lower TPP concentration, the efficiency displayed by TP1-OA is appreciable. Such low concentration of photosensitizer can be used in applications that require transparent films (e.g. medical devices, packaging, cling films and protective clothing). Also, as shown in Fig. 4.9 only light has no toxic effect on

S. aureus colonies and all the dark controls also show no reduction in the bacterial count in the same duration (90 minutes).

Table 4.5 Percentage abatement of *S. aureus* with 1% and 5% TPP-PVC

Irradiation time	LTP1-OA	LTP5-OA
30	82.57528 ± 9.78	95.64733 ± 3.2030
60	96.99165 ± 2.1412	100 ± 0
90	99.99375±0.0069	100 ± 0

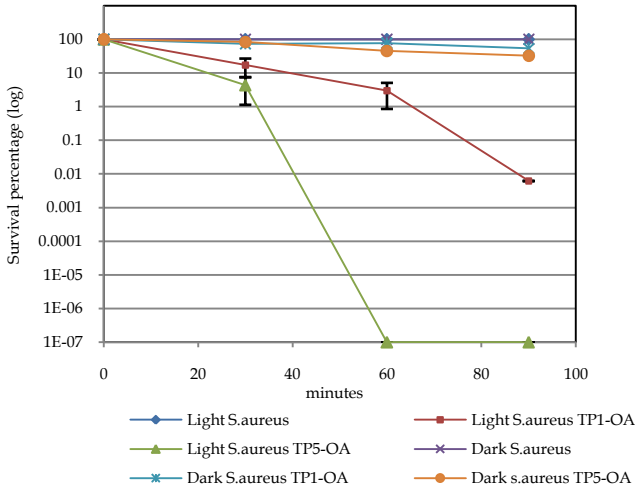

Figure 4.9 Effect of 1% and 5% TPP-PVC films on *S. aureus* in the light and dark

4.3.3 EFFECT OF VARYING CONCENTRATION OF Di n-OCTYL ADIPATE ON PHOTOEFFICIENCY OF 5% TPP-PVC

The effect of varying concentration of adipates was studied by preparing TPP-PVC films with 2 different concentrations (20 µl per 100 gm of PVC and 40 µl per 100 gm of PVC). The data for photodisinfection efficiency of the two films is plotted in fig. 4.10. The plot shows that there is a difference of approximately 2 logarithmic orders between the activities of two films. TP540 caused between 3-

4 log reduction whereas TP520 caused less than 2 log reduction in bacterial survival with almost an error bar of 1 log for TP520. This difference is less significant because after 60 minutes of illumination, both the polymeric films were capable of completely destroying the microbial polulation. However, the difference calls for an explanation and a rational reasoning can be derived from the basic properties of OA. Being a well-known and valuable plasticizer, OA imparts more free volume to the polymer and appropriately increasing the concentration of OA should increase the porosity of the polymer to a greater extent. The SEM micrographs also confirm this phenomenon (Fig. 4.2). The surface of TP540 shows dense network of porous structure which is more than in TP520. More the number of pores available; higher will be the probability of bacterial colonies to occupy these voids. *S. aureus* strains exist in colonies of about 100 individual cellular components of approximately 0.7 µm each.

Table 4.4 Abatement percentages of *S. aureus* with TP520 and TP540

Irradiation time	LTP520	LTP540
30	95.64733 ± 3.2030	99.9552 ± 0.0075
60	100 ± 0	100 ± 0
90	100 ± 0	100 ±0

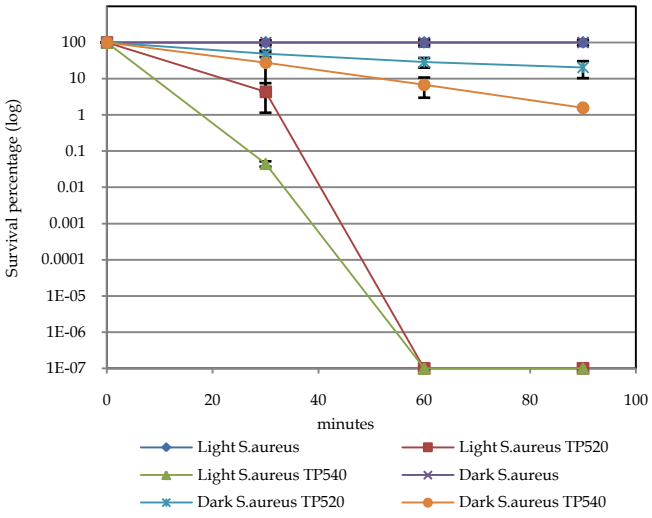

Figure 4.10 Effect of varying concentration of di n-octyl adipate on photodisinfection of *S. aureus*

4.3.4 *RECOVERY AND REUSE OF TPP-PVC FILMS*

All the films used for the evaluation of photodisinfection efficiency were recovered at the end of the experiment, washed in sterile PBS, dried and stored at 4°C in the refrigerator away from any kind of light source. Out of the many films used, 2 films of TP520 were randomly chosen for reuse in photodisinfection experiments to investigate the photoxidation ability of the used films. The data (Figure 4.11) reveal that the TPP-PVC films had reduced activity after the first use in photodisinfection trials. One film used for second time after 3 weeks showed 3 log reduction whereas the reuse after 5 weeks caused less than 1 order abatement of *S. aureus* culture.

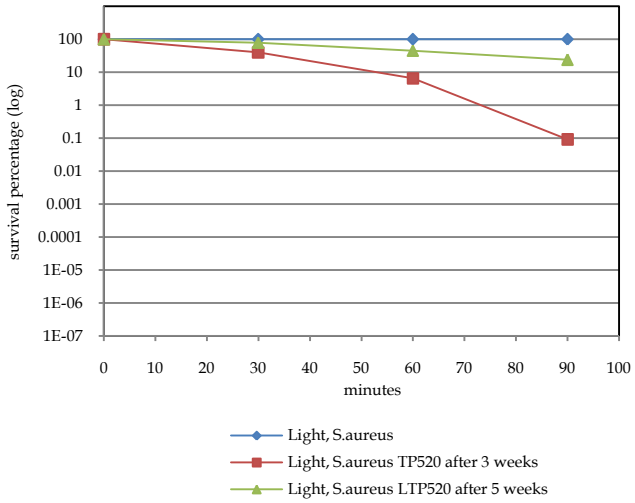

Figure 4.11 Photodisinfection ability of used TPP-PVC films

Many authors have reported to have coated PS-polymeric films in Petri dishes or other glass containers and carried out the experiments by dispensing volumes of bacterial solution into the plates. On the other hand, all of the TPP-PVC composites used in this work for the use and reuse of photodisinfection experiments were prepared in the form of thin films on glass slides and the films were removed from the slides prior to illumination. The advantage of suspending PS-polymer films in the target system is all the surfaces of the film are involved during the photooxidation process. This implies that maximum

included PS takes part in singlet oxygen generation and the total effect can be considered to be proportional to the concentration of PS in the whole film and not of the PS at only one single surface. Another benefit of suspended film technique is that once the film is used, the films can be reinforced either by cleaning the film surface with a solvent or by dissolving the film in THF and recasting.

In the present work, the light source used was emitting at a single wavelength (470 nm) and there was no temperature rise in the photodisinfection system due to the light source or other external factors. This is particularly important because PVC at higher temperatures and/or UV radiation is known to decompose releasing atomic chlorine and HCl thereby deteriorating the material. This problem was eliminated in the present case by using light from the visible part of electromagnetic spectrum and maintaining lower temperatures.

5 Poly vinyl chloride (PVC) supported pentaphyrin

5.1 INTRODUCTION

The successful incorporation and high bactericidal effect of TPP in PVC was a motivation for inclusion of new photosensitizers in PVC matrix. A new pentaphyrin synthesized and characterised previously in our laboratory was used to prepare pentaphyrin-PVC films. The pentaphyrin used in this project was 20- (4-carboxyphenyl) -2, 13-dimethyl-3, 12-diethyl [22] pentaphyrin (PCCox)[102]. PCCox belongs to a new class of expanded porphyrins with one pyrrolic unit more than regular porphyrins bearing 5 meso carbon atoms. Expanded porphyrins are discussed in detail in sec. 1.5. PCCox has already been investigated for its photodynamic activity in solution and was found to cause several order reduction of bacterial growth [46].

5.2 EXPERIMENTAL

Procedure

PVC films with 5% pentaphyrin were prepared with varying concentrations of di n-octyl adipate. The films were prepared following the same procedure as mentioned in sec. 4.2.1 and the formulations are listed in Table 5.1. The picture of the films prepared are shown in Fig 5.1

Table 5.1 Formulation of PCCox-PVC films

Name	Ingredients (mg)			
	PVC	PCCox	Adipate	Film Thickness (µm)
P-510	100	5	9.5 (10 µl)	75
P-520	100	5	19.60 (20 µl)	60
P-540	100	5	39.20 (40 µl)	70

Where,

P-510 5% PCCox-PVC film with 10 µl OA

P-520 5% PCCox-PVC film with 20 µl OA

P-540 5% PCCox-PVC film with 40 µl OA

(a) (b) (c)

Figure 5.1 Photographic pictures of (a) P-510 (b) P-520 (c) P-540

5.3 RESULTS AND DISCUSSION

5.3.1 EVALUATION OF PHOTODISINFECTION EFFICIENCIES OF PCCOx-PVC FILMS WITH DIFFERENT CONCENTRATION OF ADIPATES

The uniform inclusion of PCCox into the PVC matrix can be seen from Fig. 5.1. Similar to TPP, PCCox was also very easily incorporated into PVC polymer films using solution cast technique. But unlike TPP-PVC that had glossy facade, PCCox-PVC membranes showed more of a matt appearance. The metallic green colour of solid PCCox was also seen in the films revealing that PCCox did not undergo any transformation during film formation. Likewise, looking at the photodisinfection abilities of the films, it was observed that the films have noteworthy performance.

PCCox has previously been synthesized, studied and proved as a potential photosensitizer for PDT [103, 46]. During photodisnfection of water, PCCox was found to be capable of causing 99.997% abatement in *S. aureus* survival with blue LED light in 1 hour and 99.99997% abatement in presence of white incandescent lamp. Studies have now proven that immobilization of

photosensitizers onto a solid support like polymer does not alter its singlet oxygen generating capacity and PDT does not occur only due to the accumulation of the photo sensitizer in the microbial cell [126, 127]. This was proven in our photoxidation experiments using PCCox-PVC films. As can be seen in Fig. 5.2, P-520 caused 100% destruction in bacterial count, P-540 showed 99.783% abatement and P-510 was almost inactive in 90 minutes of illumination. The results showed that a minimum concentration of OA was essential to trigger the photosensitizing ability of PCCox. As also observed in case of TPP-PVC, OA played an important role in imparting photosensibility to the composite films. OA increases free volume in polymer structure and also enhances the mobility of polymer chains. This improved property of the polymer probably also causes singlet oxygen to move freely within the network and ultimately reaching the target cell and causing its death.

The SEM micrographs (Fig. 5.4 (a) and (c)) show that the presence of PCCox transforms the random structure of PVC (Fig. 4.2 c) into a more organized and regular pattern of pentagonal network. The free volumes in the composition can be clear seen and increasing the concentration of OA increases the size of the voids in the polymer matrix (Fig. 5.4 c). However in this case, increasing the concentration of OA did not enhance the photoactivity of PCCox-PVC film rather the efficiency was found to be reduced in presence of higher OA concentration. On the other hand, the photoactivities of TPP-PVC films were found to show dependence on concentration of OA. One explanation for the reduced behavior of P540 can be deduced from the SEM that after illumination P540 shows a significant change in its morphology. Probably, the surface of P540 differs from P520 which allows singlet oxygen to disseminate and instead in P540 the singlet oxygen does not reach the bacteria but remains in the pores and cause degradation of the PCCox in the film. However, more evidence on this performance of both the films having same concentration but differing only in the amount of adipate will be very helpful to carry on the development of such system.

Fig. 5.4 (e) and (f) show SEM micrographs of *S. aureus* culture on P-520 film. It can be seen that the bacterial strains occur as single cellular component (700-800 nm) or in clusters. The bacterial colonies are sufficiently small to rest in the voids (20 μm) of the polymer network thereby increasing the contact with the PS. Since a close proximity between the PS and the cells is necessary for

effective bacterial destruction, the probability of cells to be adsorbed is higher due to the pores in the polymeric structure. Hence, the singlet oxygen can reach the cell wall within its half life.

Table 5.2 Percent abatement caused by PCCox-PVC films under monochromatic blue LED lamp

Time of illumination	Percentage abatement (%)		
	LP-510	LP-520	LP-540
30	11.8024 ± 15.6486	97.4605 ± 0.78426	76.2484 ± 16.7949
60	-236.875 ± 163.125	99.4103 ± 0.4811	86.6984 ± 9.4056
90	27.6020 ±68.9813	100	99.783 ± 0.1534

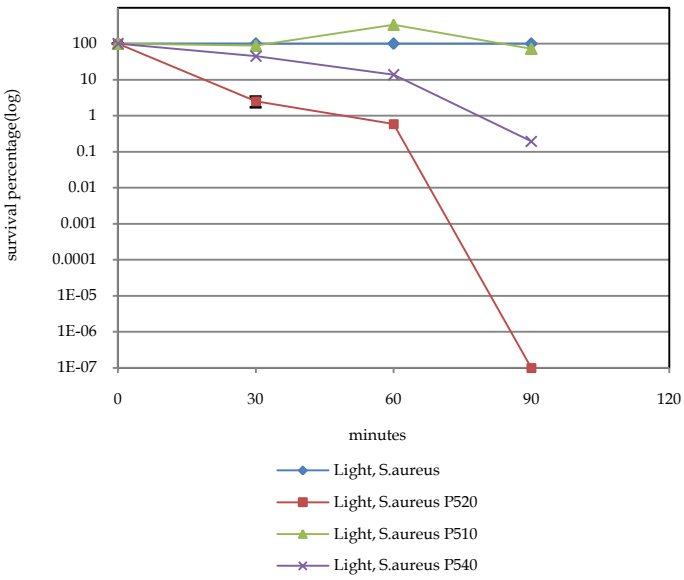

Figure 5.2 Photodisinfection of *S.aureus* with PCCox-PVC composite films

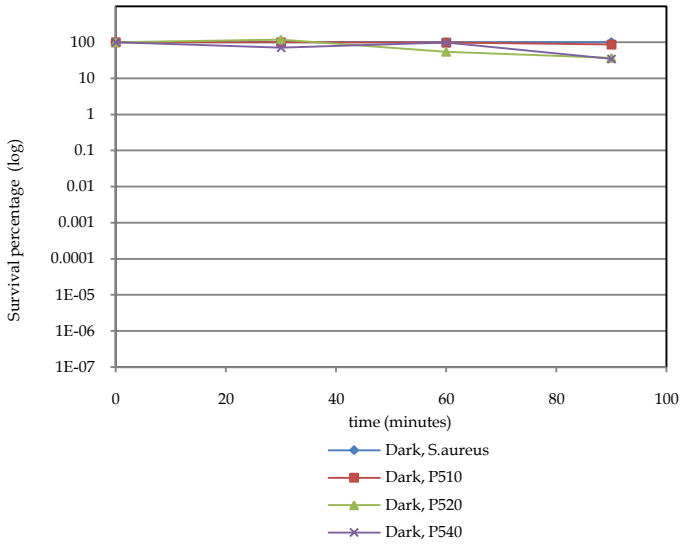

Figure 5.3 Toxicity of PCCox-PVC films on *S. aureus* evaluated by incubating the bacterial culture in the dark for similar duration of photoxidative treatment

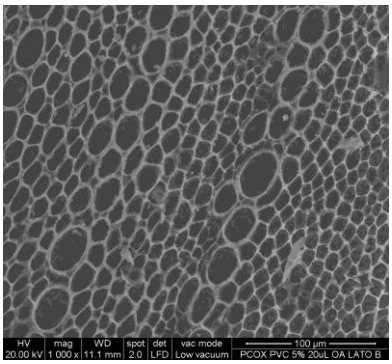

(a)

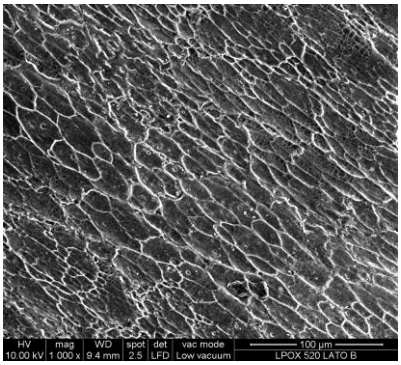

(b)

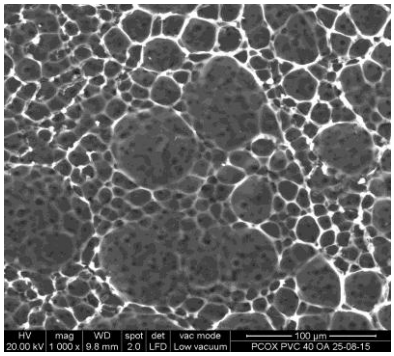

(c)

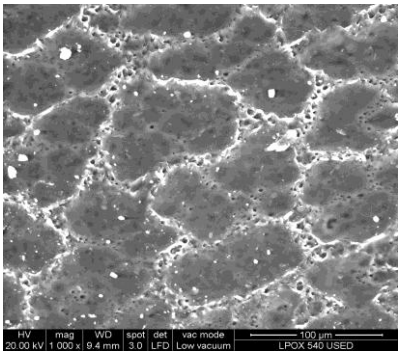

(d)

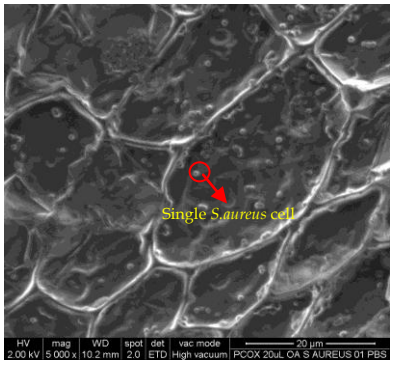

(e)

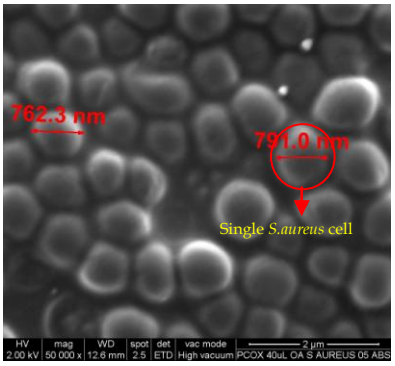

(f)

Figure 5.4 SEM micrographs of (a) P-520 x 1000 magnification (b) LP-520 x 1000 magnification (c) P-540 x 1000 magnification (d) LP-540 x 1000 magnification (e) P-520 with *S.aureus* cells x 5000 magnification (f) P-520 with *S.aureus* cells x 50000 magnification

5.3.2 PHOTOACTIVITY OF PCCox IN COMPARISON TO TPP-PVC

The photoefficiencies of P-520 and TP-520 against *S. aureus* are compared in Fig. 5.5. As can be seen, P-520 was capable to completely destroy *S. aureus* colonies in 90 minutes of illumination. On the other hand, TP-520 caused 100% destruction in 60 minutes itself at the 5% TPP concentration and same illumination conditions. Nonetheless both the films show high photoefficiency against *S. aureus*. At 60 minutes, P-520 caused 3 log reductions (99.4103%) in the bacterial survival (with an error bar of almost 1 order). The difference in the activities of the two films can be explained on the basis of light source used. PCCox (5 μM), in presence of an incandescent lamp caused more than 5-6 log reduction in *S. aureus* in 60 minutes of irradiation. Whereas the same concentration of PCCox caused between 4-5 log decrease in *S. aureus* survival when monochromatic blue LED lamp was used [46]. PCCox has a strong absorption spectrum at 480 nm (Soret band) and at 800 nm (Q-band) and hence a light source emitting a complete spectrum is necessary to fully excite PCCox. The incandescent lamp with UV cut-off emitted the whole visible spectrum When Blue LED lamp is used; only a part of the absorption spectrum is available to produce singlet oxygen. TPP has a sharp Soret band at 417 nm and small Q-bands in the region 600-800 nm. The multi-LED blue lamp emiting at 470 nm was sufficient to excite TPP completely and not so in PCCox. This makes clear the difference between the activities of the two PS-polymeric composite films.

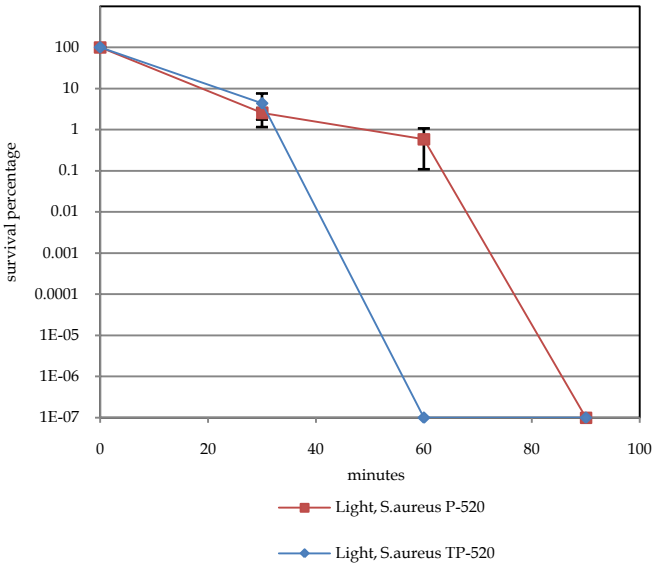

PVC has proven to be an easy and efficient carrier for the photosensitizers TPP and PCCox. In this study, it was also seen that the type of adipate plays an important role in imparting sensitivity to the films. The results of this study can be further used to develop methods to disinfect water using immobilized PS on PVC. Additional trials should be conducted to have a better understanding about the recovery and reuse of these films. Not only in water disinfection, PS-polymer inclusion also opens up the opportunity to use such materials in other anti-microbial applications like coatings, films, protective clothing etc.

6 Trial synthesis for expanded porphyrins

6.1 INTRODUCTION

Expanded porphyrins can find application in various fields from PDT to co-ordination chemistry and as sensing agents. With the aim of applying new materials for photodisinfection of water, pentaphyrinic macrocyle were synthesized and characterized. The precursors required for the macrocyle were also synthesized and are discussed below.

6.2 EXPERIMENTAL

6.2.1 SYNTHESIS OF 5-PHENYL DIPYRROMETHANE AND 5,10-DI PEHNYL TRIPYRRANE

Aryl substituted dipyrromethanes and tripyrranes are important precursors for synthesis of porphyrins and expanded porphyrins. The one pot synthesis of such compounds is a simple and high yielding route which is being followed widely [124]. Condensation of benzaldehyde with excess pyrrole in presence of TFA as catalyst resulted in a mixture of 5-phenyl dipyrromethane (**6**) and 5,10-diphenyl tripyrrane (**7**). Pyrrole (10 eq) was taken in a 3 neck round bottom flask to which benzaldehyde (1 eq) was added dropwise with bubbling nitrogen. TFA was added to the mixture and stirred under nitrogen for 15 minutes at room temperature. The reaction route is shown in scheme 6.1. The reaction was monitored by TLC (15% ethyl acetate in petroleum ether). The excess pyrrole was evaporated using a rotary evaporator and the dark viscous material was passed through a silica column to collect **6** and **7** in pure form.

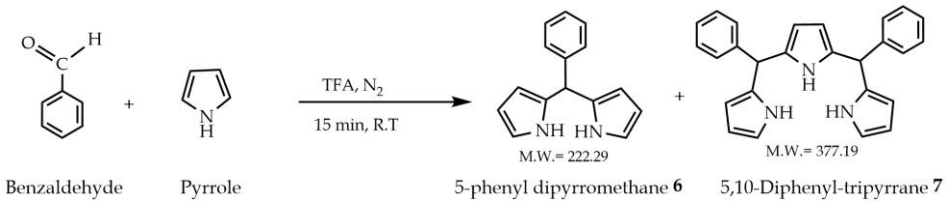

Scheme 6.1 Synthesis of compounds **6** and **7**

Table 6.1 Materials for **6** and **7**

Materials	Molecular weight	Milli moles	Weight taken (mg)	Density (g cm^{-3})	Volume
Pyrrole	67.09	100	6709	0.967	7 ml
Benzaldehyde	106	4	390	1.043	406 µl
TFA	114	0.38	44	1.48	30 µl

^{1}H NMR spectra were recorded for **6** and **7** (Figure 6.1 and 6.2). Compound **6** NMR (200 MHz, $CDCl_3$, 25°C): δ= 5.4 (s, 1H), 5.88 (m, 2H), 6.13(q, 2H), 6.61 (q, 2 H), 7.26 (m, 5 H), 7.82(br s, 2H).

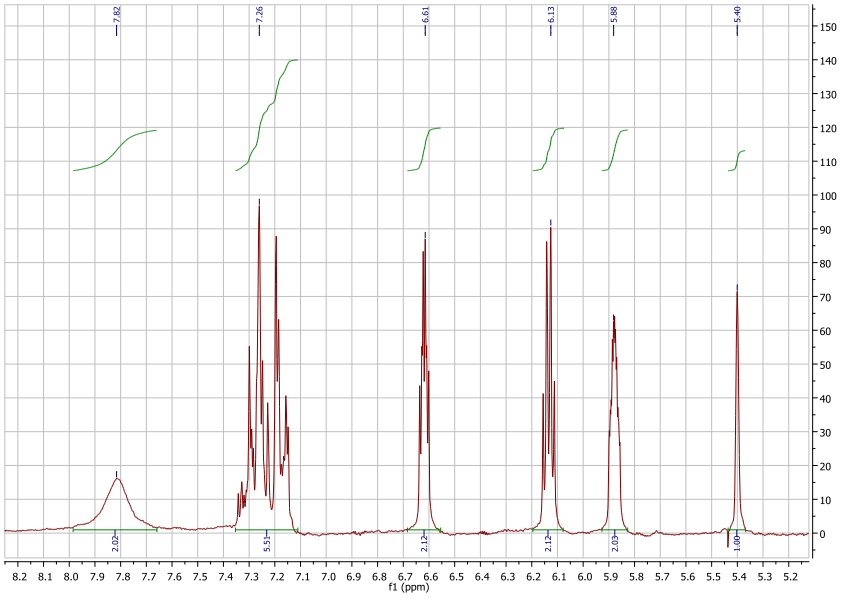

Figure 6.1 ^{1}NMR spectrum of 5-phenyl dipyrromethane **6**

Compound **7** NMR (200 MHz, $CDCl_3$, 25°C): δ=5.40 (s, 2H), 5.93 (q, 2H), 6.05 (m, 2H), 6.30 (q, 2H), 6.71 (dd, 2H), 7.44 (m, 10H), 7.97 (br s, 3H).

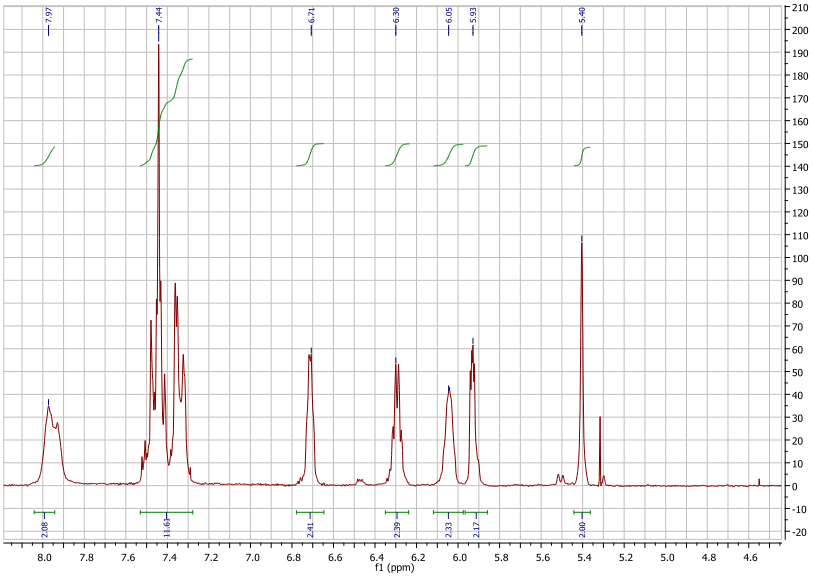

Figure 6.2 ^{1}NMR spectrum of 5,10-diphenyl tripyrrane **7**

6.2.2 FORMYLATION OF 5-PHENYL DIPYRROMETHANE

5-phenyl dipyrromethane was formylated following the Vilsmeier-Haack reaction.

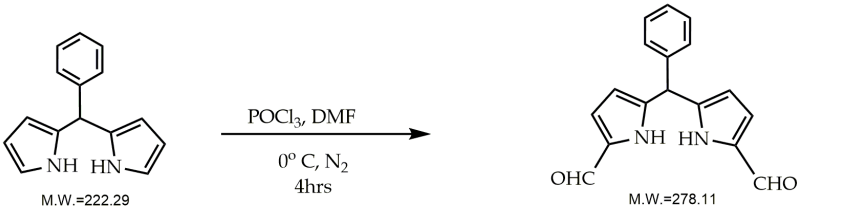

Scheme 6.2 Vilsmeier Haack formylation of **6**

650 µl (1.1 eq) of phosphoryl chloride ($POCl_3$) were added dropwise to 4 ml (8) of dimethyl formamide (DMF) under N_2 flux with stirring at 0°C. This mixture is Vilsmeier Haack reagent and was used to formylate **6**. The dipyrromethane **6** was dissolved in 3 ml of DMF in a two necked flask, cooled and fluxed with N_2.

2 ml of Vilsmeier reagent were added to the above mixture and stirred under N_2 atmosphere at 0°C. after 1.5 hours the reaction was brought to room temperature followed by addition 11.1 ml of saturated sodium acetate (CH_3COONa) solution. The reaction was allowed to stir for 4 hours at room temperature. The product was extracted using DCM (3 times), washed with water and brine (3 times). The organic phase was removed, dried using anhydrous sodium sulphate (Na_2SO_4) and evaporated to obtain 198.8 mg of pure product **8** (79.36 % yield). The product was characterized (figure 6.3) by ^{1}H NMR ((200 MHz, $CDCl_3$, 25°C): δ=5.59 (s, 1H), 6.03 (q, 2H), 6.83 (q, 2H), 7.27 (m, 5H), 9.14 (s, 5 H), 10.88 (br s, 2 H)).

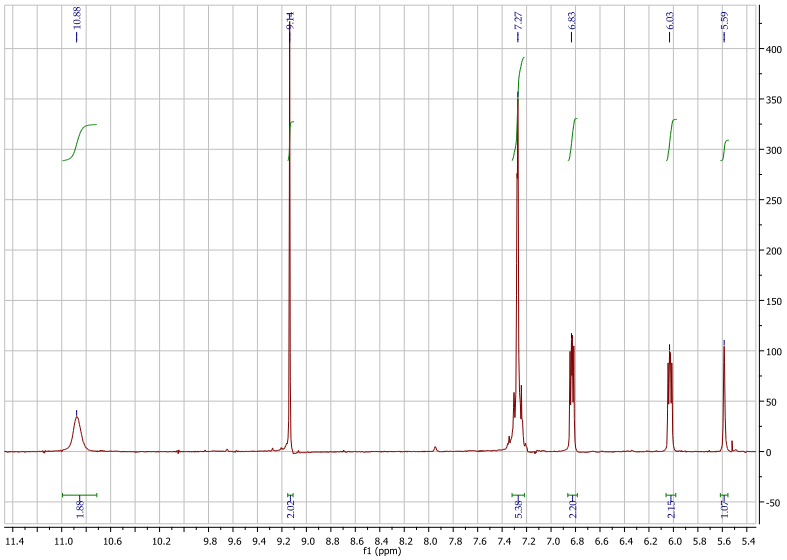

Figure 6.3 ^{1}HNMR spectrum of compound **8**

Table 6.2 Material stoichiometry for synthesis of **8**

Material	Molecular weight	Millimoles	Weight taken (mg)	Density (gcm^{-3})	Volume(µl)
Product **6**	222	0.9	200		
DMF	73.09	50.90	3270.28	0.944	4000
$POCl_3$	153.33	7.00	1073.31	1.65	650

6.2.3 SYNTHESIS OF 5-PYRIDYL DIPYRROMETHANE AND 5,10-DI PYRIDYL TRIPYRRANE

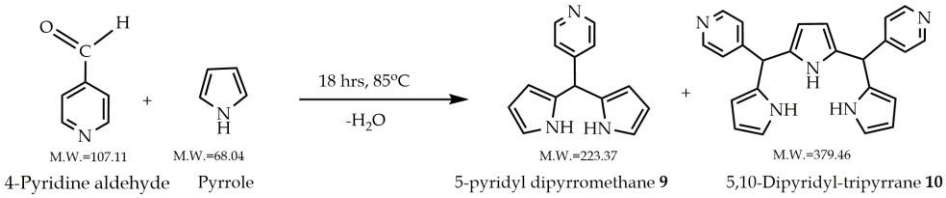

Scheme 6.3 Synthesis of compounds **9** and **10**

5-pyridyl dipyrromethane (**9**) and 5, 10-dipyridyl tripyrrane (**10**) were obtained by the condensation reaction between pyrrole and 4-pyridine aldehyde (5:1 ratio) at 85°C. Pyrrole was taken in a 50 ml 2 neck flask to which pyridine aldehyde was added dropwise and the reaction mixture was heated to 85°C. The reaction was refluxed for 18 hours with continuous stirring. The reaction was monitored by TLC on alumina (100% ethyl acetate). The excess pyrrole was evaporated on a rotary evaporator and the viscous residue was passed through an alumina column for separation and purification of **9** and **10**. **9** was eluted out with only ethyl acetate while 1% methanol in ethyl acetate was used to collect pure fractions of **10**. The two compounds were characterized by ^{1}H NMR (figure 6.3 and 6.4). Compound **9** NMR (200 MHz, $CDCl_3$, 25°C): δ=5.43 (s, 1H), 6.16 (q, 2H), 6. 70 (q, 2H), 7.09 (dd, 2H), 7.65 (dd, 2H), 8.39 (d, 2H), 8.60 (br s, 2H). Compound **10** NMR (200 MHz, $CDCl_3$, 25°C): δ=5.32 (s, 2H), 5.74 (d, 2H), 5.80 (s, 2H), 6.07 (q, 2H), 6.66 (dd, 2H), 7.01 (dd, 4H), 8.19 (d, 4H), 9.14 (br s, 3H).

Table 6.3 Reactant stoichiometry for **9** and **10**

Materials	Molecular weight	Milli moles	Weight taken (g)	Density (g cm^{-3})	Volume (ml)
Pyrrole	67.09	70	4.7	0.967	4.85
4-pyridinealdehyde	107.11	14	1.5	1.043	1.31

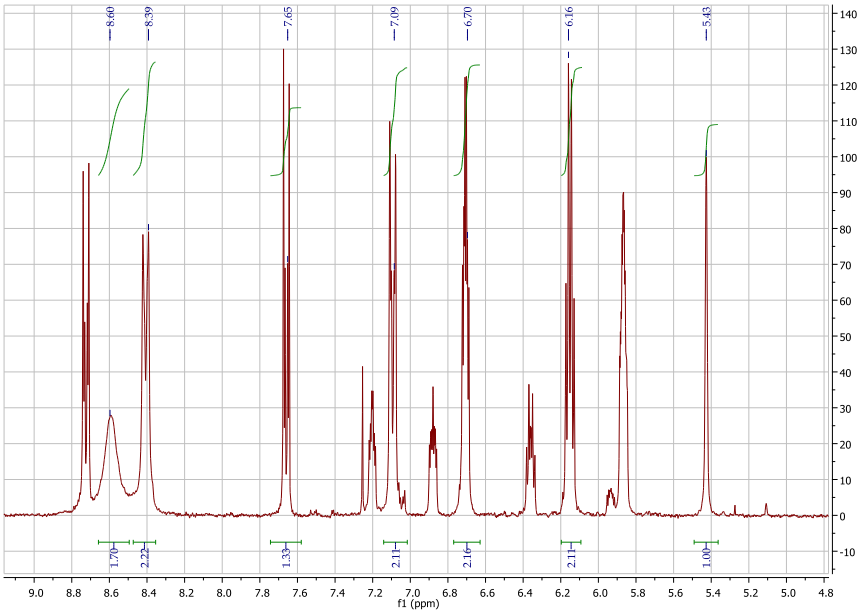

Figure 6.4 ^{1}HNMR spectrum of **9**

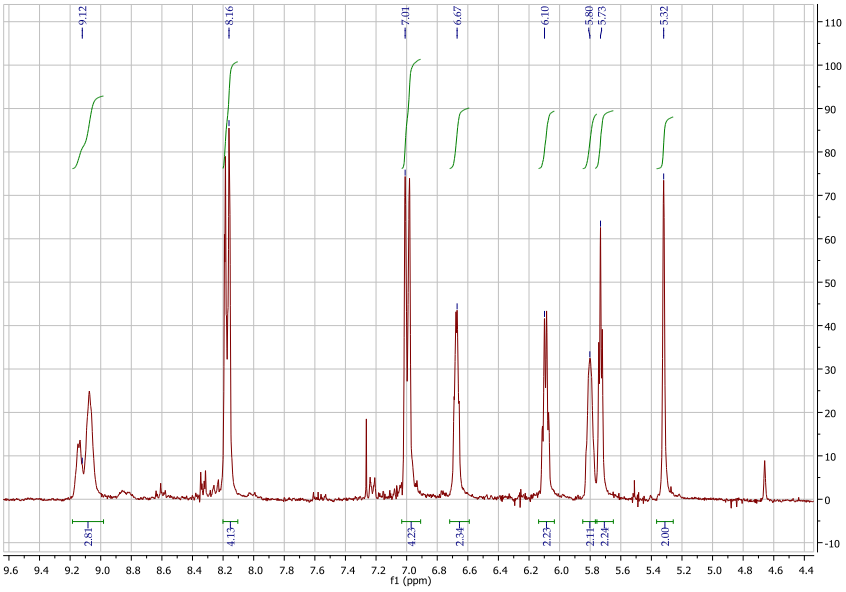

Figure 6.4 ^{1}HNMR spectrum of compound **10**

6.2.4 SYNTHESES OF THE PENTAPHYRINIC MACROCYCLE

The trial syntheses of pentaphyrinic macrocycles were carried out using the precursors **6**, **7**, **8** and **10** in different combinations at different times. Three different syntheses routes were followed:

- Condensation reaction between **7** and **8** using TFA as catalyst
- Condensation reaction between **7** and **8** using BF_3 as catalyst
- Condensation reaction between **6**, **7** and 4-pyridine aldehyde

The experimental procedure and the discussion are combined in sec. 6.3

6.3 RESULTS AND DISCUSSION

*6.3.1 SYNTHESIS OF MACROCYLE BY REACTION BETWEEN **7** AND **8** WITH TFA AS CATALYST-NO OXIDATION*

7 and **8** in equimolar ratios (table 6.4) were taken in a clean round bottom flask covered with an aluminium foil to protect from light. Dry degassed DCM was added to dissolve the reactants followed by TFA at room temperature for 20 hours under N_2 atmosphere (Scheme 6.4). The reaction was monitored by UV-visible spectroscopy (figure 6.6). The reaction mixture without any further purification was evaporated and analysed by ^1H NMR and ESI-mass spectroscopy.

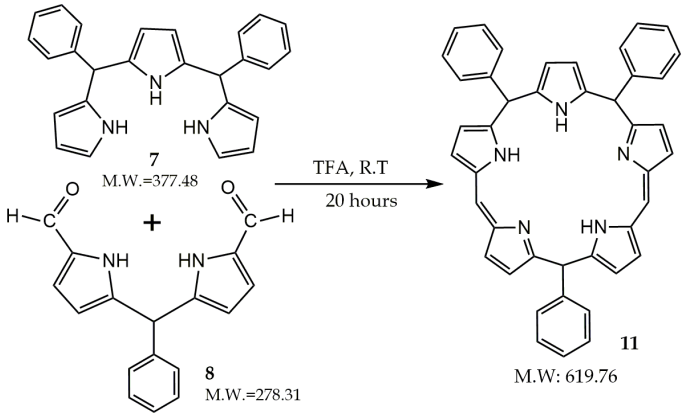

Scheme 6.4 TFA catalysed reaction between **7** and **8**

Table 6.4 Reaction stoichiometry

Materials	Molecular weight	Milli moles	Weight taken (mg)
Compound **7**	377.48	0.052	19.82
Compound **8**	278.11	0.052	14.60
TFA	114	0.525	59.85 (40.44µl)

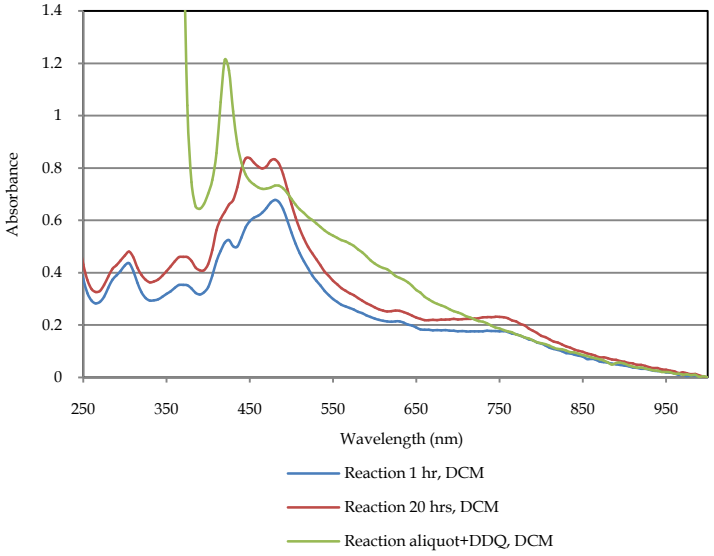

Figure 6.6 UV-visible spectral changes during the reaction

As seen in fig. 6.6, the UV-spectrum of TFA catalysed reaction between 7 and 8 shows a shoulder peak at 440 nm and 475 nm and a small absorbance peak at 750. The absorption at 475nm strongly supports the occurrence of an epanded porphyrin, whereas the absorption peak at 440 nm appears to be a porphyrin in acidic medium. A small quantity of DDQ was added in the UV-cuvette to observe the changes during oxidiation. It was observed that during DDQ-oxidation, porphyrin is rapidly formed with sharp absorption at 420 nm.

In the ^{1}H NMR spectrum are seen 2 peaks of higher intensity at δ=9.00 and 9.5. This reveals that the pyrrolic protons deshielded which can belong to either a fully oxidized porphyrin or a pentaphyrin. In the present reaction, oxidation of the product was not carried out. The deshielded protons could possibly belong to a porphyrin which is likely to be formed due to breaking of a pentaphyrinic macrocyle.

The mass spectrum also show the presence of small amount of di phenyl porphyrin (M.W= 462.18) at m/z= 463.2 $[M+1]^{+1}$. The ESI-mass also supports the formation of a pentaphyrinic macrocyle with the peak at m/z= 618.3 which corresponds to the $[M+1]^{+}$ ion of compound **12** (M.W=617.74). This mass can also belong to an N-fused pentaphyrin **13** which is also likely to be formed during condensation. There exists a severe steric congestion due to which the molecule takes up the fused-conformation with 2 inverted pyrroles. This conformation is probably easily broken to result in a meso tri-phenyl porphyrinic cycle (reduced form) **14** (M.W=540.66) during evaporation. This is confirmed by the presence of m/z=541.2. The formation of meso tri-phenyl porphyrin is only possible through the pentaphyrinic macrocylce. Hence, in this reaction it was possible to study the formation of an expanded porphyrin in its reduced form.

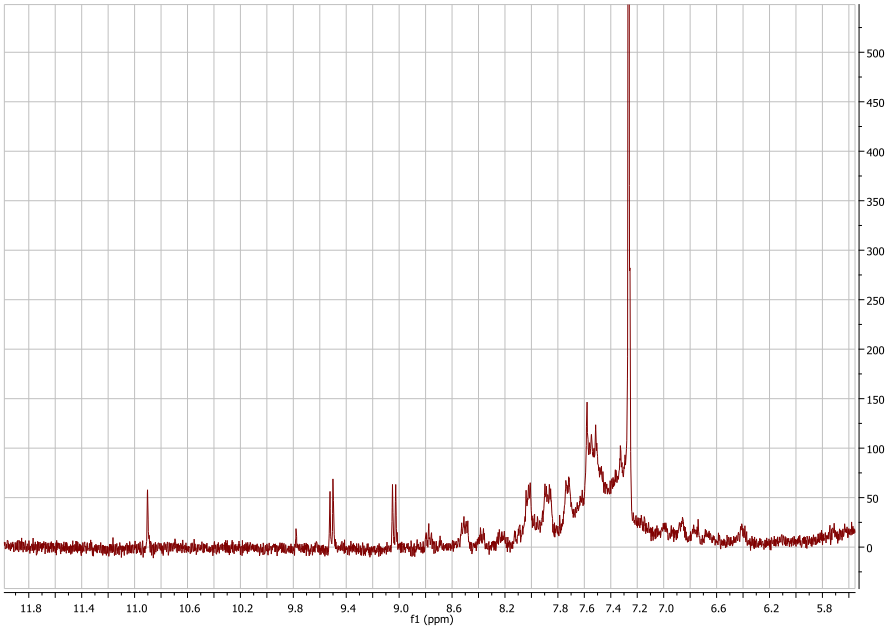

Figure 6.7 ^{1}H NMR spectrum of crude product of reaction **6.4**

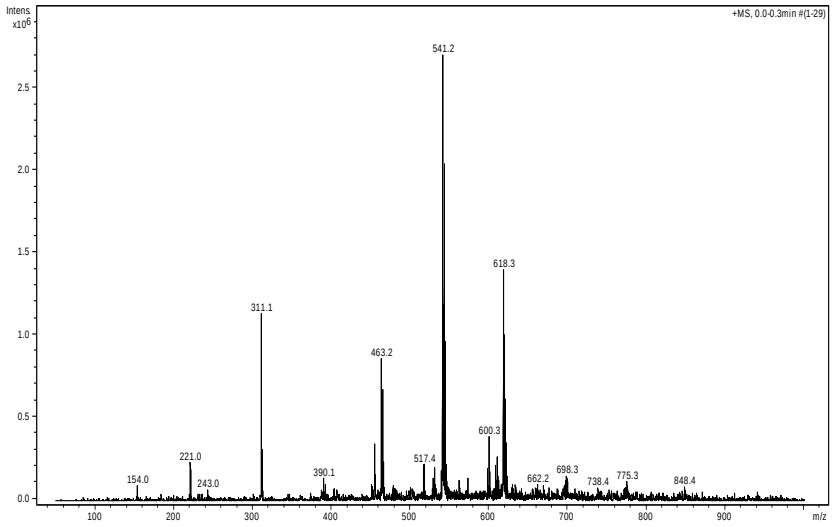

Figure 6.8 ESI-mass spectrum of crude product of reaction **6.4**

*6.3.2 CONDENSATION REACTION BETWEEN **7** AND **8** WITH TFA AS CATALYST AND DDQ OXIDATION*

In this reaction, **7** and **8** were reacted together in presence of TFA as a catalyst. Compound **8** was dissolved in dry and degassed DCM in a 2 neck round bottom flask. Compound **7** was quickly added to the mixture in absence of light. The reaction was continued for 2 hours at room temperature and N_2 atmosphere. The reaction was monitored by UV-visible spectroscopy at regular intervals. After 2 hours of reaction, a known amount of DDQ was added to the reaction and the reaction stirred for 1 hour. The reaction mixture was evaporated to obtain the crude product which was then passed through an alumina bed (petroleum ether/ethyl acetate) to separate the formed products.

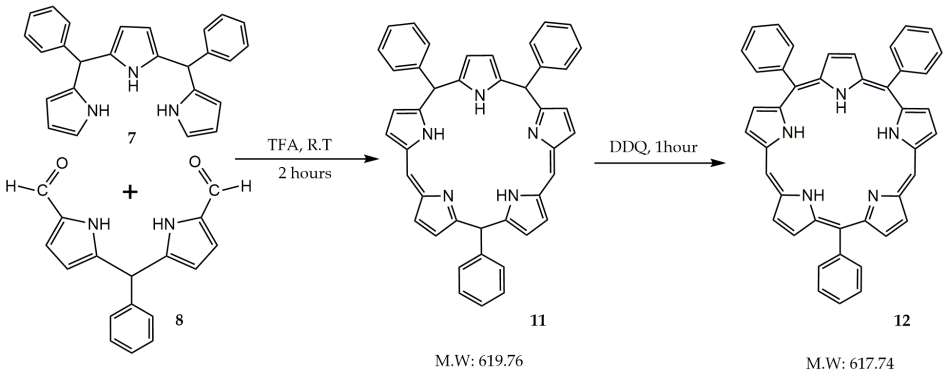

Scheme 6.5 Synthetic route for **12**

Table 6.5 List of materials and their molar quantities for **13**

Materials	Molecular weight	Milli moles	Weight taken (mg)
Compound **7**	377.48	0.052	19.82
Compound **8**	278.11	0.052	14.60
TFA	114	0.525	59.85 (40.44µl)
DDQ	227.01	0.105	23.83

In the UV-visible spectrum (Fig. 6.9), it is seen that during the reaction, the major absorption peak is at 470 nm which increases in intensity with time simultaneously with reduction in the dimer concentration 300 nm. But after DDQ oxidation, porphyrin is the major product (λmax= 435nm) as per the data obatined by absorption spectra (Fig 6.9). The formation of porphyrin is also confirmed after passing the product through alumina column. Two fractions from the column were collected. The first column fraction shows a sharp Soret band at 415 nm characterisitic of porphyrin. The column fraction was evaporated to obtain 6.8 mg of the product (porphyrin). The second fraction also shows the presence of porphyrin but with very low intensity at 415 nm and 445 nm. Both the fractions from the column were evaporated and analysed with ^{1}H NMR and ESI-mass spectroscopy.

In the NMR spectrum of the first fraction (fig. 6.10), the peaks observed can be attributed to tri-phenyl porphyrin **18** ^{1}H NMR ($CDCl_3$), δ=-3.01 (br s, 2H), 7.80 (m, 9 H), 8.28 (dd, 6 H), 9.08 (d, 4H), 9.37 (d, 4H), 10.30 (s, 1H). The ESI-mass spectrum of this fraction shows peaks at m/z= 311.1, 543.3 and 615.3 as the major signals. Tri phenyl porphyrin **18** (M.W=538.66), which was considered to

be predominantly formed showed no corresponding peak in the ESI-mass. m/z=543.3 is probably a linear fragment **15** formed during evaporation. The peak of m/z=615.3 is equal to mass of $[M+1]^{+1}$ ion of tetra phenyl porphyrin **16** (M.W=614.25) but this product is the least likely to be formed unless there existed a triphenyl tetrapyrrane as an impurity. But however, the intensity of this peak is not so low to be completely neglected.

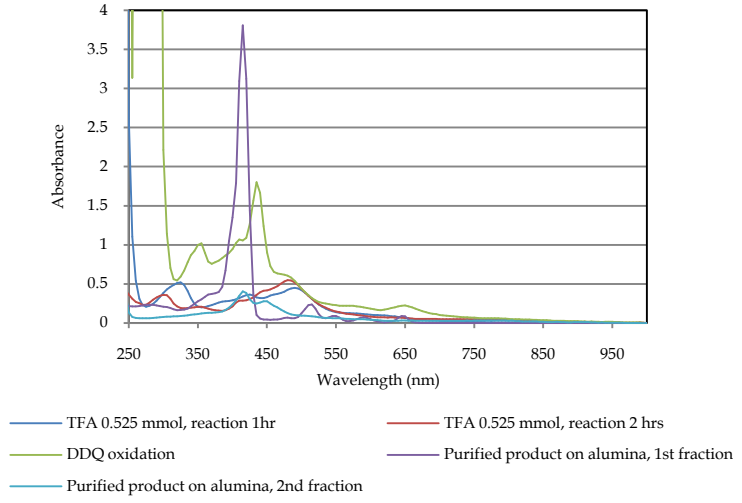

Figure 6.9 UV-visible spectral changes during reaction

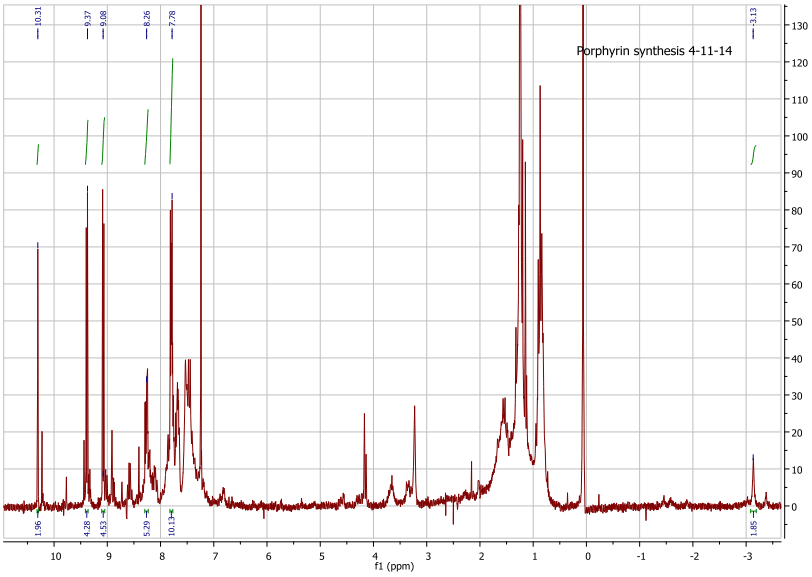

Figure 6.10 ^{1}H NMR spectrum of the product after column (first fraction)

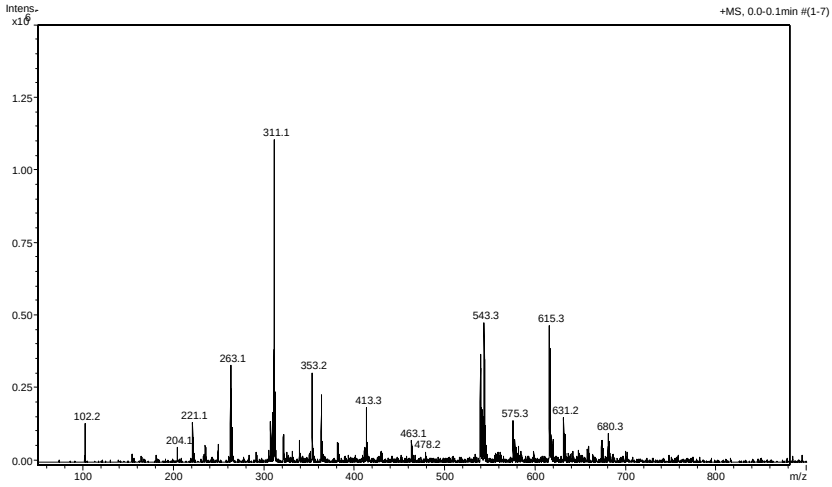

Figure 6.11 ESI-mass spectrum of product (first fraction)

The ^{1}H NMR spectrum of the second fraction show 2 different peaks in the negative region which implies that two different porphyrins were formed. The respective peaks of the deshielded porphyrin protons can be seen between 7-10 ppm. On the contrary, the ESI-mass shows no m/z corresponding to either diphenyl porphyrin **17** or tri-phenyl porphyrin **14**. The peak at m/z=543.3 is also seen here, which as previously discussed is a linear component **15** arising from a partially oxidized pentaphyrin macrocycle.

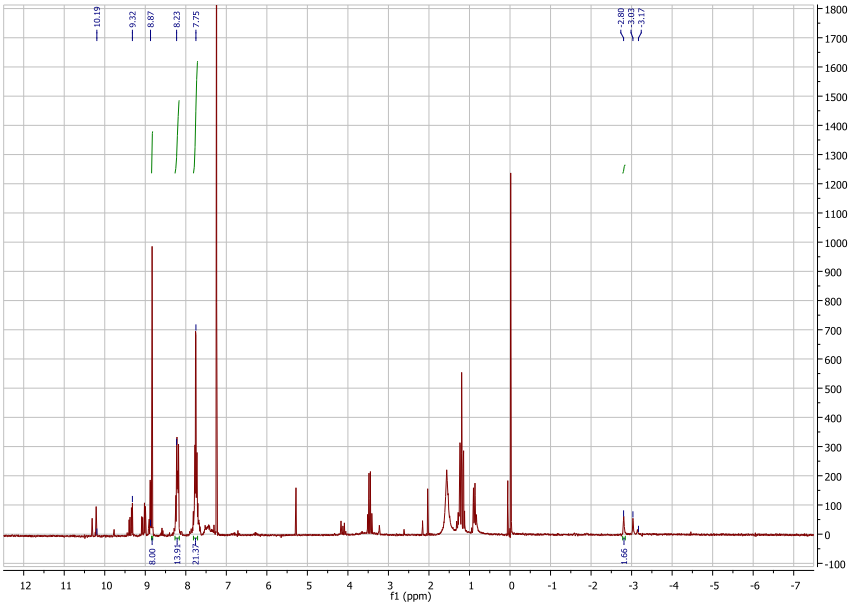

Figure 6.12 ^{1}HNMR spectrum of the column purified product (second fraction)

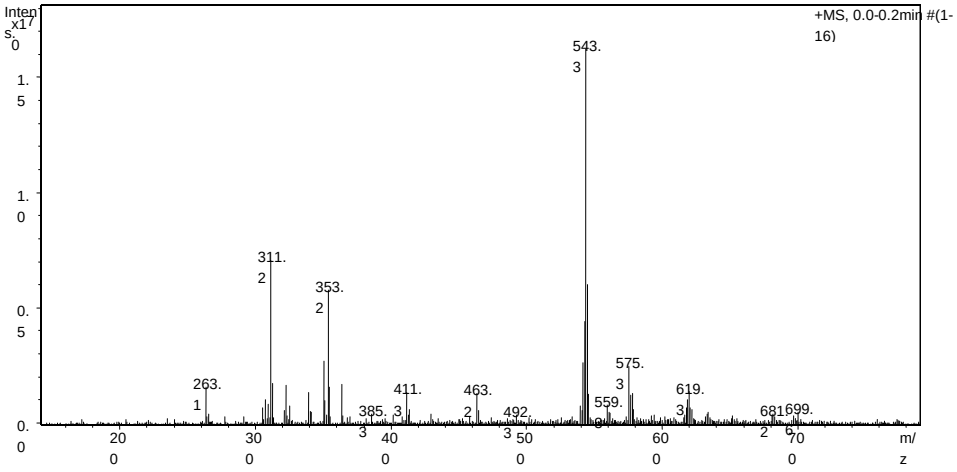

Figure 6.13 ESI-mass spectrum of purified product after column (second fraction)

6.3.3 BF_3 CATALYSED REACTION BETWEEN **7** AND **8**

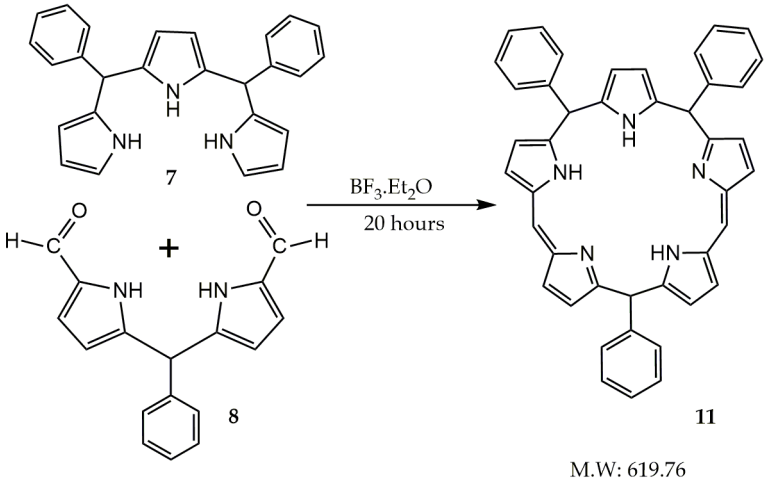

Scheme 6.6 BF_3 catalysed reaction between **7** and **8**

Table 6.6 Reaction formulation

Materials	Molecular weight	Milli moles	Weight taken (mg)
Compound **7**	377.48	0.05	19.82
Compound **8**	278.11	0.05	14.60
$BF_3.Et_2O$	141.93	0.10	14.35 (12.7µl)

In this trial reaction, **8** was dissolved in dry and degassed acetonitrile (CH_3CN) in a 2 neck flask. Boron trifluoride diethyl etherate ($BF_3{\cdot}Et_2O$) was added to the solution followed by a solution of **7** in acetonitrile protected by light. The reaction was continued at room temperature under N_2 for 20 hours. The reaction was monitored by UV-visible spectroscopy (fig.6.14). After 20 hours the reaction was divided into two parts:

- Part A: the reaction was heated to 40°C for 2 hours.
- Part B: the reaction was continued by doubling the concentration of $BF_3{\cdot}Et_2O$. The reaction was continued for 18 hours to observe some changes. After 18 hours the reaction was again divided into 2 parts

- Part B1: this part of the reaction was allowed to oxidize in presence of excess of TFA for 1 hour, evaporated and finally passed over a bed of silica
- Part B2: this part of reaction was oxidized by DDQ for 1 hour. The reaction mixture was evaporated after 1 hour and analysed by ^{1}H NMR and mass spectroscopy.

Looking at the UV-visible spectra (Figs. 6.14 to 6.18), it can be assumed that the product formed during BF_3 catalysed reaction has a strong absorbance at 485 nm. This peak increases in intensity with the reaction time at the first concentration of BF_3 (0.1 mmol). The absorption at 485 nm is consistent even after the reaction undergoes series of changes. This implies that the product formed (which is assumed to be a pentaphyrinic macrocycle) is very stable in acetonitrile as solvent. When the reaction is heated to 40°C, the intensity of the peak at 485 nm did not undergo a significant change (part A). But when DDQ was added into the UV cuvette, the peak at 485 nm was disturbed and the strong absorbance disappeared.

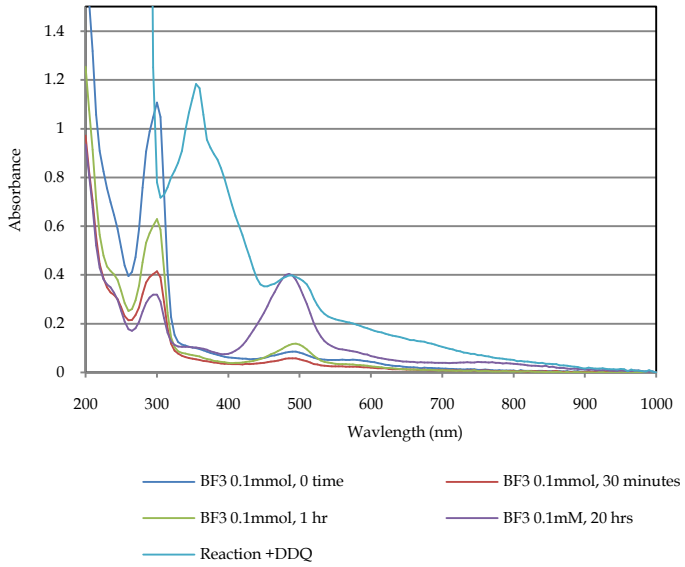

Figure 6.14 UV-visible spectrum of 0.1 mmol BF3 catalysed reaction

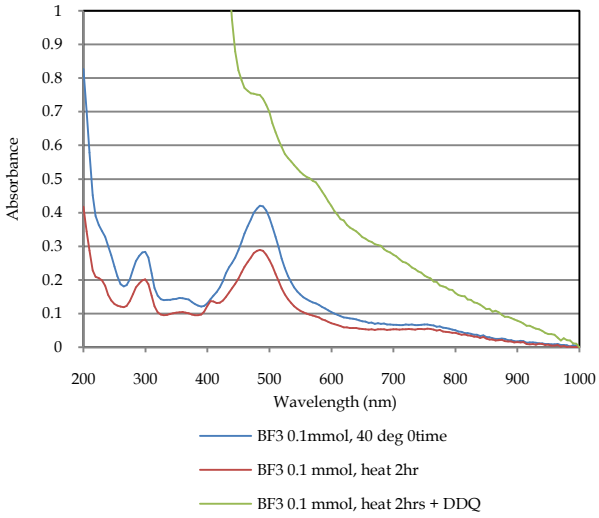

Figure 6.15 Spectral changes in the reaction after heating (part A)

In part B, when the BF_3 concentration was doubled, the absorbance at 485 nm still remained unchanged. Assuming, a pentaphyrinic macrocycle was formed, the reaction was then subjected to two different types of oxidation: TFA (part B1) and DDQ (part B2). In part B1, during oxidation with TFA the product begins to show absorbance at 750 nm and increases with time. This absorbance signal however is not sharp. It is too broad to consider as a product peak of an expanded porphyrin. This type of signal can be obtained when linear polymeric reaction takes place. The reaction was dried using N_2 gas and passed over a silica column. The fraction eluted out showed a strong and sharp absorbance corresponding to porphyrin at 415 nm. This product was later discarded as was not the desired product. Instead, B2 showed more stable state of the product even in presence of DDQ (known quantity). Also, no absorbance was observed at 750 nm. The strong absorbance at 485 nm was consistent. The reaction mixture was evaporated and analysed by ^{1}H NMR (Figs. 6.19 and 6.20) and ESI-mass spectroscopy (Fig. 6.21). The ^{1}H NMR (acetonitrile-*d*) spectrum (Fig. 6.19) does not provide much idea about the pentaphyrin. The major signal seen in the spectrum is a huge broad signal between 7.0 to 8.5 ppm and small signals between 1.0 to 3.0 pm. Addition of TFA to the sample does not resolve the ^{1}H NMR spectrum (Fig. 6.20). All the signals were unchanged and thus no structural elucidation could be generated with the ^{1}H NMR signals. However,

another aspect to be considered is that the ^{1}H NMR spectrum of this reaction was recorded using acetonitrile-*d* as the solvent instead of $CDCl_3$ (as was the case in previous section). Porphyrins and expanded porphyrins exhibit different behaviours in different solvents. The entire present reaction system was performed using acetonitrile. The solubility of the reactancts and product/s was better in acetonitrile. Also, reactions in acetonitrile have provided porphyrins in good yield and without scrambling [22A, 23A]. Acetonitrile, undoubtedly is a good solvent to carry out 3+1 or 3+2 condensation reactions and more trials should be conducted with acetonitrile as reaction solvent.

In the ESI-mass spectrum of part B2, the major signal is observed at m/z=463.5 which corresponds to diphenyl porphyrin **17** (M.W=462.18). Also, the occurrence of triphenyl porphyrin is seen as $[M+1]^{+1}$ at m/z = 539.5. However, porphyrin related signals were not observed in UV-visible as well as in ^{1}H NMR spectral analysis.

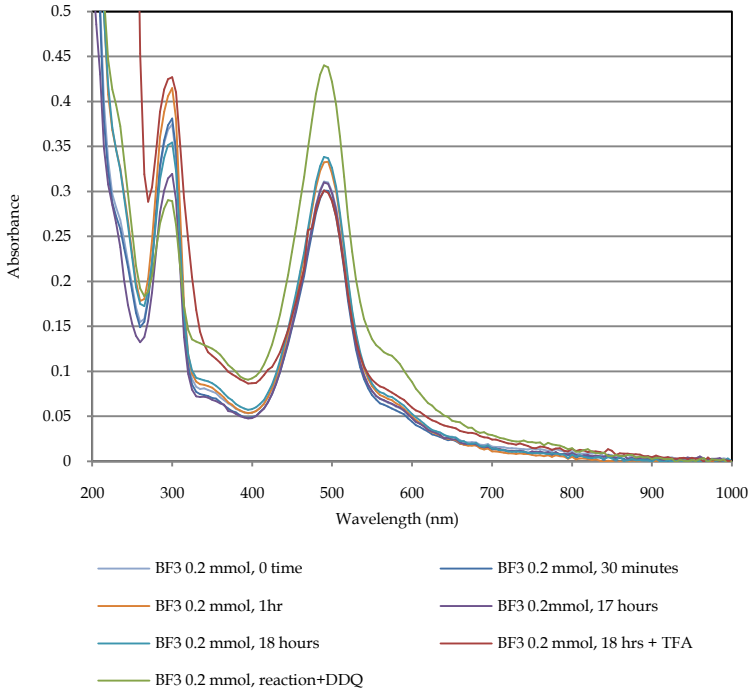

Figure 6.16 UV-visible spectral changes after increasing BF_3 concentration (part B)

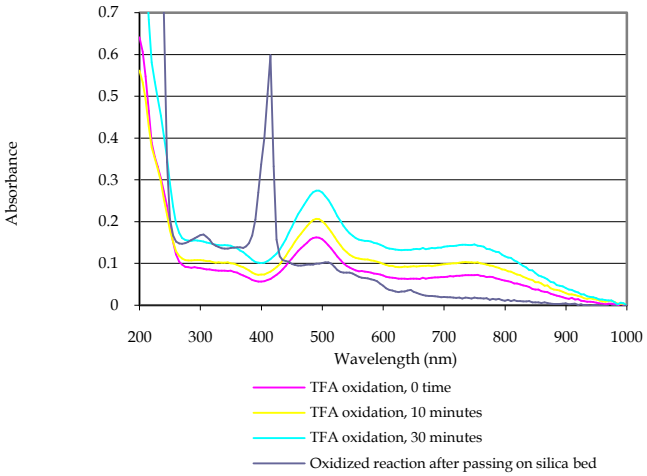

Figure 6.17 Spectral changes during TFA oxidation (part B1)

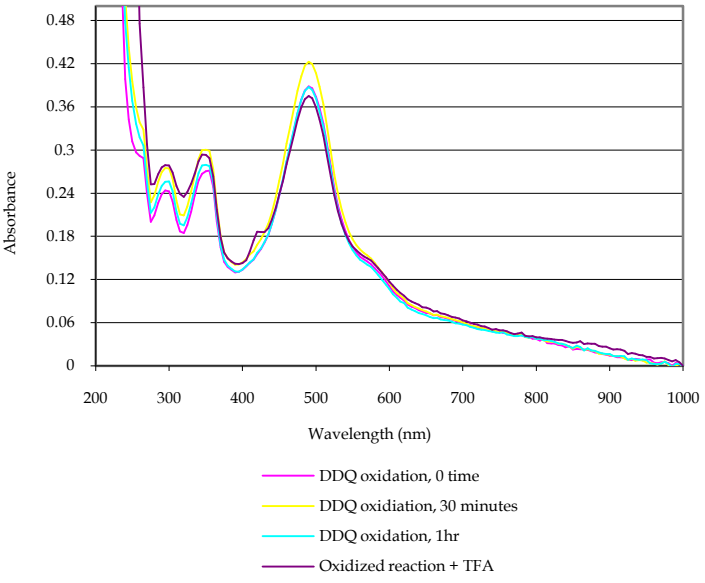

Figure 6.18 Spectral changes during DDQ oxidation (part B2)

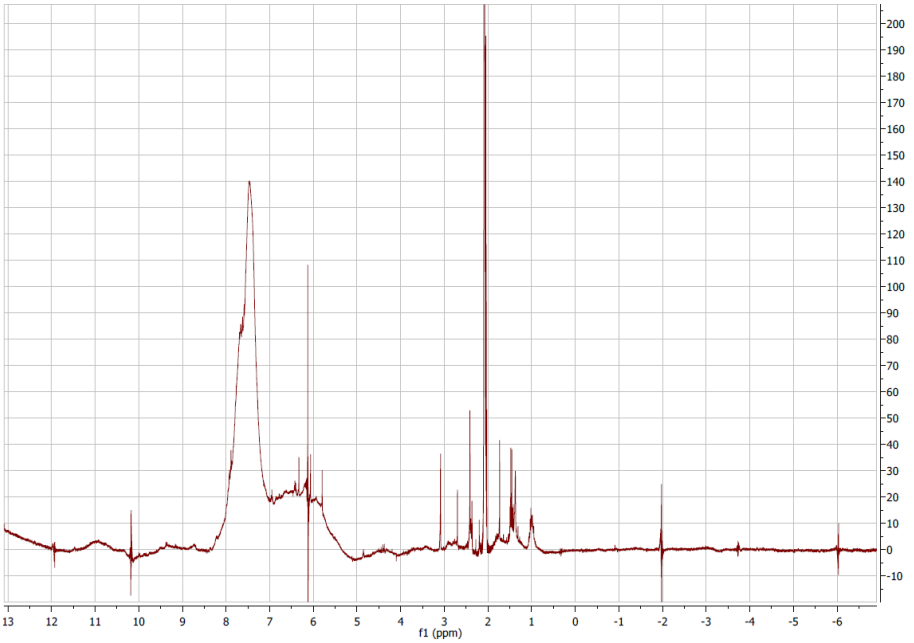

Figure 6.19 ^{1}H NMR of the DDQ oxidized product

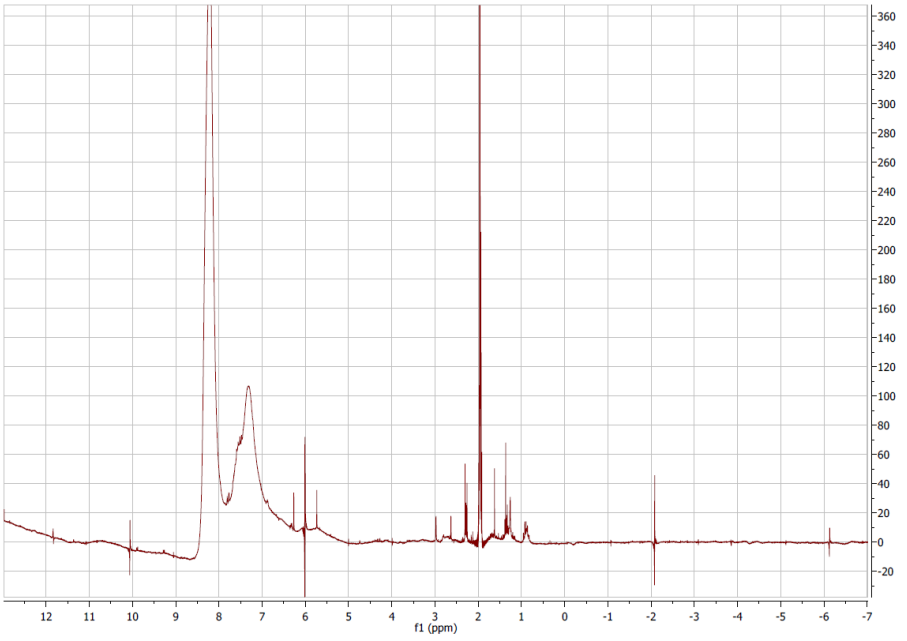

Figure 6.20 ^{1}H NMR of DDQ oxidized reaction + TFA

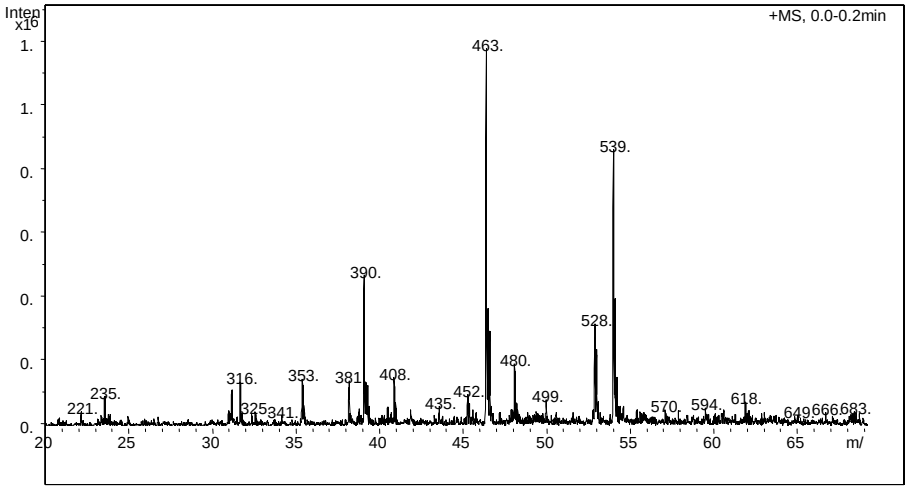

Figure 6.21 ESI- mass spectrum of DDQ oxidized product (B2)

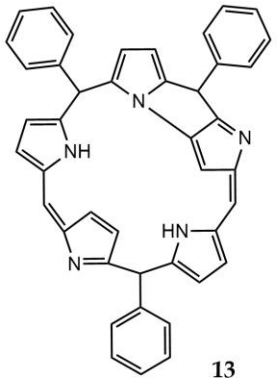

13

M.W: 617.26

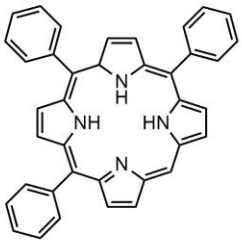

14

M.W: 540.66

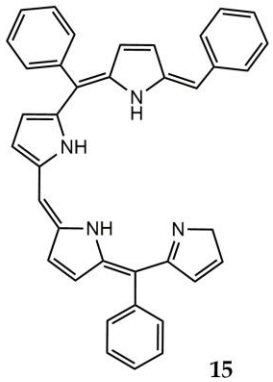

15

M.W:542.25

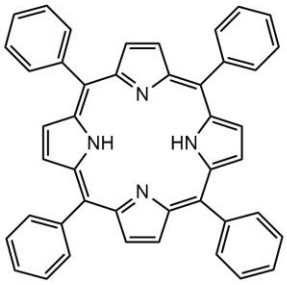

16

M.W: 614.25

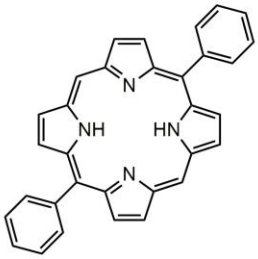

17

M.W=462.18

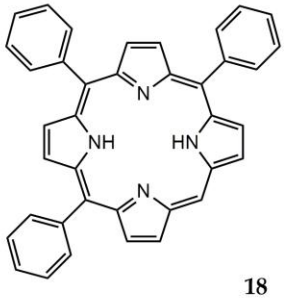

18

M.W.=538.64

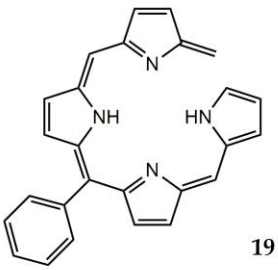

19

M.W=388.17

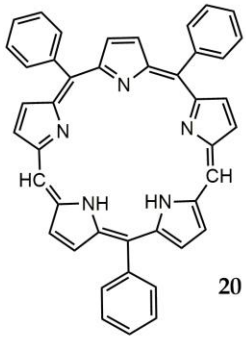

20

M.W.= 615.24

Figure 6.22 Structures of possible products during reaction between **7** and **8**

6.3.4 REACTION BETWEEN 6 AND 7 WITH 4-PYRIDINE ALDEHYDE

Photosensitizers capable of causing a photodynamic effect in a broad spectrum of microoranisms are very desirable. With this aim, 5,10-dipyridyl tripyrrane **10** and dipyrromethane dialdehyde **8** (table 6.7) were reacted in presence of TFA (scheme not shown). In this reaction though, the tripyrrane bearing 2 pyridyl groups (electron withdrawing) caused a strong –I effect in the molecule. This reduced the reactivity of the molecule causing α-carbons of pyrrole to be electron deficient and therefore unable to undergo a substitution. In order to overcome this problem, the dipyrromethane **6** and the tripyrrane **7** were reacted together with pyridine aldehyde (which reacts well with pyrroles Scheme 6.3). The reaction is represented in Scheme 6.7.

Compound **7** along with pyridine aldehyde and TFA were dissolved in dry and degassed DCM in two-necked round bottom flask. Compound **6** dissolved in DCM was added dropwise to the above mixture in absence of light. After the completion of addition, the reaction was further stirred for 1 hour. The reaction was monitored by UV-visible spectroscopy (Fig. 6.23). The reaction was then divided into 2 equal parts

- **Part A**- a known quantity of DDQ (Table 6.7) was added to this part and continued to react for 1 hour. The reaction was monitored by UV-visible spectroscopy during the 1 hour. The crude product was obtained by evaporating the reaction mixture under N_2.
- **Part B**- no changes were made in this part of reaction. The reaction mixture was evaporated with N_2 and analysed by UV-visible (DCM), ^{1}H NMR ($CDCl_3$) and ESI-mass spectroscopy.

Table 6.7 Stoichiometric ratios for the reaction 6.7

Materials	Molecular weight	Milli moles	Weight taken (mg)
Compound **6**	222.29	0.025	5.55
Compound **7**	377.48	0.025	9.42
4-pyridine aldehyde	107.11	0.05	5.53 (5.3 µl)
TFA	114	0.25	29.93 (20.22 µl)
DDQ	227	0.0125	2.8

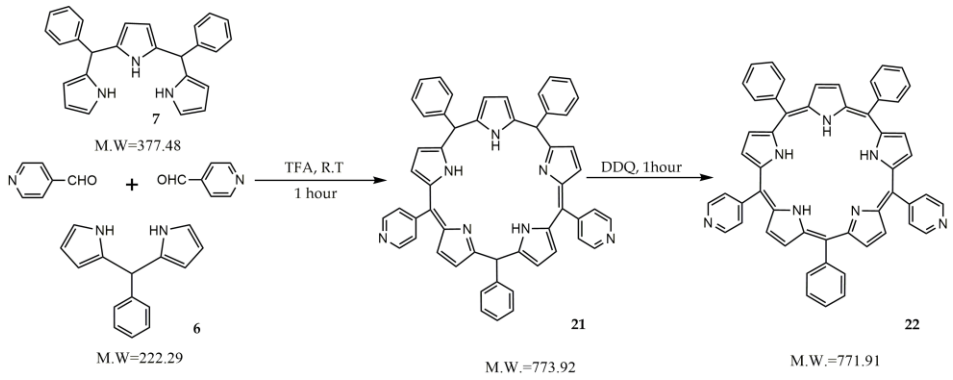

Scheme 6.7 Reaction between **6** and **7** with 4-pyridine aldehyde

During the first hour of reaction, it was observed in the absorption spectra (Fig. 6.23) that a peak at 485 nm is a prominent signal and remains so till the end of reaction. When DDQ was added in the UV-visible cell, it was seen that absorption at 438 nm appears which is typical of porphyrins.

In the UV-visible spectrum of **part A** (Fig. 6.24), a similar change was observed. The intensity of the absorption peak at 485 nm was decreased and the absorption at 438 nm increased significantly during 1 hour of oxidation with DDQ. ^{1}H NMR spectrum of part A (Fig. 6.26) showed many signals between 5.0 and 6.00 ppm that can pertain to pyrrolic protons. Also, it appears that phenylic protons lie between 7.00 and 8.00 ppm as well as pyridyl protons between 8.0 to 9.0 ppm. Two small signals are seen at 8.96 and 9.44 ppm. Such signals are characteristic of completely oxidized porphyrinic molecules or even a pentaphyrin. The ESI-mass spectrum (fig. 6.28), on the other hand shows the highest abundant ion at m/z=556.5 followed by m/z=616.5. No side product or fragment that can be formed in the reaction bears M.W=555 or M.W=615 was found. But very close is the linear fragment **23** (M.W=556.24) which can be formed only by the breaking of a pentaphyrinic cycle. Also, the porphyrin **24** has M.W=616.24.

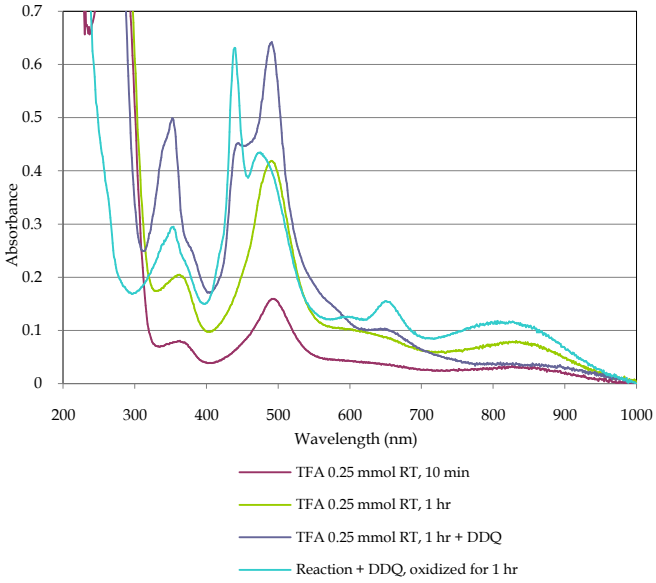

Figure 6.23 TFA catalysed reaction, UV-visible spectra

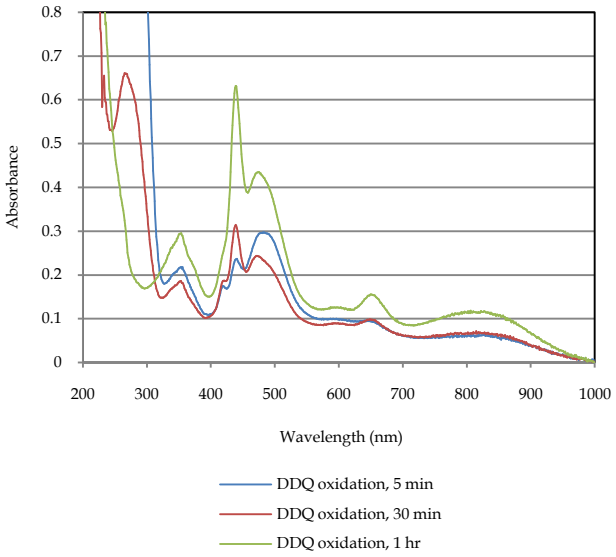

Figure 6.24 UV-visible spectral changes during DDQ oxidation

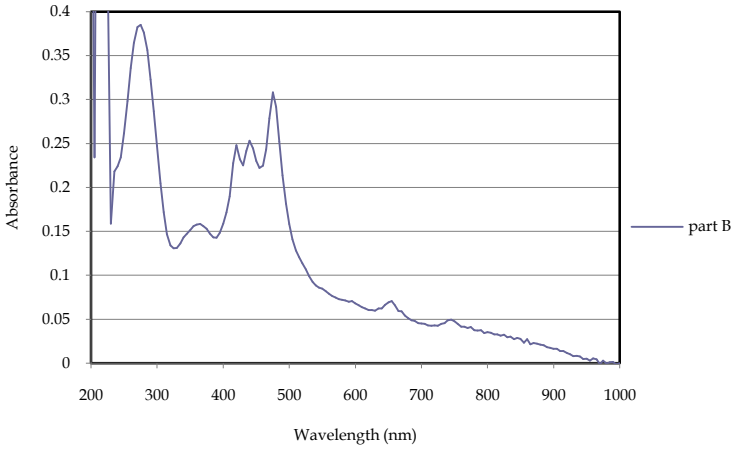

Figure 6.25 UV-visible spectra of crude without oxidation (evaporated)

The UV-visible spectrum of **part B** (Fig. 6.25) shows that the absorbance at 480 nm has the highest intensity, but also there are two other absorbances at 420 and 440 nm which can probably show the formation of small amount of porphyrin. A very small absorbance is also observed at 750 nm which supports the possibility of the success of reaction. The ^{1}H NMR spectra of **part B** (Fig.6.27) show lesser resolved signals with the major protons appearing between 5.0 to 6.5 ppm and also between 7.0 and 8.0 ppm. This nature of the spectrum is changed when TFA is added to the product with a broad signal appearing at 10.5 ppm. The ESI-mass spectrum (Fig. 6.29) interestingly show the occurrence of one major ion in much higher abundance as compared to others at m/z=622.4. The corresponding mass of this peak (M.W=621.4) is of a fragment arising from the reduced pentaphyrin **21**. This fragment is formed by the loss of two adjacent meso-phenyl groups into the structure **25**.

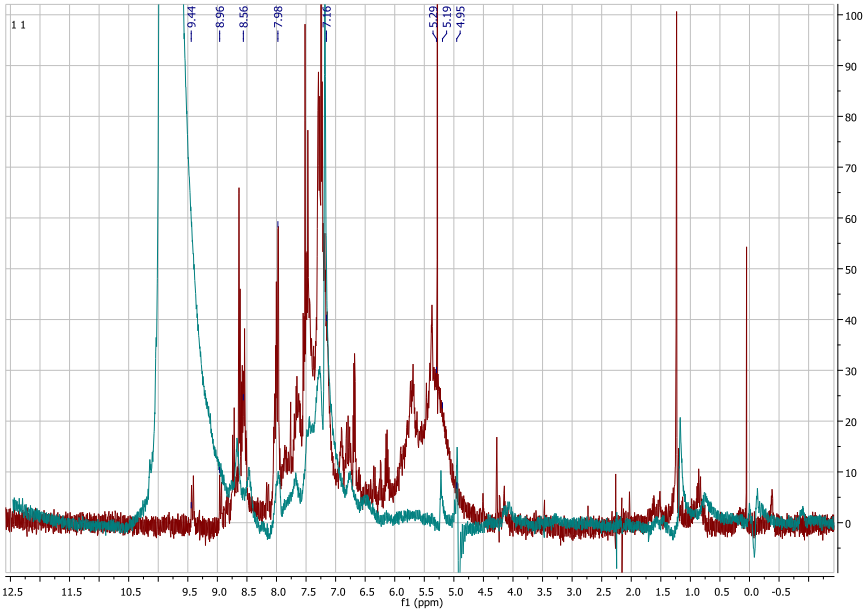

Figure 6.26 ^{1}H NMR spectra of part A and part A + TFA

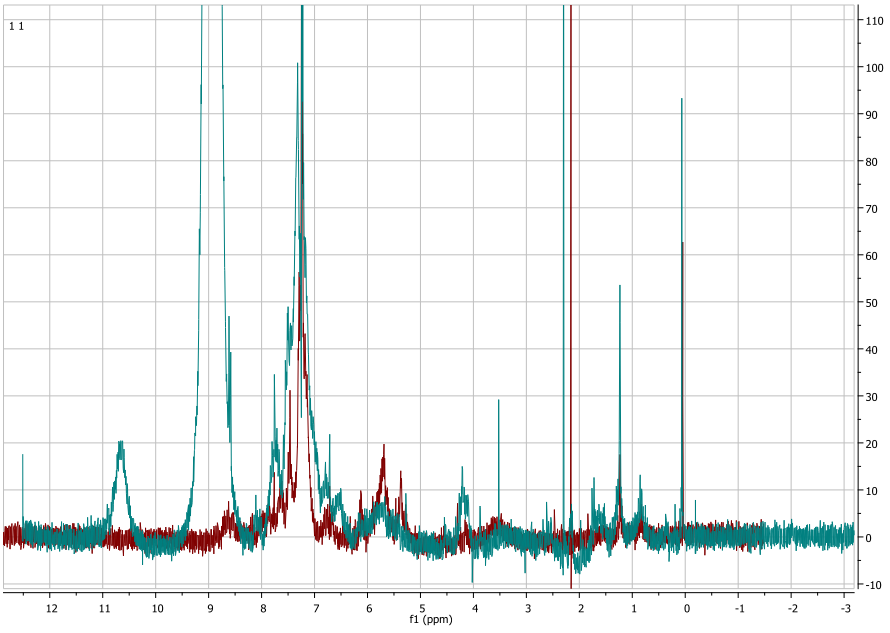

Figure 6.27 ^{1}H NMR of part B and part B + TFA

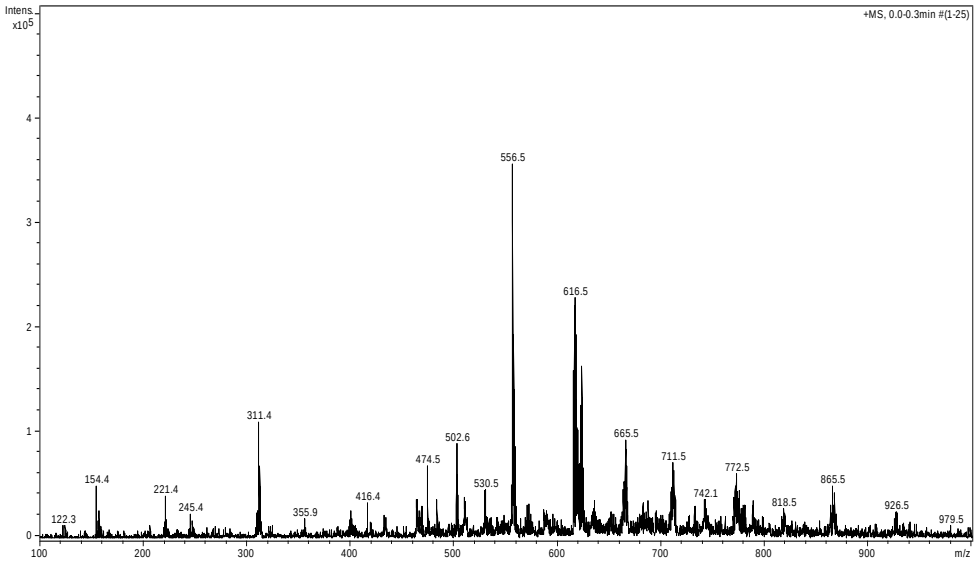

Figure 6.28 ESI-mass spectrum of part A

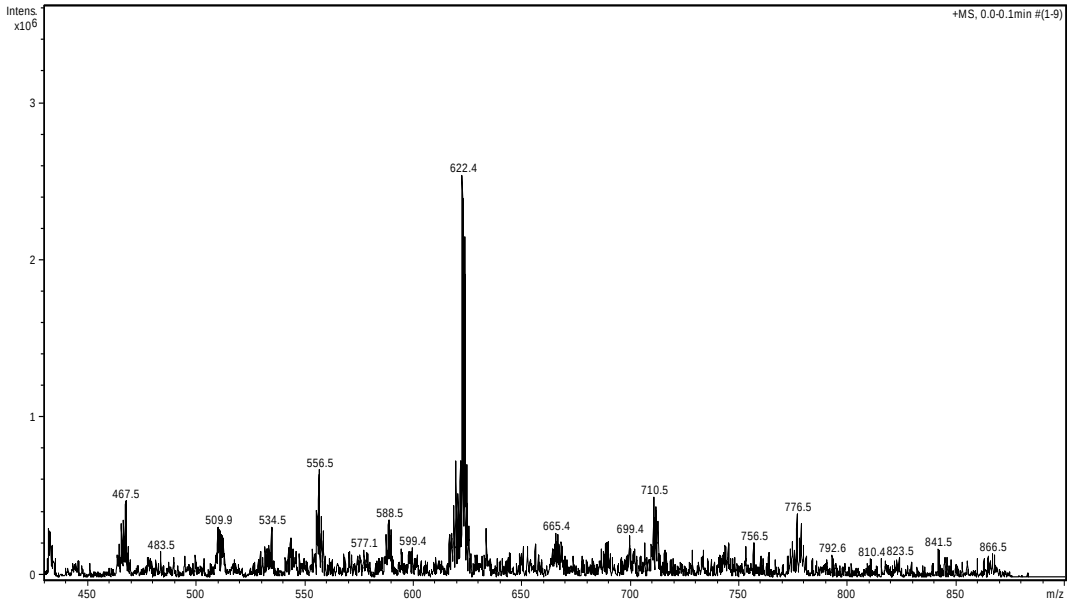

Figure 6.29 ESI-mass spectrum of part B

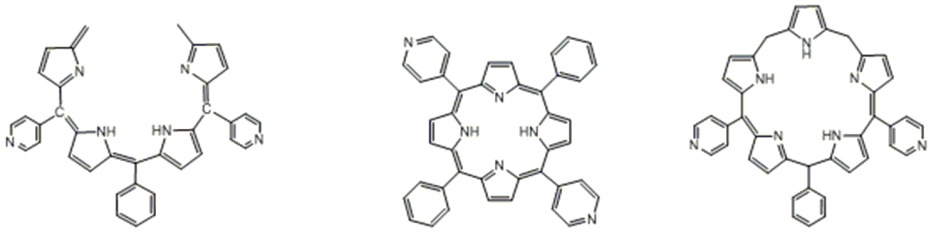

Figure 6.30 Structures of other possible products during reaction (Scheme 6.7)

The trial syntheses of expanded porphyrins show that the meso-substitution causes steric strain in the macrocyle and the expanded porphyrin failed to exist in stable form. The isolation of these compounds was also difficult as revealed by the column purification. Both TFA and BF_3 catalysed reaction between dipyrromethane dialdehyde and tripyrrane resulted in formation of an expanded porphyrin macrocylce. But however, after column purification or after evaporation the major product formed is porphyrin which is confirmed by UV-visible, mass and ^1H NMR spectroscopy.

The studies on fully meso-substituted pentaphyrin also revealed the formation of a pentaphrynic (reduced) macrocyle but however could not be isolated and purified. However, the behaviour of such macrocyles in solution and their fragmentation could be studied in these reactions.

7 CONCLUSIONS

The PhD project was aimed at synthesis of new materials with potential application in water treatment. Syntheses and application of organic photosensitizers on water photodisinfection were carried out. This study has faced gains and losses at numerous steps. But nonetheless, new horizons in the field of photodisinfection have been unveiled. In conclusion, the project can be summarised as follows

- The syntheses and characterization of new organic materials were attempted. Photosensitizers in particular expanded-porphyrins (meso-substituted) which have potential application in photodisinfection were synthesized. The study revealed that these meso-substituted macrocylces are unstable in their free form due to severe steric strain to hold the molecule in planar conformation. The macrocycles easily break to form porphyrin which has much more stable conformation.
  Since the desired pentaphyrins could not be isolated, 2 other photosensitizers (a commercially available porphyrin and a previously synthesized pentaphyrin) were used to immobilize and determine their photodisinfection efficiencies.
- 5-(4-carboxy phenyl) 10, 15, 20-triphenyl porphyrin (TPP) was used to immobilize on magnetic iron oxide nanoparticles. The use of magnetic nanoparticles for supporting porphyrin proves to be promising with several orders of reduction in the survival of Gram-positive bacterial strains. Magnetic nanoparticles used as photosenstizer supports also enables to recover the photosensitizers that can be subsequently used for futher treatment steps. The recovery is simple separation by a magnet which allows recycling the supported photosensitizer. However, reuse experiments with TPP-SPION nanoconjugate were not performed in the study as the efficiency of TPP-SPION in the first cycle was lower than free TPP by almost 4 orders. The reduced activity though, could be due to the fact that TPP-SPION molecules are in less homogenous form in the bacterial culture than free TPP. TPP is dissolved in a non-toxic amount of DMSO in order make it homogenous in water systems.

- Polymers are potential carriers for immobilizing photosensitizers. In particular in this project we have shown that, polyvinyl chloride (PVC) can be an excellent support if used with appropriate adipate. The PS-PVC films exhibited excellent photoactivity against *S. aureus* at 1 % and 5% concentration. Both TPP and PCCox display significant photodisinfection ability when immobilized on PVC but in presence of di n-octyl adipate or di-capryl adipate. The films can be prepared by simple technique of solution casting and does not involve tedious preparation methods. Their use is also trouble-free as they can be just suspended in the water systems to be treated and recovered at the end of treatment. The reuse experiments showed that the films retain activity after the first cycle but the activity drops down with storage of the film for longer time. These results of resuse require more assessment to be confirmed. Also, reinforcing the films would reveal more information about the efficiency and reuse of these films.

References

[1] S. Malato, P. Fernández-Ibáñez, M.I. Maldonado, J. Blanco and W. Gernjak, "Decontamination and disinfection of water by solar photocatalysis: Recent overview and trends," *Catalysis Today*, vol. 147, pp. 1–59, 2009.

[2] S. Baldursson and P. Karanis, "Waterborne transmission of protozoan parasites: Review of worldwide outbreaks: An update 2004-2010," *Water research*, vol. 45, pp. 6603 -6614, 2011.

[3] D. Schoenen, "Role of disinfection in suppressing the spread of pathogens with drinking water: possibilities and limitations," *Water Research*, vol. 36, pp. 3874–3888, 2002.

[4] M. Muruganandham, R. P. S. Suri, Sh. Jafari, M. Sillanpää, G. J. Lee, J. J. Wu, and M. Swaminathan, "Recent developments in homogenous advanced oxidation processes for water and wastewater treatment," *International Journal of Photoenergy*, vol. 2014, article no. 821674, 21 pages, 2014.

[5] G. Jori, M . Magaraggia, C. Fabris, M. Soncin, M. Camerin, L. Tallandini, O. Coppellotti and L. Guidolin, "Photodynamic inactivation of microbial pathogens: disinfection of water and prevention of water-borne diseases," *Journal of Environmental Pathology, Toxicology and Oncology*, vol. 30, no. 3, pp. 261-271, 2011.

[6] M. N. Chong, B. Jin, C. W .K. Chow and C. Saint, "Recent developments in photocatalytic water treatment technology: A review," *Water Research*, vol. 44, pp. 2997-3027, 2010.

[7] T. Zhang, X. Wang, and X. Zhang, "Recent Progress in TiO_2-Mediated Solar Photocatalysis for industrial wastewater treatment," *International Journal Of Photoenergy*," Vol. 2014, Article ID 607954, 12 pages, 2014.

[8] M. C. DeRosa and R. J. Crutchley, "Photosensitized singlet oxygen and its applications", *Coordination Chemistry Reviews*, vol. 233-234, pp. 351-371, 2002.

[9] Ž. Lukšienė, "New Approach to Inactivation of Harmful and Pathogenic Microorganisms by Photosensitization," Photosensitization:

An Overview, *Food Technology and Biotechnology* Vol. 43, no. 4, pp 411-418, 2005.

[10] B. D. McGinnis, V. D. Adams, and E. J. Middlebrooks, "Evaluation Of Methylene Blue And Riboflavin For The Photosensitized Degradation Of Ethylene Glycol," *Environment International*, Vol. 25, No. 8, pp. 953-959, 1999.

[11] P. Kluson, M. Drobek, S. Krejcikova, J. Krysa, A. Kalaji, T. Cajtham and J. Rakusan, "Molecular structure effects in photodegradation of phenol and its chlorinated derivatives with phthalocyanines," *Applied Catalysis B: Environmental* Vol. 80, pp. 321–326, 2008.

[12] E. Alves, M. A.F. Faustino, M. G.P.M.S. Neves, Â. Cunha, H. Nadais, and A. Almeida, "Potential applications of porphyrins in photodynamic inactivation beyond the medical scope," *Journal of Photochemistry and Photobiology C: Photochemistry Reviews*, vol. 22, pp. 34-57, 2015.

[13] A. Mills and S. L. Hunte, "An overview of semiconductor photocatalysis," *Journal of Photochemistry and Photobiology A: Chemistry*, vol. 108, pp. 1-35, 1997.

[14] O. Seven, B. Dindar, S. Aydemir, D. Metin, M. A. Ozinel, S. Icli, "Solar photocatalytic disinfection of a group of bacteria and fungi aqueous suspensions with TiO_2, ZnO and Sahara desert dust," *Journal of Photochemistry and Photobiology A: Chemistry*, vol. 165, pp. 103–107, 2004.

[15] A. K. Benabbou, C. Guillard, S. Pigeot-Rémy, C. Cantau, T. Pigot, P. Lejeune, Z. Derriche and S. Lacombe, "Water disinfection using photosensitizers supported on silica," *Journal of Photochemistry and Photobiology A: Chemistry*, vol. 219 pp. 101–108, 2011.

[16] A. K. Haylett, F. I. McNair, D. McGarvey, N. J. F. Dodd, E. Forbes, T. G. Truscott, J. V. Moore, "Singlet oxygen and superoxide characteristics of a series of novel asymmetric photosensitizers," *Cancer Letters* vol. 112, pp. 233-238, 1997.

[17] I. J. Macdonald and T. J. Dougherty, "Basic principles of photodynamic therapy," *Journal of Porphyrins and Phthalocyanines*, vol. 5, pp. 105–129, 2001.

[18] M. Pelaez, N. T. Nolan, S. C. Pillai, M. K. Seery, P. Falaras, A. G. Kontos, P. S. M. Dunlop, J. W. J. Hamilton, J. A. Byrne, K. O'Shea, M. H.

Entezari and D. D. Dionysiou, "A review on the visible light active titanium dioxide photocatalysts for environmental applications," *Applied Catalysis B: Environmental*, vol. 125, pp. 331-349, 2012.

[19] Z. Alouini and M. Jemli, "Destruction of helminth eggs by photosensitized porphyrin," *Journal of Environmental Monitoring,* vol. 3, pp. 548–551, 2001.

[20] K. H. Choi, K. K. Wang, S. L. Oh, J. E. Im, B. J. Kim, J. C. Park, D. H. Choi, H. K. Kim and Y. R. Kim, "Singlet oxygen generating nanolayer coatings on NiTi alloy for photodynamic application," *Surface & Coatings Technology*, vol. 205, pp. S62–S67, 2010.

[21] K. Ergaieg, M. Chevanne, J. Cillard and R. Seux, "Involvement of both Type I and Type II mechanisms in Gram-positive and Gram-negative bacteria photosensitization by a meso-substituted cationic porphyrin," *Solar Energy*, vol. 82 pp. 1107–1117, 2008.

[22] L. Costa, M. A. F. Faustino, J. P. C. Tomé, M. G. P. M. S. Neves, A. C. Tomé, J. A. S. Cavaleiro,. Â Cunha, and A. Almeida, "Involvement of type I and type II mechanisms on the photoinactivation of non-enveloped DNA and RNA bacteriophages," *Journal of Photochemistry and Photobiology B: Biology,* vol. 120, pp. 10-16, 2013.

[23] E. F. F. Silva, C. Serpa, J. M. Dabrowski, C. J. P. Monteiro, S. J. Formosinho, G. Stochel, K. Urbanska, S. Simões, M. M. Pereira, and L. G. Arnaut, "Mechanisms of Singlet-Oxygen and Superoxide-Ion Generation by Porphyrins and Bacteriochlorins and their Implications in Photodynamic Therapy," *Chemistry-A European Journal*, vol. 16, pp. , 2010.

[24] J. Fenoll, P. Hellín, P. Flores, C. M. Martínez, and S. Navarro, "Photocatalytic degradation of five sulfonylurea herbicides in aqueous semiconductor suspensions under natural sunlight," *Chemosphere*, vol. 87, pp. 954–961, 2012.

[25] T. Daimon, T. Hirakawa, M. Kitazawa, J. Suetake and Y. Nosaka, "Formation of singlet molecular oxygen associated with the formation of superoxide radicals in aqueous suspensions of TiO_2 photocatalysts," *Applied Catalysis A: General*, vol. 340, pp. 169-175, 2008.

[26] R. Konaka, E. Kasahara, W. C. Dunlap, Y. Yamamoto, K. C. Chien and M. Inoue, "Irradiation Of Titanium Dioxide Generates Both Singlet

Oxygen And Superoxide Anion," Free Radical Biology & Medicine, Vol. 27, Nos. 3/4, pp. 294–300, 1999.

[27] O. K. Dalrymple, E. Stefanakos, M. A. Trotz, and D. Y. Goswami, "A review of the mechanisms and modeling of photocatalytic disinfection," *Applied Catalysis B: Environmental*, vol. 98, pp. 27–38, 2010.

[28] Z. Malik, J. Hanania, and Y. Nitzan, "New trends in photobiology bactericidal effects of photoactivated porphyrins- An alternative approach to antimicrobial drugs," *Journal of Photochemistry and Photobiology B: Biology*, vol. 5, pp. 281-293, 1990.

[29] S.Ferro, L. Guidolin, G. Tognon, G. Jori, and O. Coppellotti, "Mechanisms involved in the photosensitized inactivation of *Acanthamoeba palestinensis* trophozites," *Journal of Applied Microbiology*, vol. 107, pp. 1615-1623, 2009.

[30] G. Bertoloni, F. M. Lauro, G. Cortella, M. Merchat, "Photosensitizing activity of hematoporphyrin on *Staphylococcus aureus* cells," *Biochimica et Biophysica Acta*, vol. 1475, no. 2, pp. 169-74, 2000.

[31] M. R. Hamblin and T. Hasan, "Photodynamic therapy: a new antimicrobial approach to infectious disease?" *Photochemical & Photobiological Sciences*, vol. 3, no. 5, pp. 436-450, 2004.

[32] B. Bachmann, J. K. Hopf, B. Lambrecht, and H. Mohr, "Target structures for HIV-1 inactivation by methylene blue and light," *Journal of Medical Virology*, vol. 47, issue. 2, pp. 172-178, 1995.

[33] G. Garcia, V. Sarrazy, V. Sol, C. L. Morvan, R. Granet, and S. Alves, "DNA photocleavage by porphyrin–polyamine conjugates," *Bioorganic & Medicinal Chemistry*, vol. 17, pp. 767-776, 2009.

[34] E. D. Quiroga, M. P. Cormick, P. Pons, M. G. Alvarez, and E. N. Durantini, "Mechanistic aspects of the photodynamic inactivation of *Candida albicans* induced by cationic porphyrin derivatives," *European Journal of Medicinal Chemistry*, vol. 58, pp. 332-339, 2012.

[35] K. Zupán, M. Egyeki, K. Tóth, A. Fekete, L. Herényi , Károly Módos, and G. Csík, "Comparison of the efficiency and the specificity of DNA-bound and free cationic porphyrin in photodynamic virus inactivation," *Journal of Photochemistry and Photobiology B: Biology*, vol. 90, pp. 105-112, 2008.

[36] L. Costa, M. Amparo, F. Faustino, M. G. P. M. S. Neves, Â. Cunha, and A. Almeida, "Photodynamic inactivation of mammalian viruses and bacteriophages," *Viruses*, vol. 4, pp. 1034-1074, 2012.

[37] G. Valduga, B. Breda, G. M. Giacometti, G. Jori, and E. Reddi, "Photosensitization of Wild and Mutant Strains of *Escherichia coli* by *meso*-Tetra (*N*-methyl-4-pyridyl)porphine," *Biochemical and Biophysical Research Communications*, vol. 256, pp. 84–88, 1999.

[38] S. A. G. Lambrechts, M. C. G. Aalders, and J. V. Marle, "Mechanistic Study of the Photodynamic Inactivation of *Candida albicans* by a Cationic Porphyrin," *Antimicrobial Agents And Chemotherapy*, vol. 49, no. 7, pp. 2026–2034, 2005.

[39] S. Ferro, O. Coppellotti, G. Roncucci, T. B. Amor and G. Jori, "Photosensitized inactivation of Acanthamoeba palestinensis in the cystic stage," *Journal of Applied Microbiology*, vol. 101, pp. 206–212, 2006.

[40] M. Schäfer, C. Schmitz, R. Facius, G. Horneck, B. Milow, K. H. Funken, and J. Ortner, "Systematic Study of Parameters Influencing the Action of Rose Bengal with Visible Light on Bacterial Cells: Comparison Between the Biological Effect and Singlet-Oxygen Production," *Photochemistry and Photobiology*, vol. 71, no. 5, pp. 514–523, 2000.

[41] Y. Nitzan and H. Ashkenazi, "Photo inactivation of *Deinococcus radiodurans*: An Unusual Gram-Positive Microorganism," *Photochemistry and Photobiology*, vol. 69, no. 4, pp. 505-510, 1999.

[42] C. Karunakaran, G. Abiramasundari, P. Gomathisankar, G. Manikandan, and V. Anandi, "Preparation and characterization of ZnO–TiO_2 nanocomposite for photocatalytic disinfection of bacteria and detoxification of cyanide under visible light," Materials Research Bulletin vol. 46, pp. 1586–1592, 2011.

[43] C. Arrojado, C. Pereira, J. P. C. Tomé, M. A. F. Faustino, M. G. P. M. S. Neves, A. C. Tomé, J. A. S. Cavaleiro, Â. Cunha, R. Calado, N. C. M. Gomes, and A. Almeida, "Applicability of photodynamic antimicrobial chemotherapy as an alternative to inactivate fish pathogenic bacteria in aquaculture systems," *Photochemical & Photobiological Sciences*, vol. 10, pp. 1691-1700, 2011.

[44] D. Lopes, T. Melo, N. Santos, L. Rosa, E. Alves, M. C. Gomes, Â. Cunha, M. G. P. M. S. Neves, M. A. F. Faustino, M. R. M. Domingues, and A.

Almeida, "Evaluation of the interplay among the charge of porphyrinic photosensitizers, lipid oxidation and photoinactivation efficiency in *Escherichia coli*," *Journal of Photochemistry and Photobiology B: Biology*, vol. 141, pp. 145-153, 2014.

[45] Z. Smetana, E. Ben-Hur, E. Mendelson, S. Salzberg, P. Wagner, Z. Malik, "Herpes simplex virus proteins are damaged following photodynamic inactivation with phthalocyanines," *Journal of Photochemistry and Photobiology B: Biology*, vol. 44, issue 1, pp. 77-83, 1998.

[46] G. Rossi, D. Goi and C. Comuzzi, "The photodynamic inactivation of Staphylococcus aureus in water using visible light with a new expanded porphyrin," *Journal of Water and Health*, vol 10, no. 3, pp. 390-399, 2012.

[47] F. Manjón, D. G. Fresnadillo and G. Orellana, "Water disinfection with Ru(II) photosensitisers supported on ionic porous silicones," *Photochemical & Photobiological Sciences*, vol. 8, pp. 926–932, 2009.

[48] K. Ergaieg and R. Seux, "A comparative study of the photoinactivation of bacteria by *meso*-substituted cationic porphyrin, rose Bengal and methylene blue," *Desalination*, vol. 246, pp. 353–362, 2009.

[49] Y. Nitzan, M. Gutterman, Z. Malik, and B. Ehrenberg, "Inactivation of gram-negative bacteria by photosensitized porphyrins," *Photochemistry and Photobiology*, Vol. 55, no. 1, pp. 89–96, 1992.

[50] M. Merchat, G. Bertolini, P. Giacomini, A. Villanueva and G. Jori, "Meso-substituted cationic porphyrins as efficient photosensitizers of Gram-positive and Gram-negative bacteria," *Journal of Photochemistry and Photobiology B:Biology*, vol. 32, pp. 153-157, 1996.

[51] M. Jemli, Z. Alouini, S. Sabbahi, and M. Gueddari, "Destruction of fecal bacteria in wastewater by three photosensitizers," *Journal of Environmental Monitoring*, vol. 4, pp. 511–516, 2002.

[52] C. M. B. Carvalho, E. Alves, L. Costa, J. P. C. Tome, M. A. F. Faustino, M. G. P. M. S. Neves, A. C. Tome , J. A. S. Cavaleiro, A. Almeida, A. Cunha, Z. Lin, and J. Rocha, "Functional Cationic Nanomagnet Porphyrin Hybrids for the Photoinactivation of Microorganisms," ACSnano, vol. 4, no. 12, pp. 7133–7140, 2010.

[53] J. A. Rengifo-Herrera, J. Sanabria, F. Machuca, C. F. Dierolf, C. Pulgarin and G. Orellana, "Comparison of Solar Photocatalytic Inactivation of waterborne *E. coli* using Tris (2,2'-bipyridine)ruthenium(II), Rose Bengal and TiO_2," *Journal of Solar Energy Engineering*, vol. 129, pp. 135–140, 2007.

[54] D. A. Caminos, M. B. Spesia and E. N. Durantini, "Photodynamic inactivation of *Escherichia coli* by novel meso-substituted porphyrins by 4-(3-*N*,*N*,*N*-trimethylammoniumpropoxy) phenyl and 4-(trifluoromethyl) phenyl groups," *Photochemistry and Photobiological Sciences* vol. 5, pp. 56-65, 2006.

[55] M. E. Jimenez-Hernandez, F. Manjón, D. Garcia-Fresnadillo, and G. Orellana, "Solar water disinfection by singlet oxygen photogenerated with polymer-supported Ru(II) sensitizers," *Solar Energy*, vol. 80, pp. 1382–1387, 2006.

[56] A. J. Acher and I.Rosenthal, Dye-sensitized photo-oxidation- a new approach to the treatment of organic matter in sewage effluents," *Water Research*, vol. 11, pp. 557-562, 1977.

[57] A. J. Acher and B. J. Juven, "Destruction of coliforms in water and sewage water by dye-sensitized photooxidation," *Applied and Environmental Microbiology*, pp. 1019-1022, 1977.

[58] A. G. Rincón and C. Pulgarin, "Photocatalytical inactivation of *E. coli*: effect of (continuous–intermittent) light intensity and of (suspended–fixed) TiO_2 concentration," *Applied Catalysis B: Environmental*, vol. 44, pp. 263–284, 2003..

[59] H. Schwegmann, J. Ruppert and F. H. Frimmel, "Influence of the pH-value on the photocatalytic disinfection of bacteria with TiO_2 and explanation by DLVO and XDLVO theory," *Water Research*, vol. 47, pp.1503 -1511, 2013.

[60] C. P. Gerba, C. Wallis, and J. L. Melnick, "Application of photodynamic oxidation to the disinfection of tapwater, sea water, and sewage contaminated with poliovirus," *Photochemistry and Photobiology*, Vol. 26, no. 5, pp. 499–504, 1977.

[61] N. A. Kuznetsova, O. A. Yuzhakova, M. G. Strakhovskay, A. O. Shumarina, A. S. Kozlov, A. A. Krasnovsky, and O. L. Kaliya, "New heterogeneous photosensitizers with phthalocyanine molecules

covalently linked to aminopropyl silica gel," *Journal Porphyrins and Phthalocyanines*, vol. 15, pp. 718–726, 2011.

[62] P. Parakh, S. Gokulakrishnan, and H. Prakash, "Visible light water disinfection using $[Ru(bpy)_2(phendione)](PF_6)_2.2H_2O$ and [Ru(phendione)3]$Cl_{2.2}$H2O complexes and their effective adsorption onto activated carbon," *Separation and Purification Technology*, vol. 109, pp. 9–17, 2013.

[63] F. Manjón, L. Villén, D. Garcia-Fresnadillo and G. Orellana, "On the Factors Influencing the Performance of Solar Reactors for Water Disinfection with Photosensitized Singlet Oxygen," *Environmental Science and Technology*, vol. 42, pp 301-307, 2008.

[64] A. Acher, E. Fischer, R. Zellingher, and Y. Manor, "Photochemical Disinfection of Effluents, Pilot Plant Studies," *Water Research.* Vol. 24, No. 7, pp. 837-843. 1990.

[65] A. T. Cooper and D. Y. Goswami, "Evaluation of Methylene Blue and Rose Bengal for Dye Sensitized Solar Water Treatment," *Journal of Solar Energy Engineering*, Vol. 124, no. 3, 305-310, 2002.

[66] Z. Malik, H. Ladan and Y. Nitzan, "Photodynamic inactivation of Gram-negative bacteria: problems and possible solutions," *Journal of Photochemistry and Photobiology, B: Biology*, vol. 14, no. 3, pp. 262-266, 1992.

[67] G. Jori, M. Magaraggia, C. Fabris, M. Soncin, M. Camerin, L. Tallandini, O. Coppellotti, and L. Guidolin, "Photodynamic inactivation of microbial pathogens: Disinfection of water and prevention of water-borne diseases," *Journal of Environmental Pathology, Toxicology and Oncology*, vol. 30, no. 3, pp. 261-271, 2011.

[68] R. J. Davies-Colley, R. G. Bell, and A. M. Donnison, "Sunlight Inactivation of Enterococci And Fecal Coliforms In Sewage Effluent Diluted In Seawater," *Applied And Environmental Microbiology*, vol. 60, pp. 2049-2058, 1994.

[69] A. J. Acher and Ada Elgavish, "The effect of photochemical treatment of water on Algal growth," *Water Research*, vol 14, pp. 539-543, 1980.

[70] M. Magaraggia, F. Faccenda, A. Gandolfi, and G. Jori, "Treatment of microbiologically polluted aquaculture waters by a novel

photochemical technique of potentially low environmental impact," *Journal of Environmental Monitoring*, vol. 8, pp. 923–931, 2006.

[71] A. J.Acher, E. Fischer, and Y. Manor, "Sunlight disinfection of domestic effluents for agricultural use," *Water Research*, vol. 28, no. 5, pp. 1153-1160, 1994.

[72] A. Acher, E. Fischer, R. Turnheim, and Y. Manor, "Ecologically friendly wastewater disinfection techniques," *Water Research*, vol. 31, no. 6, pp. 1398-1404, 1997.

[73] C. M. B. Carvalho, A. T. P. C. Gomes, S. C. D. Fernandes, A. C. B. Prata, M. A. Almeida, M. A. Cunha, Joa̋o P.C. Tomé, M. A. F. Faustino, M. G. P. M. S. Neves, A. C. Tomé, J. A. S. Cavaleiro, Z. Lin, J. P. Rainho, and J. Rocha, "Photoinactivation of bacteria in wastewater by porphyrins: bacterial β-galactosidase activity and leucine-uptake as methods to monitor the process," *Journal of Photochemistry and Photobiology B: Biology*, vol. 88, pp. 112–118, 2007.

[74] V. T. Orlandi, E. Caruso, G. Tettamanti, S. Banfi, and P. Barbieri, "Photoinduced antibacterial activity of two dicationic 5,15-diarylporphyrins," *Journal of Photochemistry and Photobiology B: Biology*, vol. 127, pp. 123-132, 2013.

[75] L. Villén, F. Manjón, D. García-Fresnadillo, G. Orellana, "Solar water disinfection by photocatalytic singlet oxygen production in heterogeneous medium," *Applied Catalysis B: Environmental*, vol. 69, pp. 1–9, 2006.

[76] M. Bassiouk, E. Alvarez-Zauco and V. A. Basiuk, "Adsorption of meso-tetraphenyl porphines on thin films of C-60 fullerene," *Applied Surface Science*, vol. 275, pp. 375-383, 2013.

[77] M. D. Funes, D. A. Caminos, M. G. Alvarez, F. Fungo, L. A. Otero, and E. N. Durantini, "Photodynamic properties and photoantimicrobial action of electrochemically generated porphyrin polymeric films," *Environmental Science and Technology*, vol. 43, pp. 902–908, 2009.

[78] L. Lvova, M. Mastroianni, G. Pomarico, M. Santonico, G. Pennazza, C. Di Natale, R. Paolesse, and A. D'Amico, "Carbon nanotubes modified with porphyrin units for gaseous phase chemical sensing," *Sensors and Actuators B: Chemical*, vol. 170, nos. 163-171, 2012.

[79] A. R. McDonald, N. Franssen, G. P. M. van Klink, and G. van Koten, "Click' silica immobilisation of metallo-porphyrin complexes and their application in epoxidation catalysis," *Journal of Organometallic Chemistry*, vol 694, pp. 2153–2162. 2009.

[80] E. Alves, J. M. M. Rodrigues, M. A. F. Faustino, M. G. M. S. Neves, J. A. S. Cavaleiro, Z. Lin, Â. Cunha, M. H. Nadais, J. P. C. Tome, A. Almeida, "A new insight on nanomagnet-porphyrin hybrids for photodynamic inactivation of microorganisms," *Dyes and Pigments*, vol. 110, pp. 80-88, 2014.

[81] A. Savino and G. Angeli, "Photodynamic inactivation of *E. coli* immobilized or coated dyes on insoluble supports," *Water Research*, vol. 19, no. 12, pp. 1465-1469, 1985.

[82] R. Bonnett, M. A. Krysteva, I. G. Lalov, and S. V. Artarsky, "Water disinfection using photosensitizers immobilized on chitosan," *Water Research*, vol. 40, pp. 1269 – 1275. 2006.

[83] F. Manjón, M. S. Magana, D. G. Fresnadillo, and G. Orellana, "Singlet oxygen sensitizing materials based on porous silicone: photochemical characterization, effect of dye reloading and application to water disinfection with solar reactors," *Photochemical & Photobiological Sciences,* vol. 9, pp. 838–845, 2010.

[84] F. Nakonechny, A. Pinkus, S. Hai, O. Yehosha, Y. Nitzan, and M. Nisnevitch, "Eradication of gram-Positive and gram-negative bacteria by photosensitizers immobilized in polystyrene," *Photochemistry and Photobiology*, vol. 89, pp. 671–678, 2013.

[85] S. Sabbahi, Z. Alouini, L. B. Ayed, and M. Jemli, "Inactivation of faecal bacteria in wastewater by methylene blue and visible light," *Desalination and Water Treatment*, vol. 20, nos. 1-3, pp. 209-219, 2010.

[86] D. Bai, Q. Wang, Y. Song, B. Li, H. Jing, "Synthesis of cyclic carbonate from epoxide and CO_2 catalyzed by magnetic nanoparticle-supported porphyrin," *Catalysis Communications* vol. 12, pp. 684–688, 2011.

[87] O. Sadeghi, M. M. Amini, M. F. B. Bazargani, A. Mehrani, A. Aghabali, M. Adineh, V. Amani, K. Mehrani, "Immobilization of metalloporphyrin on functionalized magnetic nanoparticles as a catalyst in oxidation of cyclohexene: novel modified Fe_3O_4

nanoparticles with triethoxysilane agent," *Journal of Inorganic and Organometallic Polymers and Materials*, vol. 22, pp. 530–535, 2012.

[88] G. Jori, C. Fabris, M. Soncin, S. Ferro, O. Coppellotti, D. Dei, L. Fantetti, G. Chiti, and G. Roncucci, "Photodynamic Therapy in the Treatment of Microbial Infections: Basic Principles and Perspective Applications," *Lasers in Surgery and Medicine*, vol. 38, pp. 468–481, 2006.

[89] A. Tavares, C. M. B. Carvalho, M. A. Faustino, M. G. P. M. S. Neves, J. P. C. Tomé, A. C. Tomé, J. A. S. Cavaleiro, Â. Cunha , N. C. M. Gomes, E. Alves, and A. Almeida, "Antimicrobial photodynamic therapy: study of bacterial recovery viability and potential development of resistance after treatment," *Marine Drugs*, vol. 8, pp. 91-105, 2010.

[90] L. Costa, C. M. B. Carvalho, M. A. F. Faustino, M. G. P. M. S. Neves, J. P. C. Tomé, A. C. Tomé, J. A. S. Cavaleiro, Â. Cunha and A. Almeida, "Sewage bacteriophage inactivation by cationic porphyrins: influence of light parameters," *Photochemical and Photobiological Sciences*, vol. 9, 1126-1133, 2010.

[91] T. K. Wong, H. J. Huang, Y. F. Wang, Y. P. Lee, C. C. Huang and C. K. Yu, "Methylene blue-mediated photodynamic inactivation as a novel disinfectant of enterovirus 71," *Journal of Antimicrobial Chemotherapy*, vol. 65, pp. 2176-2182, 2010.

[92] D. Gryglik, J. S. Miller, and S. Ledakowicz, "Singlet molecular oxygen application for 2-chlorophenol removal," *Journal of Hazardous Materials*, vol. 146, pp. 502–507, 2007.

[93] P. Kluson, M. Drobek, T. Strasak, J. Krysa, M. Karaskova, and J. Rakusan, "Sulphonated phthalocyanines as effective oxidation photocatalysts for visible and UV light regions," *Journal of Molecular Catalysis A: Chemical*, vol. 272, pp. 213–219, 2007.

[94] M. Silva, M. J. F. Calvetea, N. P. F. Gonçalves, H. D. Burrows, M. Sarakha, A. Fernandes, M. F. Ribeiro, M. E. Azenha, and M. M. Pereira, "Zinc(II) phthalocyanines immobilized in mesoporous silica Al-MCM-41 and their applications in photocatalytic degradation of pesticides," *Journal of Hazardous Materials*, vol. 233–234, pp. 79–88, 2012.

[95] C. Wang, J. Li, G. Mele, G. M. Yang, F. X. Zhang, L. Palmisano, and G. Vasapollo, "Efficient degradation of 4-nitrophenol by using functionalized porphyrin-TiO2 photocatalysts under visible

irradiation," *Applied Catalysis B: Environmental*, vol. 76, pp. 218–226, 2007.

[96] D. Li, W. Dong, S. Sun, A. Shi, and S. Feng, "Photocatalytic degradationn of acid chrome blue K with porhyrin- sensitized TiO_2 under visible light", *Journal of Physical Chemistry C*, vol. 112, no. 38, pp. 14878-14882, 2008

[97] S. Murphy, C. Saurel, A. Morrissey, J. Tobin, M. Oelgemöller, and K. Nolan, "Photocatalytic activity of a porphyrin/TiO2 composite in the degradation of pharmaceuticals," *Applied Catalysis B*, vol. 119– 120, pp. 156– 165, 2012.

[98] C. N. Street and A. Gibbs, "Eradication of the corrosion-causing bacterial strains desulfovibrio vulgaris and desulfovibrio desulfuricans in planktonic and biofilm form using photodisinfection," *Corrosion Science*, vol. 52, pp. 1447–1452, 2010.

[99] S. Ismail, S. Perni, J. Pratten, I. Parkin, and M. Wilson, "Efficacy of a novel light-activated antimicrobial coating for disinfecting hospital surfaces," *Infection Control and Hospital Epidemiology*, vol. 32, issue 11, pp. 1130-1132, 2011.

[100] Z. Luksiene and E. Paskeviciute, "Novel approach to the microbial decontamination of strawberries: chlorophyllin-based photosensitization," *Journal of Applied Microbiology*, vol. 110, pp. 1274-1283, 2011.

[101] C. Fabris, M. Soncin, G. Jori, A. Habluetzel, L. Lucantoni, S. Sawadogo, L. Guidolin, and O. Coppellotti, "Effects of a new photoactivatable cationic porphyrin on ciliated protozoa and branchiopod crustaceans, potential components of freshwater ecosystems polluted by pathogenic agents and their vectors," *Photochemical & Photobiological Sciences*, vol. 11, pp. 294-301, 2012.

[102] S. Saito and A. Osuka, "Expanded Porphyrins: Intriguing Structures, Electronic Properties, and Reactivities," *Angew. Chem. Int. Ed.* , vol. 50, pp. 4342 – 4373, 2011.

[103] C. Comuzzi, S. Cogoi, M. Overhand, G. A. Van der Marel, H. S. Overkleeft, and L. E. Xodo, "Synthesis and Biological Evaluation of New Pentaphyrin Macrocycles for photodynamic therapy", *J. Med. Chem.*vol. 49, pp. 196-204, 2006.

[104] A. K. Burrell, G. Hemmi, V. Lynch, and J. L. Sessler, "Uranylpentaphyrin: An Actinide Complex of an expanded porphyrin," *J. Am. Chem. SOC.* Vol., 113, pp. 4690-4692, 1991.

[105] R. Misra and T. K. Chandrashekar, "Structural Diversity in Expanded Porphyrins," *Accounts of Chemical Research*, Vol. 41, No. 2, pp. 265-279, 2008.

[106] E. Ganapathi, T. Chatterjee, W.Lee, and M. Ravikanth, "Synthesis, Structure, and Properties of Core-modified pentaphyrin containing six meso carbons," *Asian J. Org. Chem.*, vol. 4, pp. 638 – 645, 2015.

[107] Z. Zhang, D. S. Kim, C.-Y. Lin, H. Zhang, A. D. Lammer, V. M. Lynch, I. Popov, O. S. Miljanić, E. V. Anslyn, and J. L. Sessler, "Expanded Porphyrin-Anion Supramolecular Assemblies: Environmentally Responsive Sensors for Organic Solvents and anions," *J. Am. Chem. Soc.*, vol. 137, pp. 7769−7774, 2015.

[108] V. Král, E. A. Brucker, G. Hemmi, J. L. Sessler, J. Králová and H. Bose Jr, "A Non-Ionic Water-Soluble Pentaphyrin Derivative. Synthesis and Cytotoxicity," *Bioorganic & Medicinal Chemistry,* Vol. 3, No. 5, pp. 573-578, 1995.

[109] T. Yoneda, H. Mori, B. S. Lee, M.-C. Yoon, D. Kim and A. Osuka, "A non-fused mono-meso-free pentaphyrin and its rhodium(I) complex," *Chem. Commun.*, vol. 48, pp. 6785–6787, 2012.

[110] H. Rexhausen and A. Gossauer, "The Synthesis of a New 22 π-Electron Macrocycle: Pentaphyrin," *J. Chem. Soc., Chem. Commun.*, pp. 273, 1983.

[111] J. K. Laha, S. Dhanalekshmi, M. Taniguchi, A. Ambroise, and J. S. Lindsey, "A Scalable Synthesis of Meso-Substituted Dipyrromethanes," *Organic Process Research & Development*, vol. 7, pp. 799-812, 2003.

[112] J. L. Sessler, M. R. Johnson, and V. Lynch, "Synthesis and Crystal Structure of a Novel Tripyrrane-Containing Porphyrinogen-like Macrocycle," *J. Org. Chem.*, vol. 52, pp. 4394-4397, 1987.

[113] A. Jasat and D. Dolphin, "Expanded porphyrins and their heterologs," *Chem. Rev.*, vol. 97, pp. 2267-2340, 1997.

[114] M. Ballico, V. Rapozzi, L. E. Xodo, C. Comuzzi, "Metallation of pentaphyrin with Lu(III) dramatically increases reactive-oxygen species production and cell phototoxicity," *European Journal of Medicinal Chemistry*, vol. 46, pp. 712-720, 2011.

[115] J. L. Sessler, T. D. Mody, G. W. Hemmi, and V. Lynch, "Synthesis and Structural Characterization of Lanthanide(III) Texaphyrins," *Inorg. Chem.*, vol. 32, pp. 3175-3187, 1993.

[116] S. Mori, J.-Y. Shin, S. Shimizu, F. Ishikawa, H. Furuta and Atsuhiro Osuka, "N-Fused Pentaphyrins and Their Rhodium Complexes: Oxidation-Induced Rhodium Rearrangement," *Chem. Eur. J.*, vol. 11, pp. 2417 – 2425, 2005.

[117] N. Masilela, P. Kleyi, Z. Tshentu, G. Priniotakis, P. Westbroek, T. Nyokong, "Photodynamic inactivation of *Staphylococcus aureus* using low symmetrically substituted phthalocyanines supported on a polystyrene polymer fiber," Dyes and Pigments 96 (2013) 500-508.

[118] B. L. Carpenter, E. Feese, H. Sadeghifar, D. S. Argyropoulos and R. A. Ghiladi, "Porphyrin-Cellulose Nanocrystals: A Photobactericidal Material that Exhibits Broad Spectrum Antimicrobial Activity," *Photochemistry and Photobiology*, vol. 88, pp. 527–536, 2012.

[119] E. Feese, H. Sadeghifar, H. S. Gracz, D. S. Argyropoulos and R. A. Ghiladi, "Photobactericidal Porphyrin-Cellulose Nanocrystals: Synthesis, Characterization, and Antimicrobial Properties," *Biomacromolecules*, vol. 12, pp.3528–3539, 2011.

[120] S. Patrick, *Practical guide to polyvinyl chloride*. Rapra Technology Ltd, UK, 2005.

[121] C. E. Wilkes, C. A. Daniels, J. W. Summers, *PVC handbook*, ISBN 3-446-22714-8, Hanser Publications, 2005.

[122] P. D. Rao, S. Dhanalekshmi, B. J. Littler, and J. S. Lindsey, "Rational Syntheses of Porphyrins Bearing up to Four Different Meso Substituents," *J. Org. Chem.*, vol. 65, pp. 7323-7344, 2000.

[123] C.H. Lee, J.Y. Park, and H.J. Kim, "Studies of Porphyrin Synthesis through 3+1 Condensation," *Bull. Korean Chem. Soc.* Vol. 21, No. 1, pp. 97, 2000.

[124] C. H. Lee, J. S. Lindsey, "One-flask synthesis of *meso*-substituted dipyrromethanes and their application in the synthesis of *trans*-substituted porphyrin building blocks," *Tetrahedron*, vol. 50, pp. 11427-11440, 1994.

[125] M. Thandu, V. Rapozzi, L. Xodo, F. Albericio, C. Comuzzi, and S. Cavalli, "Clicking" Porphyrins to Magnetic Nanoparticles for Photodynamic Therapy," *ChemPlusChem*, vol. 79, pp. 90–98, 2014.

[126] K. S. Lim, K.W. Oh and S. H. Kim, "Antimicrobial activity of organic photosensitizers embedded in electrospun nylon 6 nanofibers," *Polym Int*; vol. 61, pp. 1519–1524, 2012.

[127] T.A. Dahl, W.R. Middenand, P.E. Hartman, "Pure singlet oxygen citotoxicity for bacteria," *Photochem. Photobiol.* Vol. 46, pp. 345–352, 1987.

[128] O. L. Osifeko and T. Nyokong, "Applications of lead phthalocyanines embedded in electrospun fibers for the photoinactivation of *Escherichia coli* in water," *Dyes and Pigments*, vol. 111, 8-15, 2014.

[129] M. A. D. Palma, M. G. Alvarez, A. L. Ochoa, M. E. Milanesio, and E. N. Durantini, "Optimization of cellular uptake of zinc(II) 2,9,16,23- tetrakis [4-(*N*-methylpyridyloxy)] phthalocyanine for maximal photoinactivation of *Candida albicans*," *Fungal Biology*, vol. 117, pp. 744-751, 2013.

[130] APHA, 2012 *Standard Methods for the Examination of Water and Wastewater*, 22nd edition. American Public Health Association/American Water Works Association/Water Environment Federation, Washington, DC.

[131] R. Huisgen, 1,3-Dipolar Cycloaddition Chemistry, Vol. 1, Wiley, NewYork, 1984

[132] N. J. Agard, J. A. Prescher, C. R. Bertozzi, " A strain promoted [3+2] azide-alkyne cycloaddition for covalent modification of biomolecules in living systems," *J. Am. Chem. Soc.*, vol. 126, pp. 15046 –15047, 2004.

[133] V. Rostovtsev, L. G. Green, V. V. Fokin, K. B. Sharpless, "A stepwise Huisgen cycloaddition process: copper (I) catalysed regioselctive "ligation" of azides and terminal alkynes," *Angew.Chem.*, vol. 114, pp. 2708 –2711 ,2002.

[134] W. G. Lewis, L. G. Green, F. Grynszpan, Z. Radic´, P. R.Carlier, P. Taylor, M. G. Finn, K. B. Sharpless, "Click chemistry in situ: acetylcholinestrase as a reaction vessel for the selective assembly of a femtomolar inhibitor from an array of building blocks," *Angew. Chem.*, vol. 114, pp.1095 –1099, 2002.

[135] E. J. Billo, *Excel for Chemists: A Comprehensive Guide*, Wiley, New York, 1997.

[136] S.Hamada and H. D. Slade, "Biology, Immunology, and Cariogenicity of *Streptococcus mutans*," *Microbiological Reviews*, Vol. 44, No. 2, pp. 331-384, 1980.

[137] G. Rossi, "Tecnologie sonozono e fotossidativa nel trattamento aque" PhD thesis, University of Udine, 2011.

Acknowledgement

I sincerely would like to thank many people who have been a part in the whole journey of my PhD project.

First and foremost, I am extremely grateful to my supervisor Prof. Daniele Goi to giving me this opportunity and always motivating to go ahead in this interesting field of research.

Big thanks to my co-supervisor, Dr. Clara Comuzzi for always being my friend, philosopher and guide bringing out the best in me.

Special thanks to Dr. Silvia Cavalli to help and directing me in the earlier months of my PhD project.

Heartfelt thanks to all my seniors and colleagues in the group, Giada for helping me learn new techniques in microbiology, Valentina to help me whenever needed, Caludia in working together, Matteo and Mattia always being there in some way or the other. Andrea Fattori is always a big helping hand.

Many thanks to all colleagues and technical staff at the "Department of Chemistry, Physics and Environment" for all the support during my PhD.

I like to acknowledge the support of University of Udine to support me with fellowship for PhD and also as 'Assegno di Ricerca' for postdoctoral studies and sustainability of my PhD and not forgetting Prof. Daniele Zuccaccia for being the supervisor for 'Assegno di Ricerca'.

Also I like to thank Project POCN Area di Ricerca Trieste for supporting me financially and giving the opportunity to work on this topic.

I am very much thankful to Dr. Paolo Guerrerio and his research group at IENI-CNR, Padova for helping with characterization techniquies (SEM analysis).
Thanks to all friends in Udine and Trieste for immense support and motivation.
I personally like to thank each and every one who has been part of my journey of PhD work. Also, I would like to apologize if I have unknowingly missed to acknowledge anyone.